THESIS ON NATURAL AND EXACT SCIENCES B200

Investigation of Endogenous Antioxidants and Their Synthetic Analogues by Capillary Electrophoresis

JANA KAZARJAN

TUT PRESS

TALLINN UNIVERSITY OF TECHNOLOGY
Faculty of Science
Department of Chemistry

Dissertation was accepted for the defense of the degree of Doctor of Philosophy in Natural and Exact Sciences on December 11, 2015.

Supervisors: Dr. Merike Vaher, Department of Chemistry, Faculty of Science, Tallinn University of Technology, Estonia
Professor Mihkel Kaljurand, Department of Chemistry, Faculty of Science, Tallinn University of Technology, Estonia

Opponents: Professor Tõnu Püssa, Institute of Veterinary Medicine and Animal Sciences, Estonian University of Life Sciences, Tartu, Estonia

Professor Audrius Maruška, Department of Chemistry, Vytautas Magnus University, Kaunas, Lithuania

Defense of the thesis: January 11, 2016.

Declaration:
Hereby I declare that this doctoral thesis, my original investigation and achievement, submitted for the doctoral degree at Tallinn University of Technology has not been submitted for any academic degree.

ISSN 1406-4723
ISBN 978-9949-23-878-1 (publication)
ISBN 978-9949-23-879-8 (PDF)

LOODUS- JA TÄPPISTEADUSED B200

Endogeensete antioksüdantide ja nende sünteetiliste analoogide uurimine kapillaarelektroforeesi meetodil

JANA KAZARJAN

TTÜ
KIRJASTUS

To my loved ones…

CONTENTS

CONTENTS		7
LIST OF PUBLICATIONS		9
AUTHOR'S CONTRIBUTION TO THE PUBLICATIONS		10
INTRODUCTION		11
ABBREVIATIONS		14
1	LITERATURE OVERVIEW	15
1.1	Glutathione and its analogues (UPF peptides)	15
1.2	Superoxide dismutase enzymes	17
1.3	Capillary electrophoresis in the investigation of biomolecules	18
1.4	General aspects of capillary electrophoresis	20
1.4.1	Factors affecting the electro-osmotic flow	22
1.5	Determination of acid dissociation constants of UPF peptides by CE	23
1.6	Determination of retention factors of UPF peptides by MEKC	24
1.7	Determination of metal ions in SODs by CE	26
2	EXPERIMENTAL	28
2.1	Reagents	28
2.2	Standard solutions and sample preparation	29
2.2.1	UPF peptides	29
2.2.2	SOD samples	29
2.2.3	Metal standard solutions	30
2.3	Instrumentation	30
2.3.1	Capillary conditioning	31
3	RESULTS AND DISCUSSION	32
3.1	Separation of GSH and its analogues by CE (Publication I)	32
3.1.1	Inorganic buffers	32
3.1.2	Zwitterionic buffers	33
3.1.3	Identification of peptides in a mixture	35
3.2	Determination of acidity constants of GSH and its analogues by CE (Publication I)	36
3.3	MEKC studies of UPF peptides (Publications II, III)	38
3.3.1	Choice of the micelle marker	38
3.3.2	Effect of surfactant concentration on the mobility of UPF peptides	39
3.3.2.1	Aggregation of micellar background electrolytes	42
3.3.3	Determination of retention factors of UPF peptides by MEKC	45
3.4	Determination of metal content in SODs by CE (Publication IV)	47
3.4.1	BGE optimization	47
3.4.2	Analytical performance of the CE method	49
3.4.3	Sample analysis	51
4	CONCLUSIONS	53
REFERENCES		55
APPENDICES		61
Appendix 1		61
Appendix 2		62
Appendix 3		63

Appendix 4 64
Appendix 5 65
ACKNOWLEDGEMENTS 66
ABSTRACT 67
KOKKUVÕTE 68
ORIGINAL PUBLICATIONS 71
Publication I 71
Publication II 81
Publication III 91
Publication IV 97
CURRICULUM VITAE 103
ELULOOKIRJELDUS 105

LIST OF PUBLICATIONS

This thesis is based on the following original publications, which are referred to by Roman numerals within the text:

I. Kazarjan, J., Vaher, M., Mahlapuu, R., Hansen, M., Soomets, U., Kaljurand. M. Separation of glutathione and its novel analogues and determination of their dissociation constants by capillary electrophoresis. – *Electrophoresis,* 2013, 34, 1820-1827.

II. Kazarjan, J., Mahlapuu, R., Hansen, M., Soomets, U., Kaljurand. M., Vaher, M. Investigation of the surfactant type and concentration effect on the retention factors of glutathione and its analogues by micellar electrokinetic chromatography. – *J Sep Sci*, 2015, 38, 1042-1045.

III. Kazarjan, J., Vaher, M., Kaljurand, M. Aggregation of phosphate and 1-tetradecyl-3-methylimidazolium chloride background electrolytes during micellar electrokinetic chromatography. – *Electrophoresis,* 2015, 36, 1040-1042.

IV. Kazarjan, J., Vaher, M., Hunter, T., Kulp, M., Hunter, G.J., Bonetta, R., Farrugia, D., Kaljurand, M. Determination of metal content in superoxide dismutase enzymes by capillary electrophoresis. – *J Sep Sci*, 2015, 38, 1042-1045.

AUTHOR'S CONTRIBUTION TO THE PUBLICATIONS

Publications I and II:
The author planned and carried out all the CE experiments. She interpreted the results and wrote the manuscripts. UPF peptides were synthesized and kindly provided by co-authors (Mahlapuu, R., Hansen, M. and Soomets, U.).

Publication III:
The author was mostly responsible for planning and carrying out the experimental part and participated in writing of the manuscript.

Publication IV:
The author planned and carried out all the CE experiments, (apo)SOD synthesis and purification. She interpreted the results and wrote the major part of the manuscript.

INTRODUCTION

Reactive species (RS) are formed constantly in the human body as a result of normal cellular metabolism and under pathophysiological conditions associated with an increased formation of RS. There is a complex system of different types of endogenous antioxidants that protect cells against the uncontrolled formation of reactive species or inhibit their reactions with biological structures. Hydrophilic antioxidants like glutathione (GSH) and ascorbate scavenge oxidizing free radicals and are found in cytosolic, mitochondrial and nuclear compartments. Hydrophobic scavengers (α-tocopherol, carotenoids) are found in the lipoproteins and membranes of the cell where they protect lipids from peroxidation. Along with non-enzymatic scavengers, specific endogenous antioxidant enzymes exist within the cells to destroy the superoxide (superoxide dismutase (SOD)) and hydroperoxides (catalase, glutathione peroxidase or ascorbate peroxidase). This antioxidant system controls the level of reactive species that have many important regulatory roles and at the same time it protects the cells from redox-related perturbations [1, 2]. In the present study, special attention was devoted to glutathione and its synthetic analogues, as well as superoxide dismutase enzymes that altogether contribute to the biodiversity of mechanisms for the removal of reactive species.

Glutathione is the most abundant intracellular low molecular weight non-enzymatic thiol-containing peptide in cells that has important biological functions such as direct scavenging of free radicals, detoxification and other regulatory roles[3]. After the scavenging of oxyradicals an oxidized glutathione disulfide (GSSG) is formed. Maintaining the GSH/GSSG ratio is a vital cellular mechanism for intracellular redox balance. The reducing environment within the cells ensures redox enzyme regulation, cell cycle progression, transcription of antioxidant response elements, and regulation of many other cellular processes [4-9]. At the same time, cells under stress and in many diseased states commonly experience GSH pool depletion. The administration of GSH directly to solve this problem is complicated due to an excessive extracellular degradation and poor cellular uptake of the compound. Thus, there is a high interest in designing GSH analogues as possible new bioactive compounds for pharmacological applications. In an effort toward achieving this challenging goal, new tetrapeptic analogues of GSH called UPFs (UPF1, UPF17, UPF50 and UPF51), have been synthesized [10].

The physiochemical properties of these new compounds must be precisely determined before pharmaceutical use. Amongst these properties are ionizing ability (pK_a) and hydrophobicity expressed as diverse interactions between complex biological membranes and GSH analogues (log k) that are of help in the studies of absorption, distribution, metabolism and excretion (ADME) of UPF peptides as possible drugs. In the early stages of a drug development process and exploratory studies, it is prohibitively difficult to obtain pure compounds in high quantities. Moreover, in a mixture of different GSH analogues, homo- and heterodimers are formed during natural oxidation

process. Thus, development of a method with high selectivity and sensitivity towards components of interest is a challenging and useful scientific pursuit.

In present research, close attention was paid to the development of capillary electrophoresis (CE) techniques, where the simultaneous separation of neutral and charged analytes is achieved in narrow fused-silica capillaries filled with a buffered solution under the influence of an electric field. Remarkable benefits such as high speed of separation, low consumption of buffer, requirement for a very small quantity of material, which may be relatively unstable [11], makes CE an attractive alternative analytical technique for clinical chemists and biochemists in early drug discovery. Moreover, sample preparation in CE is simple with no need for purification and/or derivatization, which allows online monitoring of the natural oxidation process of GSH analogues [12], thus making CE advantageous over other separation techniques. Last but not least, single CE methods have a potential to be adapted to a multiplexed miniaturized format, thus allowing rapid separations with improved efficiency for high-throughput applications in drug discovery.

In this research, naturally occurring antioxidant scavenger enzymes-superoxide dismutases (SODs) were also investigated by capillary electrophoresis. These metalloenzymes protect cells against oxidative damage caused by superoxide radicals that are unavoidably formed by aerobic respiration. SODs catalyze the dismutation of the superoxide radical into oxygen and hydrogen peroxide, which in turn is further eliminated by glutathione peroxidase or catalase. Hence, the biological activity of glutathione peroxidase depends on the glutathione as a cosubstrate. Eventually, GSH and SOD work synergistically to protect cells against oxidative injury.

Three forms of SODs have been investigated, each having different metal cofactors at their active site: CuZnSOD, FeSOD and MnSOD. These metal cofactors are necessary for redox cycling that result in the disproportionation of the superoxide radical into molecular oxygen and hydrogen peroxide. SODs activity therefore depends on an effective metal ion acquisition and the degree of metalation. Metal content measurement is one of the essential steps to characterize the biological activity of enzyme. It may also provide information on metal cofactor selectivity and specificity in wild type and mutant proteins [13]. Furthermore the cofactor content of cellular metalloenzymes may be a reflection of metal ion availability in the biological system. Consequently, antioxidant enzymes like superoxide dismutases are potential drug candidates and further investigation in SODs activity regulation is of substantial importance. Even more, selective superoxide dismutase mimetics have been designed as therapeutic agents against diseases caused by the superoxide anion that is known to be a crucial mediator of inflammation [14]. Thus, a capillary electrophoresis protocol was developed for the simultaneous determination of transition metal content in superoxide dismutase enzymes as an essential step in the further understanding of SODs activity. As discussed above, CE is a fast and simple method that has advantages such as high separation ability of mixtures of ions, low sample and background electrolyte consumption and ease of automation.

The main goal of the present research was to show the diverse opportunities that capillary electrophoresis opens for the investigation of endogenous antioxidants and their synthetic analogues as possible drugs for preclinical investigations, as well as the determination of metal content in superoxide dismutase enzymes for the accurate measurement of their activity. More specifically, individual studies aimed at the following:

- developing a separation protocol for glutathione and its analogues and determining the dissociation constants of these peptides by CE;
- investigating the influence of surfactant type and concentration on retention factors of GSH and UPF peptides and their homodimers by micellar electrokinetic chromatography (MEKC);
- developing a CE protocol for the separation, identification and quantification of metal content in naturally occurring and metal substituted SODs using a novel IL-based background electrolyte.

ABBREVIATIONS

BGE	Background electrolyte
CE	Capillary electrophoresis
CHES	2-(Cyclohexylamino)ethanesulfonic acid
C_{14}MImCl	1-Tetradecyl-3-methylimidazoilum chloride
DAD	Diode array detector
DMF	*N*,*N*-Dimethylformamide
DMSO	Dimethyl sulfoxide
EOF	Electro-osmotic flow
FAAS	Flame atomic emission spectrophotometry
FDA	Food and Drug Administration
GFAAS	Graphite furnace atomic emission spectrophotometry
GSH	Glutathione
GSSG	Glutathione disulfide
HEPES	2-[4-(2-Hydroxyethyl)piperazin-1-yl]ethanesulfonic acid
MS	Mass spectrometry
MEKC	Micellar electrokinetic chromatography
MOPS	3-Morpholinopropane-1-sulfonic acid
$O_2^{\cdot -}$	Superoxide radical (superoxide radical anion)
RS	Reactive species
SDS	Sodium lauryl sulfate
SDS-PAGE	Sodium lauryl sulfate polyacrylamide gel electrophoresis
SOD	Superoxide dismutase

1 LITERATURE OVERVIEW

1.1 Glutathione and its analogues (UPF peptides)

Glutathione is a soluble thiol-containing compound composed of cysteine, glycine and glutamate. It is a powerful antioxidant that is found in most of the cells in millimolar concentrations. GSH's free radical scavenging properties rise from the presence of the sulfhydryl group (pK_a= 8.93), hence, only 1.2 % of GSH is in the thiolate form under physiological conditions (pK_a=7.4)[15].

Reduced glutathione reacts with reactive oxygen species (ROS) to form oxidized glutathione (GSSG), which, in turn, is recycled back to two GSH molecules by enzyme called GSH-reductase. An imbalance between the production and elimination of ROS triggers oxidative stress and, as a result, cells activate adaptive responses in order to restore the redox balance. Besides, the redox regulation of ROS is critical to many cellular functions such as ion transport, cell signaling, apoptosis program activation and many more[16, 17]. The level of GSH is decreased in neurodegenerative diseases such as Alzheimer's disease (AD), Parkinson's disease (PD) and amyotrophic lateral sclerosis (ALS), and with age[18, 19]. Hence, the GSSG/GSH ratio is used as an indicator of oxidative stress. The regulation of the level of endogenous GSH is vital in maintaining redox homeostasis and in protecting cells against ROS of either endogenous or exogenous source (smoking, air pollution, UV radiation). Unfortunately, the GSH molecule transport into the cells is rather poor. Besides, L-cysteine, which is the rate-limiting amino acid in GSH synthesis, is toxic for humans.

Different strategies have been tried to compensate for the low level of GSH and/or mimic its functions. One of the possible approaches is the administration of N-acetyl cysteine (NAC), which is a FDA approved drug, being a precursor to intracellular cysteine and glutathione. Though NAC has proven anti-inflammatory and antioxidative effects, these are specific and concentration dependent. Consequently, the drug has low bioavailability and a higher dosage is needed to ensure the stated effects of NAC. At the same time, it is expected that GSH synthesis machinery is unaffected and is perfectly functioning. Another approach to overcome problems with GSH pool depletion is the synthesis of chemically modified analogues with GSH-like activity regarding redox function. Various compounds have been designed in order to mimic the various physiological and pharmacological effects of glutathione. YM737 (N-(N-gamma-L-glutamyl-L-cysteine) glycine L-isopropyl ester sulfate monohydrate) is a monoester of GSH that has a beneficial effect in rat cerebral ischemia model. To protect GSH analogues from the degradative effects of various enzymes cyclic peptide homologues of glutathione cyclo(Glu[Cys-ß-Ala-]-OH) and cyclo(Glu[Cys-Gaba-]-OH) have also been generated and their anti-tumor activity has been established [20, 21].

A library of tetrapeptic GSH analogues that are called UPF peptides (Fig. 1) was designed as another possible approach to enhance the GSH-related detoxification capacity. These UPF peptides contain the *O*-methyl-L-tyrosine

residue that is added to the N-terminus of glutathione, as presence of methoxy groups is thought to be responsible for antioxidant activities in molecules like melatonin, as well as carvedilol and its metabolite SB 211475. In this research, four of the UPF peptides referred to as UPF1, UPF17, UPF50 and UPF51 were investigated. UPF1 (Tyr(Me)-γ-Glu-Cys-Gly) and UPF17 (Tyr(Me)-α-Glu-Cys-Gly) molecules posses the *O*-methyl-L-tyrosine residue that is added to the N-terminus of the GSH-like Glu-Cys-Gly sequence in order to increase not only their antioxidativity but also hydrophobicity. At the same time, there is a slight difference between UPF1 and UPF17 in moiety; namely, UPF1 has the γ-glutamyl moiety similarly to GSH, while UPF17 has the α-glutamyl moiety. This minor discrepancy resulted in an improved hydroxyl radical scavenging ability of UPF17 by approximately 500-fold compared to UPF1, which in turn is an about 60-fold better hydroxyl scavenger than glutathione. Along with its *in vitro* antioxidant abilities, UPF1 has also shown antioxidative effects in an ischemia/ reperfusion model on an isolated heart of Wistar rats. UPF1 and UPF17 have shown no toxic effects in different cell types either [22-24]. In addition to UPF1 and UPF17 other GSH analogues, namely UPF50 (β-Ala-His-Tyr(Me)-γ-Glu-Cys-Gly) and UPF51 (β-Ala-His-Tyr(Me)-α-Glu-Cys-Gly, are described in this work for the first time ever. These two novel UPF peptides (UPF50 and UPF51) have an additional carnosine (β-Ala-His) dipeptide in their N-termini. Carnosine, being naturally found in several tissues like skeletal muscle, heart muscle, skin, stomach, nerve tissue and brain, has many beneficial properties such as ion chelating and wound-healing promoting capabilities and the ability to scavenge free radicals [25, 26].

Unfortunately, the therapeutic potential of carnosine is limited due to its rapid degradation upon oral or intravenous administration by serum carnosinase [27]. Thus, the addition of carnosine moiety to UPF50 and UPF51 peptides has at least two promising goals: (a) avoiding carosinase hydrolysis and (b) enhancing the antioxidative properties of UPF50 and UPF51 in addition to the *O*-methyl-L-tyrosine moiety already present in the mentioned analogues.

In addition to important biological effects like antioxidativity, the physicochemical properties of these new GSH analogues should be determined prior to pharmaceutical applications. Knowledge of dissociation constants (pK_a) and partitioning behavior expressed as various interactions between the charged and anisotropic biological membranes and ionized potential pharmaceuticals like UPF peptides (log *k*) are of crucial importance in understanding the possible outlying mechanisms of drug transport into the cells. Nevertheless, investigation of GSH analogues is problematic due to the oxidation processes resulting in the formation of homo- and heterodimers of the mentioned peptides. Also, in the early phases of preclinical investigations, the amount of synthesized compounds like GSH analogues is relatively low, so, a method that takes into account this "drawback" should be developed. Moreover, GSH and its analogues under physiological conditions (pH 7.4) are most probably ionized, thus, not purely hydrophobic interactions but also ionic bonds and charge transfers participate in the transport of these peptides across anisotropic biological membranes. In view of the above, a fast, precise, versatile and

sensitive analysis method for the simultaneous determination of pK_a and log k is highly needed.

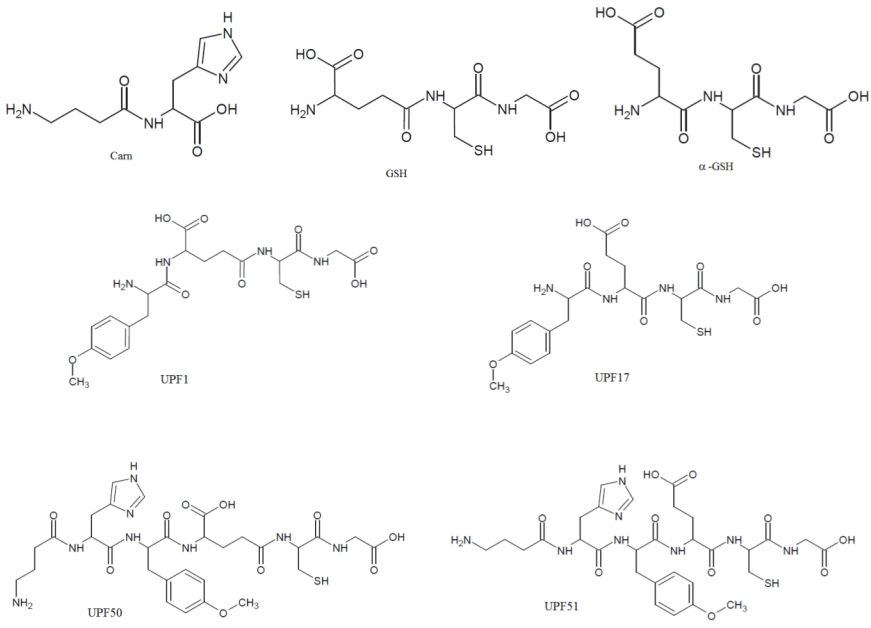

Figure 1. General structure of GSH, UPF peptides and carnosine.

1.2 Superoxide dismutase enzymes

During aerobic respiration, oxygen undergoes a series of reactions, leading sequentially to the production of a superoxide radical anion ($O_2^{\cdot -}$). In most cells degradation of the superoxide radical is under exclusive control of superoxide dismutase enzymes that catalyze the dismutation of $O_2^{\cdot -}$ into hydrogen peroxide and oxygen [28]. The function of SODs to control the level of steady-state $O_2^{\cdot -}$ is vital as superoxide radicals are strongly toxic, being a precursor to extremely oxidizing species like hydroxyl radicals: the rate constants of their reactions with many biological molecules are close to the diffusion limit. This means that the functioning of SODs in eliminating of $O_2^{\cdot -}$ is crucial for the survival of cells. Furthermore, it has been found that SODs are associated with atherosclerosis, hypertension and increased risk of ischemic heart diseases [29]. Thus, studies of superoxide dismutases to understand the activity regulation of the mentioned enzymes for future SOD-dependent therapeutic strategies are of great importance.

The SOD family consists of four enzymes according to their central metal ion (Fe, Mn, Cu/Zn, and Ni) at the active site [30]. The SOD isoforms found in mammals include CuZnSOD (cytoplasm, nucleus, extracellular matrix) and MnSOD (mitochondria matrix), which require catalytic metal (Cu or Mn) for their activation and Zn for a proper enzyme folding and stability. CuZnSOD and MnSOD are found in prokaryotic and eukaryotic organisms as well. FeSOD is

found in prokaryotes and in plants, while NiSOD is present in aerobic bacteria. Although, all SODs share similar enzymatic activity, the protein structure and metal binding sites differ for each central metal ion. However, FeSOD and MnSOD (Fig. 2) are quite similar in structure and have identical metal binding sites. Though metal up-take is non-specific and both Mn and Fe can occupy the active site of MnSOD, only the Mn form is catalytically active. Meanwhile, Cu/Zn and Ni enzymes have different structures [13, 29, 30].

The enzymatic activity of superoxide dismutases depends on the presence of the specific metal ion cofactor existing in the active site of the corresponding SOD enzyme. Understanding the effects of metal ion(s) in SOD function(s) is essential for further investigations of these enzymes [31]. Therefore, determination of metal content in SODs is of utmost importance. A simple and fast method for the separation of mixtures of metal ions, with small sample volume and low running electrolyte consumption is of considerable interest.

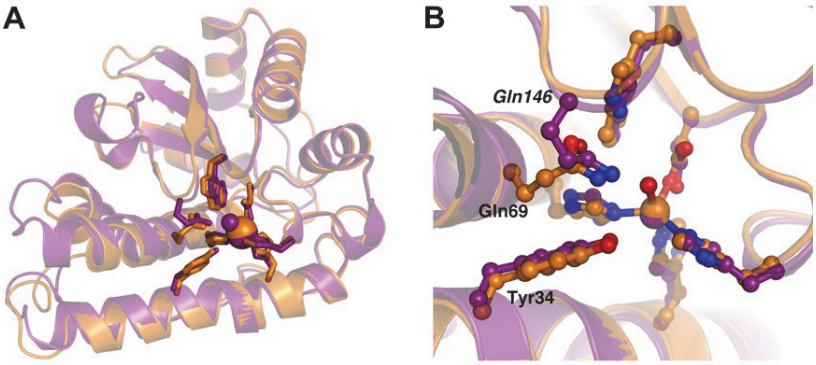

Figure 2. (A) Overlay of the backbones of *E.Coli* FeSOD (orange) and Fe-substituted *E.Coli* MnSOD (Fe(Mn)SOD), magenta) and (B): detail of the active sites of the overlaid proteins. Reproduced from Anne-Frances Miller [32].

1.3 Capillary electrophoresis in the investigation of biomolecules

The increasing demand of the pharmaceutical industry for new alternative and/or complementary analytical techniques for drug screening purposes has led to the establishment of capillary electrophoresis as an alternative separation technique that is effective for a wide spectrum of analytes and analyses. Compared to the existing chromatographic methods CE offers advantages such as high degree of automation, possibility of miniaturization and parallelization, low consumption of sample and electrolytes, minimal sample preparation procedure and rapid analysis time [33]. Nearly 15 years ago the introduction of the CE method to the Human Genome Project remarkably increased the throughput for DNA sequencing [34]. Nowadays CE is used for routine analyses in many hospitals, clinics and has many application areas in the pharmaceutical community. Numerous CE modes can be used to characterize the analytes to be separated. Capillary zone electrophoresis (CZE) is the simplest and most popular form of CE, where separation is based on the electromobility of charged

compounds (charge to size ratio) that migrate at different velocities under an applied voltage. Micellar electrokinetic chromatography (MEKC) is a hybrid of electrophoresis and chromatography that is able to separate both charged and neutral species in the same run. The separation mechanism in MEKC is based on both the electromobility and differential partitioning into a micellar pseudophase. Capillary isoelectric focusing (CIEF) is a CE mode used for the separation of amphoteric species like peptides, amino acids and proteins. In CIEF separation is pH gradient driven and is based on an isoelectric point (pI value) of analytes that under electric field start to migrate so long as they are charged until a point where they have no net charge (isoelectric point). Capillary gel electrophoresis is often used for the size- and shape-based separations of biological macromolecules like proteins, oligonucleotides and DNA. Affinity CE is an electrophoretic mode that measures specific molecular interactions of receptors, ligands or antibodies with solutes. Cyclodextrin-modified CE is demonstrated to be very sensitive and robust in thousands of examples of enantioseparations of chiral drugs [35]. Recently, such modes of capillary electrophoresis as CZE and MEKC have been also employed for the investigation of different types of antioxidants [36-38].

Various types of detectors can be interfaced to CE. These include mass spectrometry (MS), contactless conductivity (CC), laser induced fluorescence (LIF) and Ultraviolet (UV) detection methods. Recent advances in providing appropriate conditions for capillary electrophoresis-mass spectrometry interfacing remarkably increased the number of CE-MS applications in pharmaceutical applications. On the other hand, contactless conductivity detection in CE is limited yet, as more efforts are needed to provide robustness, ease of operation and suppression technology and, finally, cost-effectiveness in order to increase the potential of this detection method in the studies of drug candidates. While LIF is the most sensitive detection method, it is not desired in drug discovery and development as most analytes do not fluoresce naturally and thus require derivatization. However, systems like multiplexed CE for DNA sequencing require ultra high sensitivity and therefore use LIF detection. Many drug-like compounds contain aromatic rings or conjugated double bonds in their structures and thus absorb in the 195-254 nm UV region without the need for derivatization of molecules.

Constant developments regarding capillary electrophoresis techniques have led to the establishment of CE as a complementary or alternative separation method for drug discovery and development applications. The possibility to transform single capillary electrophoresis methods to multiplexed format allows CE to emerge as a routine analytical method in drug development.

Continuous screening and/or synthesis of thousands of compounds generate the selection of *hits*, which are then further enhanced by chemical modifications to produce so-called *leads*. These leads are then tested to possess druglikeness by various *in vivo* and *in vitro* tests for the estimation of the adsorption, distribution, metabolism and excretion properties of a compound, and for toxicological investigations. For the estimation of the passive absorption

of biochemicals across biological membranes, the knowledge of compound acid dissociation constants (pK_a values) and partitioning behavior of ionized compounds (retention of MEKC (log k)) are of utmost importance as the ionization state of these compounds affects ADME properties [39, 40].

1.4 General aspects of capillary electrophoresis

Capillary electrophoresis is a separation technique where the simultaneous separation of all solutes, regardless of charge, is achieved in narrow fused-silica capillaries filled with a conductive background electrolyte (BGE) solution under the applied voltage. Qualities like high efficiency and selectivity of separation, fast analysis time, minimal sample injection volume and ease of operation make CE an efficient and versatile approach for a wide spectrum of scientific researches.

In CE the sample is introduced into a capillary tube filled with an electrolyte solution. Under an electric field of intensity E, the analytes start to move with a characteristic migration velocity (ν_{ep}) due to the electrophoretic mobility of analytes and electro-osmotic mobility of the electrolyte solution inside the capillary:

$$\nu_{ep} = \mu_{ep} \times E \tag{1}$$

The electrophoretic mobility of an analyte (μ_{ep}) is determined by the electric charge (q), molecular size and shape (6πr coefficient) of the solute and depends on the characteristics of BGE in which migration occurs (viscosity (η), pH, ionic strength of the electrolyte solution). The solute's electrophoretic mobility is expressed as follows:

$$\mu_{ep} = \frac{q}{6\pi\eta r} \tag{2}$$

Taken together the electrophoretic velocity (ν_{ep}) of the spherically shaped solute can be given by the equation:

$$\nu_{ep} = \mu_{ep} \times E = \frac{q}{6\pi\eta r} \times \frac{V}{L} \tag{3}$$

where q is the charge of the solute, η is the viscosity of BGE, r is the Stokes radius of the solute; V is the applied voltage, L is the total capillary length.

When voltage is applied through the capillary filled with BGE, not only the solute starts to migrate with the characteristic electrophoretic velocity (ν_{ep}), but also the bulk migration of the electrolyte solution is generated, called electro-osmotic flow. In general, the surface of uncoated fused-silica-capillaries contains a large number of silanol groups (Si-OH) that become ionized at pH levels above 2-3 and negatively charged silanate (Si-O$^-$) are formed. Cations that are present in BGE are attracted to the negative Si-O$^-$ to maintain the charge balance of the capillary surface: part of these cations binds tightly to silanate ions forming a fixed layer (Stern layer), the other part of loosely bound cations

forms the mobile or diffusive layer (Gouy-Chapman layer). Together these two layers form the so-called double layer. After the application of the voltage, the solvated cations in the mobile layer start to migrate from anode to cathode, thus producing electro-osmotic flow (EOF).
The velocity of the electro-osmotic velocity (v_{eof}) can be expressed as:

$$\nu_{eof} = \mu_{ep} \times E = (\frac{\xi\varsigma}{\eta}) \times (\frac{V}{L}) \quad (4)$$

where ξ is the dielectric constant of BGE and ζ is the zeta potential of the capillary.

EOF velocity is affected by zeta potential, which in turn is determined by two factors. First, the zeta potential is directly proportional to the charge density on the capillary walls. With the increase of the pH of BGE, more silanol groups dissociate and the zeta potential as well as the velocity of EOF increases. Second, the zeta potential is proportional to the thickness of the double layer: the increased ionic strength of BGE and consequently a higher concentration of cations results in the compression of the double later, thus decreasing the zeta potential and reducing the EOF velocity.
Taken together, the solute's total velocity is the sum of its electrophoretic velocity and the velocity of the electro-osmotic flow and can be described as follows:

$$\nu_{tot} = \nu_{ep} + \nu_{eof} \quad (5)$$

and

$$\mu_{tot} = \mu_{ep} + \mu_{eof} \quad (6)$$

In normal CE (negatively charged capillary surface), anions migrate in the opposite direction with respect to the electro-osmotic flow and the velocities of anions will be smaller than the electro-osmotic velocity. At the same time, cations migrate in the same direction as the electro-osmotic flow, thus having greater velocities than the electro-osmotic velocity. If $\nu_{eof} > \nu_{ep}$, both cations and anions can be separated in the same run. Eventually, the highly charged small cations (largest charge-to-size ratios) elute first, followed by larger cations of smaller charge. Neutral species are not separated during normal CE and they elute as a single band with the elution rate corresponding to the electro-osmotic flow velocity. Finally, the smallest highly charged anions elute last with the longest migration time.
For practical applications the solute's total velocity may be expressed as:

$$\nu_{tot} = \frac{L_{eff}}{t_m} \quad (7)$$

where L_{eff} corresponds to the effective capillary length (length to detector) and

t_m is the migration time of the solute. It gives

$$\nu_{tot} = \mu_{tot} \times \frac{V}{L} = \left(\mu_{ep} + \mu_{eof}\right) \times \frac{V}{L} \quad (8)$$

Rearranging equations (7) and (8) yields

$$t_m = \frac{L_{eff} \times L}{(\mu_{ep} + \mu_{eof}) \times V} \quad (9)$$

As seen from equation (9), the solute's migration time can be decreased by applying a higher voltage (V) or by using a shorter capillary (L) [43].

1.4.1 Factors affecting the electro-osmotic flow

Electro-osmotic flow is the bulk flow of electrolyte solution in the capillary resulting from the surface charge of the double-layer at the capillary wall under the applied voltage. Electro-osmotic flow is usually beneficial; nevertheless, it needs to be controlled. In principle, the control of EOF is achieved by modification of the capillary surface charge or viscosity of BGE. Parameters that affect the surface charge of the wall also affect the solute properties (like pH of BGE). Conditions that optimize both the velocity of EOF and mobility of the solute are required for successful separations.

At low or moderate pH the small negative charge density of the capillary wall causes adsorption of cationic solutes via Coulombic interactions. When pH is high, the EOF velocity may be too high, thus resulting in the elution of analytes before separation has occurred. Adjusting the pH of the electrolyte solution, which also affects the solute charge and therefore its mobility, can make the most remarkable changes in EOF. When lowering the pH of BGE, protonation of the acidic solute and the surface of the capillary wall will occur, while the high pH of BGE will result in deprotonation of both the solute and capillary surface. Knowledge of the solute's dissociation constant(s) is therefore of utmost importance in selecting the right pH range of the running BGE. Additionally, lowering the voltage can decrease the velocity of EOF as well, though at the expense of prolonged analysis time.

EOF can also be adjusted by changing the ionic strength and/or concentration of BGE. The higher concentration of BGE will result in a decreased effective charge at the wall, thus limiting Coulombic interactions of the solute with the capillary surface. At the same time, high concentrations of BGE induce the current increase, leading to Joule heating, while buffer capacity decreases with lowering the BGE's ionic strength. The instrumentally controlled temperature changes the viscosity of the separation medium: with increasing temperature the viscosity decreases, resulting in the EOF increase. Different organic modifiers (isopropanol, ethanol, acetonitrile) affect the viscosity of BGE and also the zeta potential of the capillary surface.

Lastly, buffer additives like surfactants modify the capillary wall by the means of dynamic coatings. Use of these coatings increases, decreases or reverses the surface charge of the capillary and thus the EOF [41, 42].

1.5 Determination of acid dissociation constants of UPF peptides by CE

Traditionally, the established method for pK_a determination has been titration with either potentiometric or UV spectral detection. However, these methods have disadvantages and limitations, namely the relatively large amounts of stable high-purity water-soluble compounds and preparation of carbonate free solutions for measurements at neutral to high pH for potentiometric titrations. If UV detection is employed, then the compound must have a chromophore and the UV absorbance of that compound needs to change as a function of ionization. Like in potentiometric detection, the UV detection also requires compounds of high purity, but if impurities are still present, then they shall not interfere with spectroscopic measurements. In the early phases of drug discovery and developments, newly synthesized compounds have relatively low purity. Therefore, use of titration methods is limited due to the mentioned drawbacks [43].

Recently, capillary electrophoresis became an alternative method for the pK_a measurement. The determination of acid dissociation constants by capillary electrophoresis is based on the measurement of variation of migration times of the analyte as a function of pH of the background electrolyte of a constant ionic strength. As can be seen from Fig. 3, the fitting of effective mobilities as a function of pH also provides information about the charge distribution and ionization profile of an analyte over a wide pH range, thus aiding in the understanding of possible pH-dependent transport mechanisms.

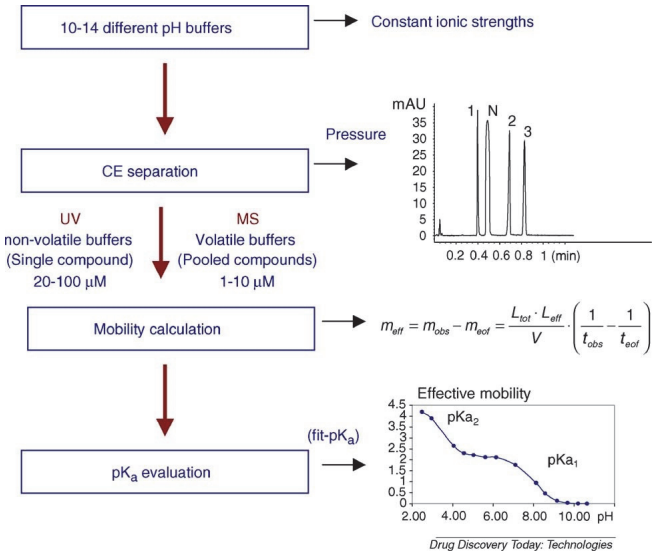

Figure 3. Schematic work flow of pK_a screening by CE-UV and CE-MS.
m_{eff} is the effective mobility of the compound; N is a neutral marker (DMSO); 1 and 2 are basic and acidic compounds separated from the neutral marker. (Reproduced from Hong Wan, Thompson, R.A.) [44].

The advantages of CE over other methods are the following [45]:

(1) impurities of the sample do not disturb pK_a measurements as CE is a separation method;

(2) use of automated CE instruments;

(3) as only mobilities of compounds are used in calculations, knowledge of an exact concentration of compounds is not necessary;

(4) low sample and background electrolyte consumption;

(5) absence of special purity demands for BGE solutions;

(6) ability to determine pK_a values of sparingly soluble compounds (with suitable chromophore(s)).

Due to the above-listed advantages over traditional titration methods CE has been gaining popularity within pharmaceutical community. Several research groups have demonstrated medium- to high-throughput screening of pK_a values of pharmaceuticals by using capillary electrophoresis with UV or MS detection [44, 46].

Experimentally, pK_a values are measured on the basis of migration times of analytes and the neutral marker in the background electrolyte of constant ionic strength at a given temperature and by varying pH over a certain range.

The effective mobility (μ_{eff}) of an ion is calculated as follows:

$$\mu_{eff} = \frac{L \times L_{eff}}{V} \left(\frac{1}{t_{app}} - \frac{1}{t_{eof}} \right) \quad (10)$$

where t_{app} is the apparent migration time of the analyte, t_{eof} is the migration time of the neutral marker .

From the relationship between the calculated effective mobilities and the pH of the electrolyte, a sigmoid-shaped titration curve (Eq. (11)) is obtained, where the inflection point(s) corresponds to the pK_a value(s) of the analyte:

$$\mu_{eff} = \frac{\mu_{A^-}}{1 + 10^{(pH - pK_a)}} \quad (11)$$

The curve can be fitted with the nonlinear regression model where two unknowns – the mobility of the fully ionized species (μ_{A^-}) and pK_a (depends on the number of the ionizable groups) are regression parameters [39, 47].

1.6 Determination of retention factors of UPF peptides by MEKC

In micellar electrokinetic chromatography separation of charged and neutral solutes takes place in a BGE solution that contains added surfactant molecules, which above their critical micelle concentration (CMC) form aggregates called micelles. The solute molecules are distributed according to their partition coefficients between the aqueous BGE and micelles that constitute the pseudo-stationary phase (PSP). Therefore, MEKC is considered a hybrid of electrophoresis and chromatography. If analytes are charged, the migration velocity depends on both the partition coefficient of the analytes between the

micelles and the aqueous BGE and on the electrophoretic mobility if no micelles are present. Neutral analytes do not have electrophoretic velocity; therefore the migration velocity depends only on the partition coefficient between micelles and aqueous BGE [48].

There are a number of surfactants used in MEKC, anionic sodium dodecyl sulfate (SDS) being the most widely employed surfactant to generate micelles as it has several advantages, such as high solubilization capability, low UV absorbance and easy availability. Another popular surfactant used in MEKC is cationic cetyltrimethylammonium bromide (CTAB) that adsorbs on the capillary wall and reverses the direction of EOF. Along with these conventional surfactants, ionic liquid (IL) type surfactants, namely alkylimidazolium-based ILs, are gaining popularity as PSPs in MEKC [49, 50]. In general, IL is a salt that is liquid below 100 °C. The most remarkable properties of ILs are negligible vapor pressure, miscibility with water and many organic solvents, as well as prominent catalytic properties. Analysis of the structure-activity relationship of a typical imidazolium IL showed that ILs possess surface active properties that are similar to those of surfactants and, as a result, in aqueous solution micelles are formed. This property makes ILs a possible new class of surface-active agents that have the properties of classical cationic surfactants (ability to reverse the direction of EOF). Compared to traditional PSPs, IL-type surfactants with alkyl chains longer than four behave as amphiphilic compounds that offer versatile interaction types like electrostatic, ion–dipole, π-π, van der Waals, hydrogen-bonding interactions with the imidazolium cation head and hydrophobic interactions because of the long alkyl tail [51].

In general, approximately 90% of drugs is considered to be chargeable under physiological conditions [33]; thus not only hydrophobic interactions but also ionic bonds and charge transfers constitute to diverse interactions between biomembranes and ionized compounds like UPF peptides. The partition coefficients rationalized in terms of retention factors (k) of ionized compounds are described as a ratio of how long a compound interacts with PSP to retention in BGE. Possible ways to measure the partition coefficients of ionized compounds by CE modes involve using artificial membranes, i.e. liposomes [52], vesicles [53], immobilized artificial membranes (IAM) [54], microemulsions [55] and micelles [56]. The preparation of liposomes, vesicles, IAMs, and microemulsions that are used to monitor the partition coefficients of ionized compounds is tedious and time-consuming. On the other hand, the use of micelles in MEKC allows an optimal modeling of intermolecular interactions present in biological systems by a simple change of the surfactant type of the micellar pseudo-stationary phase (PSP). Moreover, the use of micelles is cost-effective compared to artificial membranes. For amphoteric compounds like UPF peptides the overall retention factor is the weighted sum of the retention factors of all species present [49]. The UPF peptides can interact with positively charged micelles (C_{14}MImCl and CTAB) by electrostatic interaction due to the negative net charges acquired by dissociation and possible complexation (borate buffer, pH 8.2). As seen from the equations in Supporting Information Table S1, the described dissociation (Eq. 1a), possible complexation (Eqs. 1b–c) and

association (Eqs. 1d–g) equilibria have to be considered in the overall retention factor determination of UPF peptides. It can be predicted that for cationic micelles (C_{14}MImCl, CTAB) and negatively charged UPF peptides a strong electrostatic interaction takes place and an electrostatic repulsion is expected to occur with anionic micelles (SDS). The impact of equilibria described by Eqs. 1(f)–(g) (Appendix 1) is negligible as the possible complexation of UPF peptides with a tetrahyhydroxyborate anion is considered to be very low, due to the absence of vicinal hydroxyl groups. Additionally, SDS as a negatively charged micelle-forming surfactant with borate buffer (pH 8.2, I = 35 mM) was used to determine the retention factors of negatively charged peptides. Thus, it is expected that $k_{(BP)^-}$ and $k_{(BP\text{–}O^-)^{2-}}$ will be very small (Appendix 1).
To calculate the retention factors of UPF peptides the following equation can be employed [49, 57]:

$$\mu = \frac{1}{k+1}\mu_{eff} + \frac{k}{1+k}\mu_{mc} \qquad (12)$$

where μ is the pseudoeffective electrophoretic mobility of the UPF peptide in micellar BGE, k is the overall retention factor of the UPF peptide, μ_{eff} is the effective electrophoretic mobility of the UPF peptide in micelle-free BGE and μ_{mc} is the electrophoretic mobility of micelles in micellar BGE. From Eq. (12) the following expression can be derived, which allows calculation of the true retention factor k in MEKC from the mobilities μ, μ_{eff}, and μ_{mc} :

$$k = \frac{\mu - \mu_{eff}}{\mu_{mc} - \mu} \qquad (13)$$

The mentioned mobilities have to be determined in separate measurements: μ and μ_{mc} are determined in the presence of micelles (MEKC condition) and μ_{eff} is determined in the absence of the surfactant (CZE condition).

1.7 Determination of metal ions in SODs by CE

Metal ions present in superoxide dismutases ensure SOD enzyme activity, which in turn depends on effective metal ion acquisition and the degree of metalation. Determination of metal ions is crucial in order to characterize enzyme ability to scavenge superoxide radicals. Additionally, metal ion content of cellular metalloenzymes like SODs may be a reflection of general metal ion availability in biological systems. Having knowledge of metal ion content in order to get more insights into how these SOD enzymes are regulated in living organisms may be important for superoxide dismutase engineering and design as possible pharmaceuticals [58].

Currently, there are several methods to measure the metal content in proteins. The most common ones are graphite furnace or flame atomic absorption spectrophotometry (GFAAS or FAAS), which, however, can only measure one element at a time. Quantitative determination of metals in proteins can also be achieved by using inductively coupled plasma (ICP). ICP connected with atomic emission spectrometer (ICP-AES) allows sensitive multielement

detection. ICP-MS, especially hyphenated with multi-dimensional capillary and nanoflow HPLC, offers highly sensitive element analysis [59, 60]. However, all types of ICP equipment require high operational cost and therefore routine analysis is prohibited in most laboratories.

Compared to these techniques, CE is a fast and simple method that has advantages such as high separation ability of mixtures of ions, small sample and BGE consumption and ease of automation [61]. CE has been extensively used for the determination of metal ions in different matrices [62, 63].

In general, there are two possible ways to measure metals by CE. Pre-column complexation, where an excess of ligand is added to the sample to ensure the complete complex formation is one method. As the complexes formed before injection may dissociate during CE run, it is necessary to add ligand to BGE to ensure the stability of the complexes [64].

Another, simpler approach is on-column complexation, which allows direct injection of sample into capillary where a rapid complexation reaction between metal ions and ligand(s) occurs [65]. On-column complexation of metal ions with direct UV detection is possible when using 2, 6-pyridinedicarboxylic acid (PDC) as a ligand that chelates metal ions producing anionic complexes which are then separated under an anionic separation mode. In order to get a fast CE separation of anionic metal complexes, addition of a cationic surfactant is necessary. Although, many surfactants like cetyltrimethylammonium bromide (CTAB), tertadecyltrimethylammoium bromide (TTAB), tetramethylammonium hydroxide (TMAH), have already been used to analyze metal complexes, no baseline separation between $Cu^{2+}$and Zn^{2+} (present in CuZnSOD simultaneously) was achieved [66, 67]. Nowadays ionic liquids have numerous chemical applications by various analytical techniques, including HPLC, GC, and MS [68-71]. ILs have been also used as BGE additives in CE for the analysis of different samples [74, 75.] Once again, an imidazolium based ionic liquid (IL), 1-tetradecyl-3-methylimidazolium chloride (C_{14}MImCl), which has a long alkyl chain on the cation, may be also used as an additive in BGE to reverse the direction of EOF (dynamic coating of the capillary wall) and thus, the detection of the chelated metals will be performed in a reverse polarity separation mode.

2 EXPERIMENTAL

2.1 Reagents

All chemicals and reagents were of analytical grade and were used as received. Milli-Q water (Milli-Q, Millipore S. A. Molsheim, France) was used for the preparation of all standard solutions, preparation of BGEs, dilution of SOD samples, preparation and dilution of stock solutions of GSH, UPF1, UPF17, UPF50 and UPF51. All stock solutions were stored at −18 °C. Peptides GSH and GSSG were obtained from Sigma-Aldrich (Steinheim, Germany).

Background electrolytes: disodium hydrogen phosphate, sodium dihydrogen phosphate, 2-(cyclohexylamino)ethanesulfonic acid (CHES), 3-morpholinopropane-1-sulfonic acid (MOPS), 2-[[1,3-dihydroxy-2-(hydroxymethyl)propan-2-yl] amino] ethanesulfonic acid (TES), 2-[4-(2-hydroxyethyl)piperazin-1-yl]ethanesulfonic acid (HEPES), sodium dodecyl sulfate, cetyltrimethylammonium bromide, ammonium acetate, 2,5-dihydroxybensoic acid (used as the MALDI matrix), hydrogen peroxide were obtained from Sigma-Aldrich (Steinheim, Germany) and 1-tetradecyl-3-methylimidazoilum chloride (C_{14}MImCl) was supplied by IoLiTec Ionic Liquids Technologies (Heilbronn, Germany). Pyridine-2,6-dicarboxylic acid was from Merck (Darmstadt, Germany). Sodium hydroxide, boric acid, hydrochloric acid, phosphoric acid and acetic acid were purchased from Riedel-de Haën (Germany).

Buffers for CE procedures:

Publication I: $B(OH)_3/B(OH)_4^-$ (pK_a = 9.24, pH = 8.45–10.00), $H_2PO_4^-/HPO_4^{2-}$ (pK_a = 7.21, pH 7.40–8.20), CH_3COOH/CH_3COO^- (pK_a = 4.76, pH 6.10–5.50), CHES/CHES$^-$ (pK_a = 9.39, pH 8.45–10.00), TES/TES$^-$ (pK_a = 7.55, pH 7.80–8.45), MOPS/MOPS$^-$ (pK_a = 7.18, pH 7.40–7.80) buffers were used in concentrations from 50 to 200 mM with pH adjusted to the respective pH level by 1 M sodium hydroxide or 1 M ammonium hydroxide. For determination of the pK_a of GSH analogues, the ionic strength of buffers was held constant and equal to 50 mM.

Publication II: Buffers used in the experiments were $H_2PO_4^-/HPO_4^{2-}$ (stock 100 mM, pH 7.4 and 8.2), $B(OH)_3/B(OH)_4^-$ (stock 500 mM, pH 8.2), MOPS/MOPS$^-$, TES/TES$^-$, HEPES/HEPES$^-$ (stock 500 mM, pH 7.4). The pH of solutions was adjusted to the respective pH level by 1 M sodium hydroxide, 1 M phosphoric acid or 1 M hydrochloric acid.

Micellar BGEs were: (i) phosphate buffer (pH 7.4) containing 10, 20, 30, 36, 50 or 60 mM C_{14}MImCl; or (ii) phosphate buffer (pH 7.4) containing 10, 20, 30, 36, 50 or 60 mM CTAB; or (iii) phosphate buffer (pH 8.2) containing 10, 20, 30, 36, 50 or 60 mM C_{14}MImCl: or (iv) borate buffer (pH 8.2) containing 10, 20, 30, 36, 50 or 60 mM SDS. Despite the different buffer compositions employed in CZE/MEKC experiments, the ionic strength (I) of all buffers was held constant and equal to 35 mM.

Publication III: Micellar BGEs used were 5, 10, 15, 20, 25, 30, 35 and 45 mM

phosphate buffers, each containing 30, 36, 38, 40, 45, 50, 55, and 60 mM C_{14}MImCl (pH 7.4).

Publication IV: BGEs used were 5−20 mM PDC and 1 mM C_{14}MImCl at pH 3.6−5.0. Real sample analysis was carried out with an optimized BGE containing 10 mM PDC and 1 mM C_{14}MImCl at pH 3.8.

All BGEs were freshly prepared and filtered through a 0.45 μm membrane filter (Millipore, Bedford, MA, USA) and stored at 8 °C until used, except ammonium acetate that was made freshly just before analysis.

Neutral markers: mesityl oxide, benzene, acetone, dimethyl sulfoxide (DMSO), *N*, *N*-dimethylformamide (DMF) were obtained from Lachema (Brno, Czech Republic).

Micellar markers: dodecanophenone, α-tocopherol, vitamin K1 and dodecylbenzene were purchased from Sigma-Aldrich (Steinheim, Germany).

2.2 Standard solutions and sample preparation

2.2.1 UPF peptides

All Fmoc-L-amino acids were purchased from Novabiochem (Merck-Millipore, Hohenbrunn, Germany), except Fmoc-L-Tyr(Me)-OH, which was sourced from CBL Patras (Patras, Greece). All the other reagents used to synthesize peptides were purchased from Merck Chemicals (Merck-Millipore). Peptides UPF1 (Tyr(Me)-γ-Glu-Cys-Gly), UPF17 (Tyr(Me)-α-Glu-Cys-Gly), UPF50 (β-Ala-His-Tyr(Me)-γ-Glu-Cys-Gly), and UPF51 (β-Ala-His-Tyr(Me)-α-Glu-Cys-Gly) were synthesized on a Fmoc-Gly-Wang resin obtained from Novabiochem (Merck-Millipore), utilizing a standard Fmoc solid-phase peptide synthesis [25]. In order to enhance the antioxidant properties and bioavailability of GSH analogues UPF1 and UPF17, two novel analogues with additional carnosine (β-Ala-His) dipeptides in the N-termini of the peptides were designed. These were named UPF50 and UPF51, respectively (Fig. 1). An aqueous solution of each peptide (including GSH and GSSG) was prepared at a concentration of 1 mM. For CE analysis a mixture of peptides (Publication I, each peptide's concentration 200 μM) was injected into the capillary and individually at a concentration of 200 μM (Publication II).

2.2.2 SOD samples

The analyzed protein samples included bovine CuZnSOD, *Escherichia coli* FeSOD and *Caenorhabditis elegans* MnSOD, all of which were purified to more than 95% purity based on SDS-PAGE analysis. The bovine CuZnSOD was kindly provided by Prof. J.V. Bannister (Cranfield University, Bedford, England). The lyophilized bovine CuZnSOD was resuspended in 10 mM potassium phosphate buffer (pH 7.8) at a concentration of 5 mg/mL. The *E.coli* FeSOD protein was purified as previously described by Hunter et al. [73]. The Fe-substituted *C.elegans* MnSOD was prepared by culturing *E.coli* OX326A cells (SOD deficient) harboring the pTrc99-sod-3 vector in defined media composed of M9 salts (2.4 g/L Na_2HPO_4, 1.2 g/L KH_2PO_4, 0.4 g/L NH_4Cl, 0.2 g/L NaCl,

1.2 mg/L $CaCl_2$), 1 mM $MgCl_2$, 0.2% (w/v) fructose, $5x10^{-5}$ % (w/v) thiamine, 1% (w/v) casamino acids in deionized water. This defined medium was supplemented with 20 mg/mL ampicillin and 200 μM $FeSO_4$ as appropriate. All solutions were made using Amberlite-treated water to reduce the amount of manganese present. The expressed protein was also purified by the technique described by Trinh et al. [74].

The lyophilized bovine CuZnSOD was resuspended in 10 mM potassium phosphate buffer (pH 7.8) at a concentration of 5 mg/mL. The *E.coli* FeSOD was resuspended in 10 mM Tris buffer (pH 7.8) at a concentration of 1 mg/mL. The *C.elegans* MnSODs were resuspended in 10 mM KH_2PO_4/K_2HPO_4 buffer (pH 7.8) at a concentration of 8.1 mg/mL and Fe-substituted MnSOD at 2 mg/mL.

For CE analysis of metals the SOD stocks were (0.44–1.62 mg, 200–976 μL) freeze-dried at 0.040 mbar which corresponds to -50 °C. The residues were resuspended in 35% HCl (1:1) and the hydrolysis was performed overnight at 100 °C. Then hydrogen peroxide was added (1:1) and the mixture was incubated for 5 h at 85 °C in a water bath. Finally, the mixture was dried under reduced pressure and then dissolved in an appropriate amount of Milli-Q water (100–200 μL).

For AAS analysis nitric acid (65%) of ”suprapure“ grade (Sigma-Aldrich, USA) was used for protein sample (1 mL) digestion. Metals were extracted from the samples with concentrated nitric acid (1:1) in the water bath at 85 °C for 120 min. After cooling down the samples were diluted with Milli-Q water at least five times.

2.2.3 Metal standard solutions

For CE procedures the standard metal solutions were prepared by dissolving appropriate amounts of metal sulfate or chloride salts in deionized water (Milli-Q, Millipore, USA, resistivity >18 MΩ·cm) at a final concentration of 500 μg/mL and then filtered through a 0.45-μm-membrane filter before use.

For AAS procedures the stock atomic spectroscopy standard solutions (1000 mg/L) of Fe, Mn, Cu and Zn were purchased from Fluka (Switzerland). Multielement Quality Control Standard 26 (high-purity standards, Charleston, USA) was gradually diluted with 4% nitric acid solution before use.

2.3 Instrumentation

All CE experiments were performed on an Agilent 3D instrument (Agilent technologies, Waldbronn, Germany) equipped with a UV/Vis DAD detector. A fused-silica capillary (Polymicro Technologies, Phoenix, USA) with an internal diameter of 50 μm (Publications I−III) or 75 μm (Publication IV) and a length of 51.5/60 cm (L_{eff}/L_{tot} , effective capillary length (length to detector) / total capillary length, respectively) was used in the experiments. The separation voltage was set to +20/+25 kV (Publication I), -10 kV (Publication II), -5, -10 and -15 kV (Publication III) and -20 kV (Publication IV). The injection pressure was set to 50 mbar for 10 s (Publications I-III) and for 6 s (Publication IV). The

temperature of the capillary was kept at 25 °C (Publications I–III) and 30 °C (Publication IV). The analytes were detected at various wavelengths depending on the UV absorption spectra (195−230 nm). All the electropherograms were recorded and integrated with Agilent ChemStation software.
The pH value of the electrolyte solutions was measured with a Metrohm 744 pH Meter equipped with a combination electrode (Metrohm, Herisau, Switzerland) that had been calibrated with commercial buffers at pH 7.00 (± 0.01) and 10.00 (± 0.01) (Sigma–Aldrich).
MALDI-TOF-MS analysis was carried out in the delayed extraction (20–100 ns) positive-ion reflection mode on a Bruker Autoflex II mass spectrometer (Bruker Daltonics, Denmark) equipped with a nitrogen laser (337 nm). The laser power was set to obtain a good S/N (approx. 50%), and the mass range of 250–1650 *m*/*z* was scanned.
The concentration of SODs was measured using Varian Cary 50 Bio UV/Visible Spectrophotometer (McKinley Scientific, USA).
The protein samples (SODs) were lyophilized using Christ Alpha 1-2 LDplus (Fisher Bioblock Scientific, Illkirch, France). Hydrolyzed mixture of SODs was dried under vacuum at 85 °C by using the Heidolph rotary evaporator (Nuremberg, Germany).
A Spectra AA 220F flame atomic absorption spectrometer (Varian, Mulgrave, Australia) equipped with a deuterium lamp for background correction was used. Acetylene of 99.99% purity (AGA, Helsinki, Finland) was used as the fuel gas.
A Spectra AA 220Z atomic absorption spectrometer (Varian, Mulgrave, Australia) equipped with a side-heated GTA-110Z graphite atomizer, a Zeeman-effect background correction and an integrated autosampler was used. Graphite tubes with coating and platforms made of pyrolytic graphite were used throughout the work. Argon of 99.99% purity (AGA, Helsinki, Finland) was used as the purge gas.

2.3.1 Capillary conditioning

New capillaries were conditioned by flushing them first with 1 M NaOH solution for 30 min, then with Milli-Q water for 15 min and finally with a BGE solution for 5 min. Between the runs the capillary was rinsed using different procedures for every experiment:
Publication I: with 1 M NaOH for 5 min, with Milli-Q for 3 min, with BGE for5 min;
Publications II, III: with 1 M NaOH for 2 min, with Milli-Q for 2 min, with MeOH for 2 min, with BGE for 5 min;
Publication IV: with MilliQ for 2 min, with BGE for 5 min.

3 RESULTS AND DISCUSSION

3.1 Separation of GSH and its analogues by CE (Publication I)

The separability of peptides was inspected in the pH range from 5.50 to 10.00 and the results were in agreement with the rule of thumb, which states that the separation of peptides is most likely to be achieved in BGEs of pH around the pK_a values of analytes. The pK_a values of the peptides under study were expected to be around 9, according to that of the reduced GSH. Two buffer types (inorganic and zwitterionic, Table 1) were tested for the simultaneous separation and identification of two mixtures of peptides: (a) UPF1+UPF50+GSH (and their homo- and heterodimers), (b) UPF17+UPF51+GSH (and their homo- and heterodimers). The separation of UPF1, UPF17, UPF50 and UPF51 as well as the mixture of their homo- and heterodimers was not achieved because of the same molecular weight of the analytes.

3.1.1 Inorganic buffers

At first the separation of both mixtures consisting of GSH and UPF peptides and their homo- and heterodimers was performed using 50 mM phosphate buffers (pH 7.40, 7.80 and 8.20), but no baseline separation of peptides was achieved. Next, boric acid at different concentrations (50–250 mM) and pH values (7.40–10.00) was investigated to improve separation selectivity. With increasing borate concentration, the migration times of peptides increased and resolution improved as well. At higher boric acid concentrations (≥250 mM) and pH values (>9), the heat dissipation was insufficient, resulting in destabilized current and corrupted signal due to the baseline fluctuation. On the other hand, when the boric acid concentration was lower than 200 mM, the heat dissipation problem was solved even at high pH values. However, the separation of some peptides was poor with no baseline separation achieved. As seen from Fig. 4, the boric acid concentration of 200 mM with pH 8.45 was optimal for the separation of the peptide mixture (b) (UPF17+UPF51+GSH). The total selectivity decreased and the baseline separation of some peaks was not achieved when pH values higher or lower than the optimal pH of 8.45 were used. As also seen from Fig. 4, peak intensities increased with pH 7.40 (Fig. 4B) contrary to those when pH was 8.45 (Fig. 4A) since the CE analysis of the peptide mixture (b) with pH values 8.45 and 7.40 was performed at different times, the formation of homo- and heterodimers increased in time.

The migration order of peptides (Fig. 4A*,* pH 8.45*)* was as follows: UPF51, UPF51 homodimer, UPF51–GSH heterodimer, UPF51–UPF17 heterodimer, GSH, GSSG, UPF17, UPF17–GSH heterodimer, with the last migrating species being the UPF17 homodimer. When compared to the migration order of peptides with pH 7.40, (Fig. 4B), that of UPF51 and UPF17 heterodimer, GSH, UPF17 and GSSG peptides had changed, indicating that the

migration behavior depended not only on the pK_a value, but also on the possible specific interactions between the peptides and the borate BGE [75].

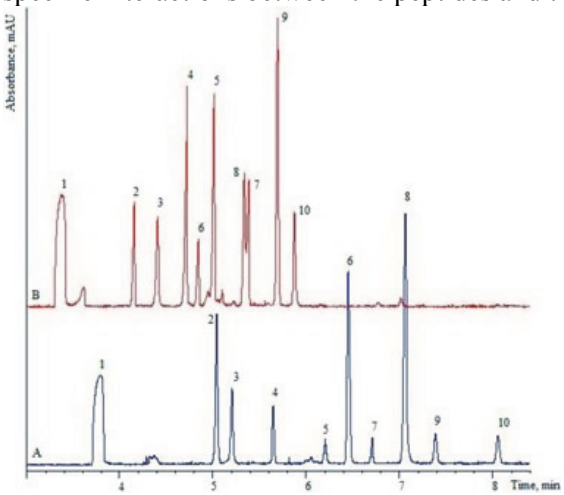

Figure 4. Electropherograms of UPF51, UPF17 and GSH and their homo- and heterodimers at different pH values.
CE conditions: 200 mM boric acid as BGE, capillary length 60 cm (51.5 cm to detector), detection at 195 nm, capillary temperature 25 °C, injection pressure 50 mbar for 10 s, applied voltage 25 kV. (A) pH 8.45 and (B) pH 7.40.
Peak identification: 1 DMF, 2 UPF51, 3 UPF51 homodimer, 4 UPF51−GSH heterodimer, 5 UPF51−UPF17 heterodimer, 6 GSH, 7 GSSG, 8 UPF17, 9 UPF17−GSH heterodimer, 10 UPF17 homodimer.

3.1.2 Zwitterionic buffers

Zwitterionic buffers (CHES, TES, MOPS) with a concentration range from 50 to 200 mM and pH indicated in Table 1 were also tested for the separation of a mixture consisting of UPF1/17, UPF50/51 and GSH peptides.

Table 1. Composition of buffers

pH range covered	Buffer constituents	pK_a [a)]
8.45−10.00	$B(OH)_3/B(OH)_4^-$	9.24
7.40−8.20	$H_2PO_4^-/HPO_4^{2-}$	7.21
5.50−6.10	CH_3COOH/CH_3COO^-	4.76
8.45−10.00	$CHES/CHES^-$	9.39
7.80−8.45	TES/TES^-	7.55
7.40−7.80	$MOPS/MOPS^-$	7.18

[a)] pK_a values from Goldberg, R.N., et al. [76]

$CHES/CHES^-$ (pK_a 9.39) and $B(OH)_3/B(OH)_4^-$ (pK_a 9.24) buffers were tested for the ability to separate the mixture of peptides (a) (b) by varying the buffer concentration from 50 to 200 mM and pH from 8.45 to 10.00 and the obtained results were compared. It was estimated that the optimal pH for the separation of peptides was the same (pH 8.45) for both the CHES and borate buffers. The selectivities remained in the range of 1.02–1.27 with CHES and borate buffers

with fixed pH of 8.45 with no significant differences in selectivities noted between the buffers of different concentrations (50–200 mM). The CHES buffer had a slightly higher selectivity at 50 mM and the borate buffer at 200 mM, though. The number of theoretical plates for CHES and borate buffers (50–200 mM, pH 8.45) was also calculated: the average efficiency turned to be more than one million.

The migration order of peptides (CHES buffer at pH 8.45) was as follows: UPF51 peptide, UPF51 homodimer, UPF51–GSH heterodimer, GSH, UPF51–UPF17 heterodimer, GSSG, UPF17, UPF17–GSH heterodimer, the last migrating species being the UPF17 homodimer (Fig. 5A). Compared to the borate buffer at the same pH of 8.45, the migration order of GSH and UPF51–UPF17 heterodimer had changed.

The TES buffer at pH 8.45 (50 mM) was also tested and the migration order of the analytes was similar to that in case of the CHES buffer at the same pH of 8.45 (50 mM). Compared to pH of 8.45, at pH 7.80 (TES, 50 mM) the migration order of UPF17 and GSSG had changed, though (Fig. 5B). The migration order variations could also be observed when 50 mM CHES buffer was used at different pH values (e.g. 8.45, 8.70 and 9.55). These variations are probably due to the differences in the distribution order of pK_a values of individual ionogenic groups between GSH and UPF51–UPF17 heterodimer and UPF17 and GSSG. The MOPS buffer showed analogous results. The same procedures were performed with the mixture (a) of (UPF50, UPF1 and GSH) peptides and the results were in accordance with those obtained with other buffers.

Altogether, an inorganic buffer such as borate and zwitterionic buffers like CHES, TES and MOPS showed good separability within the pH range from 7.40 to 9.05. Thus, they can be used in separation of the mixture consisting of UPF1/17, UPF50/51 and GSH peptides as well as their homo- and heterodimers. The borate buffer may be preferred for separation of the above-mentioned peptides because of the higher transparency of boric acid in the UV light compared to zwitterionic buffers.

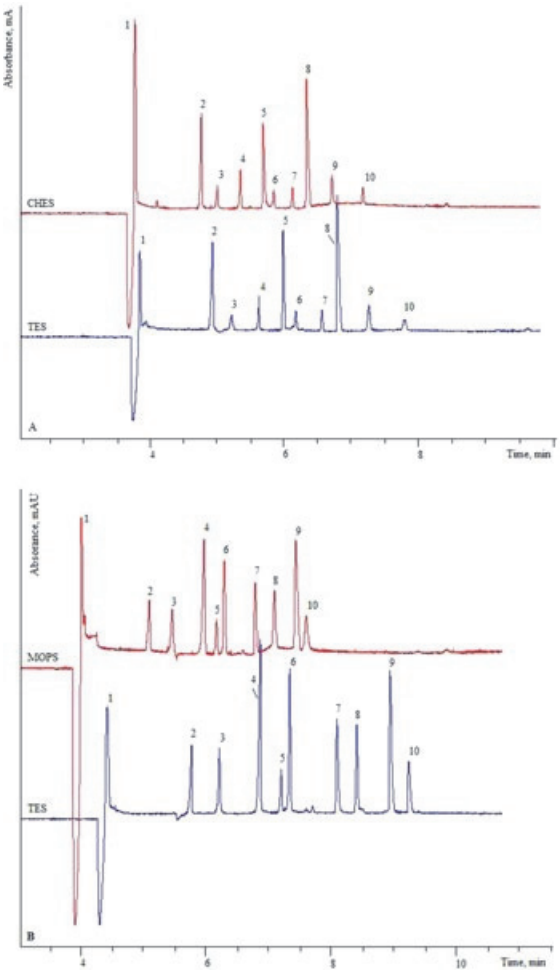

Figure 5. Separation of peptides using CHES, TES and MOPS buffers.
CE conditions: ionic strength 50 mM, other conditions as in Fig. 4. (A) CHES, TES buffers at pH 8.45, (B) TES and MOPS buffers at pH 7.80.
Peak identification: (A) 1 DMF, 2 UPF51, 3 UPF51 homodimer, 4 UPF51—GSH heterodimer, 5 GSH, 6 UPF51–UPF17 heterodimer, 7 GSSG, 8 UPF17, 9 UPF17–GSH heterodimer, 10 UPF17 homodimer.
Peak identification: (B) same as (A) with the exception of 7: UPF17, 8: GSSG.

3.1.3 Identification of peptides in a mixture

The peaks of peptides in each electropherogram (Figs. 4, 5) were identified using the standard addition method and comparing their UV spectra. First, the solution of the corresponding individual peptide was kept at room temperature for 24 h in order to allow peptide to dimerize (oxidize) (confirmed by MALDI-TOF-MS). The CE separation of this dimerized (oxidized) sample was carried out resulting in an electropherogram with one peak corresponding to the homodimer. Then this homodimer's electropherogram was compared with that of the unoxidized standard that had two peaks, one corresponding to the reduced form of the peptide and the other to its oxidized form (homodimer).

Similarly, the solution of two different peptides was allowed to form homo- and heterodimers for 24 h at room temperature. The combinations of pairs were as follows: UPF51+UPF17, UPF51+GSH, UPF17+GSH and UPF50+UPF1, UPF50+GSH, UPF1+GSH. The CE separation of the mixture of two peptides resulted in five peaks on the electropherogram whose two peaks corresponded to the reduced form of peptides, two to their oxidized forms – homodimers, and one extra peak was associated with the corresponding mixed dimer–heterodimer (also confirmed by MALDI-TOF-MS). The peptide mixture (b) consisting of UPF51, GSH and UPF17 was made and kept at room temperature for 24 h in order to let homo- and heterodimers form. Then the reaction mixture (b) was subjected to MALDI-TOF-MS analysis and the mass spectra of the oxidation reaction products of the mixture of UPF51, GSH and UPF17 were obtained (Fig. 6). Shortly, the CE separation was carried out with the same mixture and the electropherogram obtained once again showed five peaks, two belonging to homodimers and three to heterodimers, the reduced forms were absent, which meant that the peptides were completely oxidized. The same procedures were performed with the mixture (a) and the results obtained were in agreement with the above.

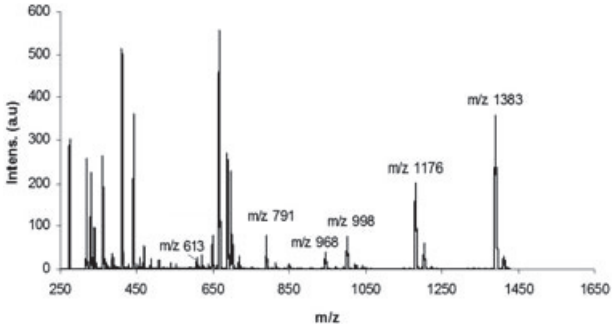

Figure 6. Mass spectra of the oxidation reaction products of the mixture of UPF51, GSH and UPF17. GSSG 613 Da, GSH–UPF17 heterodimer 791 Da, UPF17 homodimer 968 Da, GSH–UPF51 heterodimer 998 Da, UPF51–UPF17 heterodimer 1176 Da, UPF51 homodimer 1383 Da.

3.2 Determination of acidity constants of GSH and its analogues by CE (Publication I)

Since it is known that most biological reactions take place at or near neutral/basic pH between 6 and 8, it was decided to measure the pK_a values of imidazolyl, thiol (if present in the molecule) and/or amino groups.

Generally, in order to measure the pK_a value of an unknown substance, it is necessary to cover a wide pH range. In this work, we employed buffers that covered the pH range from 5.50 to 10.00 (Table 1).

As shown above, the baseline separation was achieved in the pH range of 7–9. Generally it allowed the peptides UPF1/17, UPF50/51 and GSH to be injected as a mixture. If baseline separation was not achieved (pH<7, pH>9), the peptides were injected in pairs: UPF51+UPF17, UPF51+GSH, UPF17+GSH and UPF50+UPF1, UPF50+GSH, UPF1+GSH.

In order to get an exact pH value, the stock solutions used were mixed in an appropriate way and diluted to obtain the desired ionic strength. Since the determination of pK_a depends on the ionic strength of the background electrolyte, this parameter should be held constant throughout the buffer series. The constituents of running buffers were selected to achieve a compromise between buffering capacity, effective stacking of analytes, low Joule heating, small temperature gradients and viscosity differences. Taking into account all the mentioned requirements for buffers for pK_a determination, an ionic strength of 50 mM was chosen. The buffers used for pK_a determination were CHES, TES, MOPS and acetate (used for determination of pK_a of the imidazolyl group). As already mentioned, the borate buffer may interact with the peptides used, therefore it was not employed in pK_a measurement experiments.

For the determination of dissociation constants, the effective mobility (μ_{eff}) of each peptide was presented as a function of pH. The obtained plots (Fig. 7) were resolved using statistical software *SigmaPlot 11.0.*

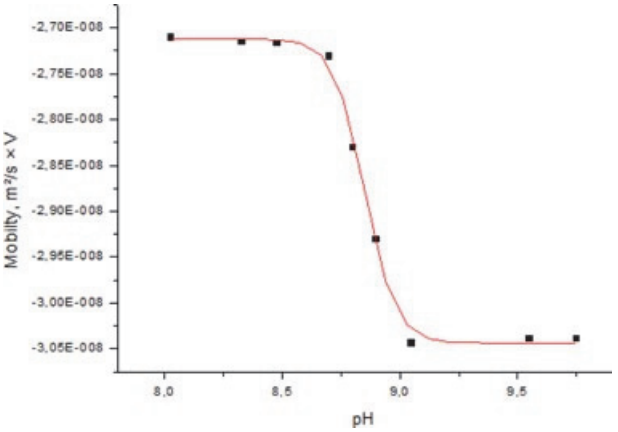

Figure 7. Plot of μ_{eff} vs pH for UPF17 homodimer.
Conditions are the same as in Fig. 4, except that 50 mM buffers were used and the borate buffer was not used. The inflexion point of the sigmoidal curve corresponds to the pK_a value of amino group of the UPF17 homodimer.

The pK_a values obtained are presented in Table 2. Among the thiol groups, the pK_a value of UPF17 is the lowest (7.86 ± 0.03), while that of GSH is the highest (8.13 ± 0.4). Among the amino groups, the pK_a value of the UPF50–UPF1 heterodimer is the highest (9.10 ± 0.07). The pK_a value of the imidazolyl group of the UPF51–UPF17 heterodimer is the highest (6.29 ± 0.04) and that of the UPF50 homodimer the lowest (5.94 ± 0.03). As also seen from Table 2, some differences in pK_a between the peptides may be observed when determined by CE and other methods [22].

Table 2. pK_a values of some GSH analogues measured by CE.

Peptide	pK_a ± SD		
	Imidazolyl	Amino	Thiol
UPF1		8.91 ± 0.05	8.03 ± 0.02/9.3 ± 0.1[a)]
UPF17		8.83 ± 0.07	7.86 ± 0.03/9.4 ± 0.2[a)]
UPF50	6.21 ± 0.05	9.06 ± 0.11	7.89 ± 0.12
UPF51	6.24 ± 0.07	9.00 ± 0.10	7.99 ± 0.10
UPF1 homodimer		9.03 ± 0.08	
UPF17 homodimer		8.84 ± 0.01	
UPF50 homodimer	5.94 ± 0.03	8.95 ± 0.03	
UPF51 homodimer	6.05 ± 0.04	9.01 ± 0.04	
UPF1−GSH heterodimer		8.90 ± 0.02	
UPF17−GSH heterodimer		8.96 ± 0.04	
UPF50−GSH heterodimer	6.19 ± 0.06	8.81 ± 0.04	
UPF51−GSH heterodimer	6.01 ± 0.02	9.03 ± 0.06	
UPF50−UPF1 heterodimer	6.20 ± 0.07	9.10 ± 0.07	
UPF51−UPF17 heterodimer	6.29 ± 0.04	8.93 ± 0.06	
GSH		8.93 ± 0.06	8.13 ± 0.4/9.0 ± 0.3[a)]
GSSG		9.05 ± 0.04	

[a)] Measured pK_a values of thiol groups in GSH, UPF1 and UPF17 by titration [22].

3.3 MEKC studies of UPF peptides (Publications II, III)

3.3.1 Choice of the micelle marker

At the beginning of the MEKC investigation of UPF peptides different compounds like dodecanophenone, α-tocopherol, vitamin K1 and dodecylbenzene were tested as possible micellar markers [77]. Dodecanophenone, α-tocopherol and vitamin K1 did not give reproducible migration times of micelle when using BGE composed of phosphate buffer (pH 7.4) and different surfactants like C_{14}MImCl (CMC 2.5 mM/3.5 mM in 25 mM phosphate/water, respectively [78]), CTAB, SDS (CMC 3.27 mM in 20 mM phosphate buffer, pH 7.0 [79]) probably due to the strong absorption on the capillary wall and high methanol content needed in the marker sample solution [49, 57]. When phosphate buffer (pH 7.4) was replaced with MOPS, TES and/or HEPES buffers (pH 7.4) in order to improve the migration time reproducibility of the mentioned micelle markers, no positive results with the same surfactants (C_{14}MImCl, CTAB, SDS) were obtained. Dodecylbenzene gave reproducible migration times (t_{mc} RSD <10%) of micelles when BGE composed of phosphate buffer (pH 7.4) and

surfactants like C_{14}MImCl and CTAB were used. When dodecylbenzene was used as an SDS micelle marker in the BGE composed of phosphate, MOPS, TES and/or HEPES buffer (pH 7.4), the migration time of SDS micelles did not improve. Only with the use of the borate buffer (pH 8.2) a positive effect on the migration time of the SDS micelle (t_{mc} RSD <10%) was obtained when dodecylbenzene was used as a marker. The RSD% of the migration time of C_{14} MImCl micelles was 10.38 and of CTAB micelles 6.91 (RSD% of the migration time of micelles was calculated on the basis of all UPF peptides).
For MEKC experiments dodecylbenzene was dissolved in MeOH at a concentration of *ca.* 2 mg/mL.

3.3.2 Effect of surfactant concentration on the mobility of UPF peptides

Since the studied UPF peptides are hydrophilic compounds with pK_a values of imidazolyl, amino and thiol moieties in the range of 5.94–6.29, 8.81–9.10 and 7.86–8.13, respectively (Publication I), it is expected that these GSH analogues are negatively charged at physiological pH (7.4) and the electrostatic interactions between these analytes and charged micelles (C_{14}MImCl, CTAB, and SDS) should contribute to the overall retention factors. As discussed before, UPF peptides exist in two forms in an aqueous solution: reduced monomeric peptide and oxidized homodimeric peptide (kindly refer to section 3.1.3).
In Fig. 8 the pseudoeffective electrophoretic mobility μ of the investigated UPF peptides, GSH and GSSG is plotted against the concentration of the surfactant (conc(C_{14}MImCl, CTAB and/or SDS)) ranging from 10 to 60 mM with conc(surfactant) increments of 10 mM. The further study of Fig. 8 reveals that the surfactant concentration of 36 mM has been used instead of 40 mM. The reason for this was the micelle aggregation (kindly refer to section 3.3.3) of BGE composed of phosphate buffer (pH 7.4) and 40 mM 1-tetradecyl-3-methylimidazolium chloride during MEKC experiments. This aggregation was seen as spikes on the output electropherogram and therefore the identification of analytes was hindered. To avoid the aggregation of micellar BGE, the concentration of C_{14}MImCl was gradually lowered and 36 mM 1-tetradecyl-3-methylimidazolium chloride was chosen (Publication II). In order to match the other surfactant concentrations used in MEKC experiments with C_{14}MImCl, the same concentration range of CTAB and SDS was employed.

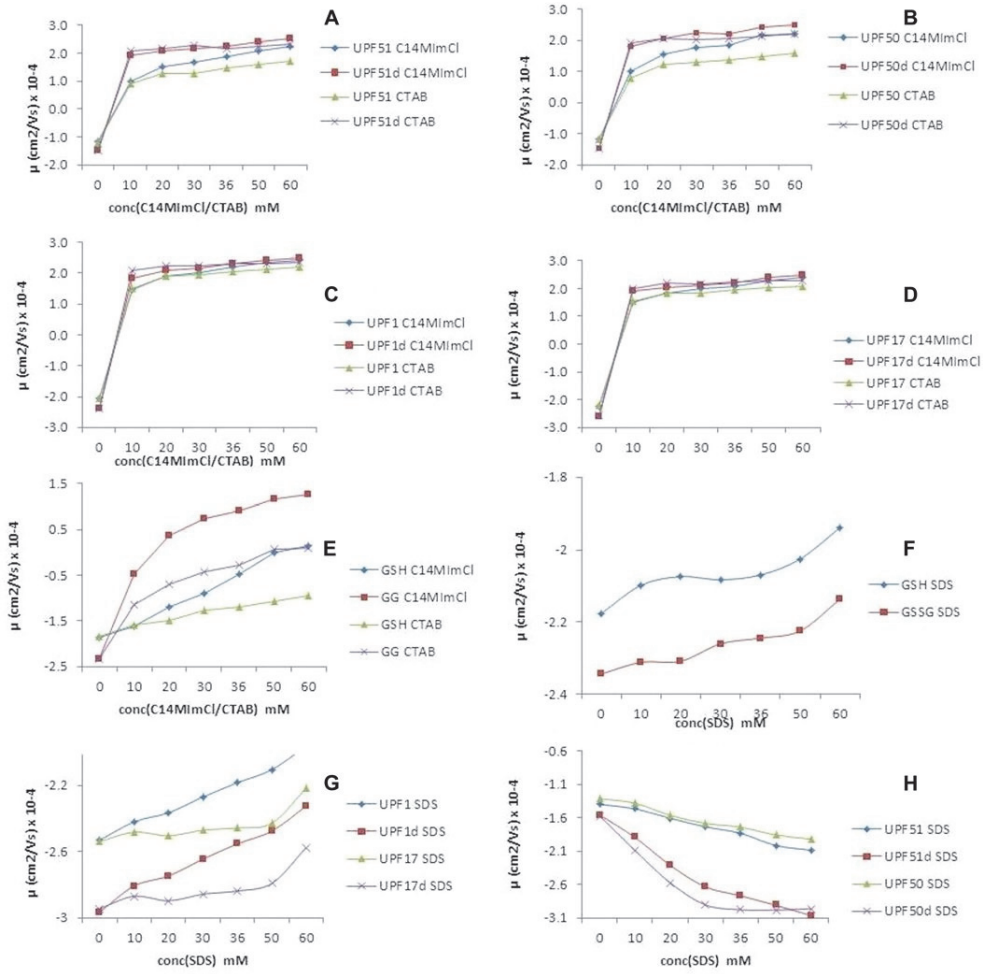

Figure 8. Effect of the surfactant concentration of C_{14}MImCl, CTAB and SDS on the pseudoeffective mobility of peptides.
(A–E) phosphate buffer (pH 7.4) and 0–60 mM C_{14}MImCl/CTAB;
(F–H) borate buffer (pH 8.2) and 0–60 SDS.
CE and MEKC conditions: fused-silica capillary 60/51.5 cm (L_{tot}/L_{eff}), id 50 μm, detection 200 nm and 230 nm, capillary temperature 25 °C, applied voltage –10 kV (micellar BGE with C_{14}MImCl and CTAB) and +10 kV (non-micellar BGE and micellar BGE with SDS). The ionic strength of all buffers was held constant at 35 mM; *d* represents homodimer.

When further studying Fig. 8A–D, it can be seen that the μ values obtained in MEKC experiments are positive unlike the effective mobility μ_{eff} measured in BGE without surfactant due to the interaction of negatively charged peptides with positively charged micelles (C_{14}MImCl, CTAB). Also, a slight increase in the μ values of UPF peptides of both reduced and oxidized forms with increasing PSP concentration is obtained. This result confirms that the mode of interaction between these UPF peptides and positively charged micelles is not

purely electrostatic interaction but hydrophobically assisted electrostatic interaction. The obtained outcomes are different from those reported in case of charged analytes where a plateau curve is obtained when μ is plotted against surfactant concentration [49]. As can also be seen form Figs. 8A–D, the contribution of the hydrophobic interaction between UPF1 and UPF17 (and their corresponding homodimers) and cationic micelles is lower compared to that between UPF50 and UPF51 that have carnosine moiety present in their structures. A totally different situation was observed with GSH and GSSG: the pseudoeffective electrophoretic mobility of reduced and oxidized glutathione significantly increased with increasing concentration of C_{14}MImCl and/or CTAB from 0 to 60 mM, indicating that these analytes have a relatively strong interaction with micelles (Fig. 8E). Moreover, GSSG has a more powerful interaction with both C_{14}MImCl and CTAB than with GSH, this being stronger when 1-tetradecyl-3-methylimidazolium chloride was used. When comparing the resolution between UPF peptides, it was slightly better when CTAB was employed as PSP than in the case of C_{14}MImCl (Figs. 1A–D). At the same time, for GSH and GSSG the resolution was better when C_{14}MImCl was used as PSP (Fig. 1E). On the whole, in the case of UPF peptides the extent of micelle complexation for C_{14}MImCl was higher than that for CTAB: doubling the surfactant concentration from 30–60 mM increased the pseudoeffective electrophoretic mobility by 12.7% with C_{14}MImCl versus 6.7% with CTAB for UPF17 and by 10.8% with C_{14}MImCl versus 3.1% with CTAB for the UPF17 homodimer. This result can be ascribed to the versatile electrostatic interaction sites provided by the polar imidazolium functional group of the imidazolium based IL, C_{14}MImCl. Besides, the hydrophobic interactions with the long alkyl tail of C_{14}MImCl are also possible. The imidazolium moiety can cause ion-dipole interactions and hydrogen bonding with the C-2 hydrogen of the imidazolium cation [80]. In addition to C_{14}MImCl and CTAB, the pseudoeffective electrophoretic mobility of peptides was plotted against the concentration of SDS (Figs. 8F–H). When the SDS surfactant in the concentration range from 0 to 60 mM was employed, the borate based BGE (pH 8.2) was used, instead. The pseudoeffective electrophoretic mobilities are negative due to the absence of the interaction between the negatively charged peptides and negatively charged micelles. As can be seen from Figs. 8F–G, μ increases (becomes more positive) with increasing PSP in the case of GSH, GSSG, UPF1 and UPF17 (monomer and homodimer) due to the absence of the interaction between the mentioned peptides and SDS micelles.

At the same time, μ decreases (becomes more negative) with increasing PSP in the case of UPF50 (monomer and homodimer) and UPF51 (monomer and homodimer) due to the complexation of the corresponding peptides with SDS micelles (Fig. 8H). Apparently, there is a hydrophobic interaction between UPF50, UPF51 (and their corresponding homodimers) and SDS micelles since peptides under study and SDS micelles are negatively charged and an electrostatic repulsion should exist between them. This hydrophobic interaction

is due to the carnosine moiety present in UPF50/51 and their dimers' structure. In order to compare pH 8.2 with physiological pH of 7.8, BGE composed of phosphate buffer (pH 8.2) and C_{14}MImCl/CTAB with the concentration range 0–60 mM was also studied. The obtained results were alike to those obtained with phosphate buffer (pH 7.4), the pseudoeffective mobility values being slightly higher when pH 8.2 was used (data not shown).

The reproducibility of the migration times (Figs. 8A–H) of peptides ranged from 0.061% to 1.49% in the case of CTAB, from 0.045% to 1.15% in the case of C_{14}MImCl and from 0.068% to 1.96% in the case of SDS. The differences in RSD% values obtained with different concentrations of surfactants can be ascribed to the unique micelle structures of PSPs and the dynamic coating of the capillary of cationic surfactants [49, 81].

3.3.2.1 Aggregation of micellar background electrolytes

During the investigation of UPF peptides by MEKC with the use of different background electrolytes, the formation of micelle aggregates was observed as a random sequence of spikes on a UV detector signal. This phenomenon appeared when C_{14}MImCl and phosphate buffer (pH 7.40) were used in different concentration combinations.

In the micelle aggregation experiments, the capillary was filled with the micellar BGE at known concentrations (5−45 mM phosphate buffers (pH 7.40), each containing 30, 36, 38, 40, 45, 50, 55 and 60 mM C_{14}MImCl) and the response of the UV detector (at a wavelength of 200 nm) was monitored as a function of time directly after the application of the voltage (-5 kV, -10kV or -15 kV). Other instrumental parameters were identical to the parameters used in the MEKC studies of UPF peptides.

The field was applied over the homogenous solution, thus it was expected that the only source of variations in the detector output (other than noise) could be the formation of micelle aggregates that blocked the light path of the UV detector. Moreover, the aggregation could be only observed after the application of voltage, no spiking was seen if the micellar BGE was pumped through the capillary under pressure. An example of electropherograms of micelle aggregates is presented in Fig. 9. As seen from Fig. 9, in the beginning the detector signal is constant as is expected for the homogenous and stable micellar solution. After a few minutes, the spiking in the signal starts to increase progressively, which indicates the onward formation of aggregates that pass in front of the UV detector. After approximately 5 min (Fig. 9A) the pattern of spikes stabilizes, indicating that the formation of aggregates came to an apparent stationary state, which means that the aggregates have reached the size comparable to that of the capillary.

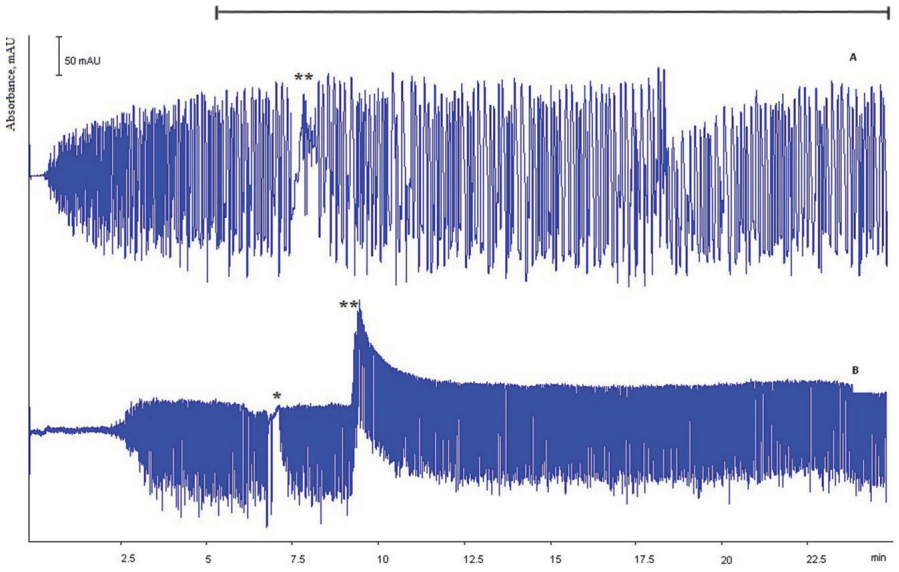

Figure 9. The evolution of the UV detector response at the capillary window from the time the high voltage of –10 kV was applied.
MEKC conditions: fused-silica capillary (id 50 μm, total length 60 cm, length to detector 51.5 cm), detection at 200 nm, capillary temperature 25 °C, applied voltage –10 kV.
(A) 10 mM phosphate buffer and 30 mM C_{14}MImCl-based BGE (pH 7.4);
(B) 25 mM phosphate buffer and 45 mM C_{14}MImCl-based BGE (pH 7.4).
The ├──┤ represents an apparent stationary state.

Next, the estimation of the aggregation potential of BGE of different concentrations was carried out. The root mean square (RMS) value of the signal fluctuation over the stationary area, i.e. area of the constant fluctuation size (please refer to Fig. 9A–B) was chosen as a reproducible and unique criterion for all BGE concentrations. RMS was more intensive when 10 and 15 mM phosphate buffers were used after the application of -5, -10 and -15 kV voltages with the highest RMS belonging to -10 kV. At the same time, the lowest RMS belonged to 5 and 45 mM phosphate buffers with the application of -5, -10 and -15 kV voltages. Altogether, the application of -10 kV produced the highest and -5 kV the lowest RMS values (Fig. 10A). From Fig. 10B it can be seen that the highest RMS value was with 50 mM C_{14}MImCl when -15 kV was applied and the lowest one corresponded to 45 mM C_{14}MImCl with the application of -5 kV. In all, with the application of the -10 kV voltage, the RMS values were high, being the greatest with 40 and 45 mM C_{14}MImCl.

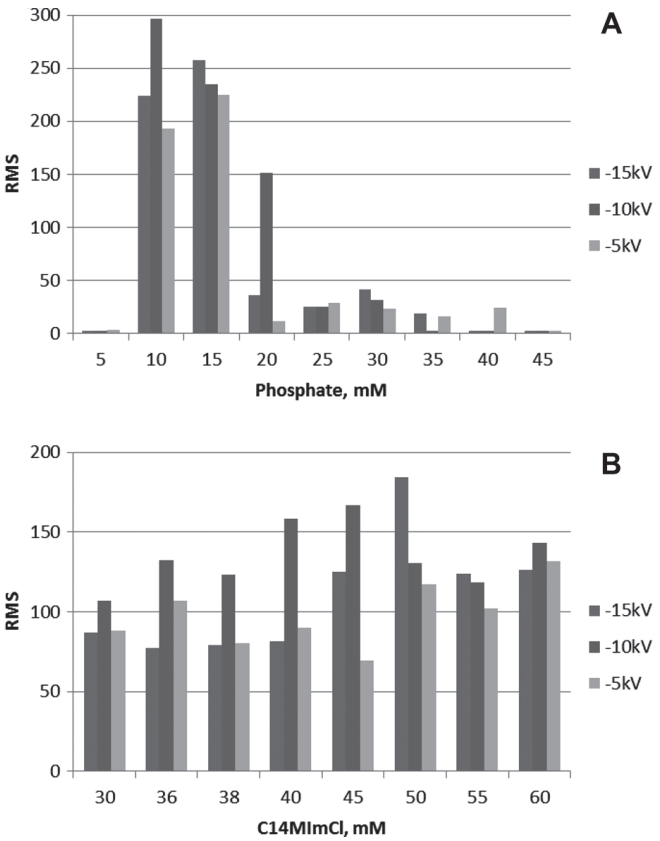

Figure 10. RMS of spikes as a function of phosphate buffer (pH 7.4) concentration (A) and C_{14}MImCl concentration (B).

Experimental conditions: applied voltage –5, –10 and –15 kV, other conditions as in Fig. 9.

The aggregation time shortened when BGE became more dilute: on the electropherogram the pattern of spikes appeared from 30 to 45 mM C_{14}MImCl when voltage was set to -10 kV and the phosphate buffer concentration was kept constant at 10 mM with the IL concentration varying from 30 to 60 mM. On the other hand, the aggregation time became more prolonged as BGE became more dilute: spikes on the electropherograms appeared from 40 to 60 mM C_{14}MImCl when the IL concentration was varied over the same range and the phosphate buffer concentration was held at 15 mM. The aggregation time was constant when -5 and -15 kV were applied regardless of phosphate buffer and IL concentrations. So it may be concluded that the appearance of aggregates depends on the concentration of BGE components. Aggregates appear at a certain threshold concentration of phosphate buffer and C_{14}MImCl (BGE) and cease to appear at higher concentrations of BGE.

On the whole, it seems that micelle aggregation may be interpreted as a failure of the electrophoretic run (e.g. " uneven" concentration increments and the inability to study peptides within a certain concentration range of C_{14}MImCl);

on the other hand MEKC may be an excellent technique for micelle (and probably other substances') aggregation studies.

3.3.3 Determination of retention factors of UPF peptides by MEKC

Under physiological conditions (pH 7.4) the studied analytes are negatively charged [81]; therefore their separation by MEKC is based not only on chromatographic but also on electrophoretic principles as well. The overall retention factor of peptides is the weighted average of the retention factors of all species (neutral and charged) that are present in the solution. The retention factors were calculated according to Eq. 12 with several assumptions made: the influence of PSP on the ionic strength, viscosity and dielectric constant of BGE is considered very low and the interaction of the peptide with surfactant monomers is neglected. The true retention factor k in MEKC was calculated from the mobilities μ, μ_{eff} and μ_{mc} (Eq.13) that have to be determined in different CE modes under the same conditions: μ and μ_{mc} were measured in the MEKC mode and μ_{eff} in the CZE mode.

In Fig. 11 the dependence of the retention factors of reduced and oxidized forms of UPF peptides and glutathione on the concentration of the surfactant (C_{14}MImCl, CTAB and SDS) is depicted. As seen from Figs. 11A–D, G and H, the retention factors of monomeric UPF peptides increase and that of dimeric UPF peptides decrease with increasing surfactant concentration. The dependence of the retention factor on the C_{14}MImCl and CTAB micelle concentration is non-linear and the obtained curves converge to a limiting value. The absorption of monomeric UPF peptides in micelles achieves saturation approximately when the concentration of C_{14}MImCl/CTAB reaches 36 mM. Afterwards, the increase of the C_{14}MImCl/CTAB concentration only performs the function of "dilution" (and a more "plateau-like" curve is obtained, see Figs. 11 A–D, G and H).

When pH of the phosphate buffer was set to 8.2, the retention factors of monomeric UPF peptides increased (Figs. 11C–D) and decreased when pH was 7.4 (Figs. 11A–B). This was probably due to the higher net negative charge of peptides at pH 8.2. Negative monomeric UPF peptides interact more strongly with oppositely charged micelles like C_{14}MImCl and CTAB mainly by electrostatic interaction. At the same time, the retention factors of GSH and GSSG increased with increasing surfactant concentration (C_{14}MImCl and/or CTAB). When C_{14}MImCl was employed as PSP, the retention factors of GSH and GSSG were higher compared to that of CTAB. With the increase of pH of the phosphate buffer from 7.4 to 8.2, the retention factors of GSH and GSSG were increased as well (Fig. 11E). Altogether, with C_{14}MImCl used as PSP, the retention factors of UPF peptides, GSH and GSSG were higher compared to that of CTAB; this could be ascribed to the versatility of interaction sites provided by the imidazolium cation.

The homodimeric forms of UPF peptides should have a greater net negative charge compared to their corresponding monomeric forms [82] and therefore have

a more explicit electrostatic interaction with positively charged micelles. Remarkably, the retention factors of homodimeric forms of UPF peptides decreased with the increase of PSP concentration (C_{14}MImCl and CTAB) (Figs. 11 A–D, G and H). A possible explanation for this phenomenon is the pK_a shift of UPF homodimers that is caused by their interaction with cationic micelles [83, 84] that results in a change of the net charge of peptides from negative to neutral. Since GSH analogues under investigation are hydrophilic, the interaction of neutral homodimeric forms of these peptides with charged micelles is considered to be very weak. Therefore, with the increase in PSP concentration, the UPF homodimers acquire a more positive charge and the interaction between peptides and micelles weakens, resulting in lower retention factors.

Another possible explanation may be the influence of peptide conformation stabilized by intermolecular hydrogen bonds. A bend in the UPF homodimers' backbone may again induce a change in pK_a. Moreover, the hydrophobicity of the neighboring amino acids may also influence the peptide ionization constants [85]. The homodimers of UPF1 and UPF17 have hydrophobic methoxy-tyrosine moieties, while UPF50 and UPF51 have histidine residues in addition to methoxy-tyrosine moieties that may change the pK_a values of the neighboring amino acids and therefore alter the backbone stereochemistry and hinder the complex formation with the micelle. As a result, the electrostatic interaction between the micelles and UPF homodimers is decreased. Indeed, as seen from Appendix 4, a stronger interaction between the UPF50 homodimer and C_{14}MImCl micelle is observed when the concentration of 1-tetradecyl-3-methylimidazolium chloride is lower.

A further possible explanation for the reduced retention factors of UPF homodimers with increasing concentration of cationic surfactants is that the shape of micellar associates changes, suggesting that the homodimers of UPF1, UPF17, UPF50 and UPF51 preferably bind to C_{14}MImCl and/or CTAB of a specific shape [81]. When SDS was used in the MEKC experiments as PSP, only the reduced and oxidized forms of UPF50 and UPF51 interacted with SDS micelles. The retention factors of UPF50 and UPF51 peptides increased with increasing SDS concentration (Fig. 11F).

The log k values of the retention factors of monomeric and dimeric forms of GSH analogues can be found in Appendix 5.

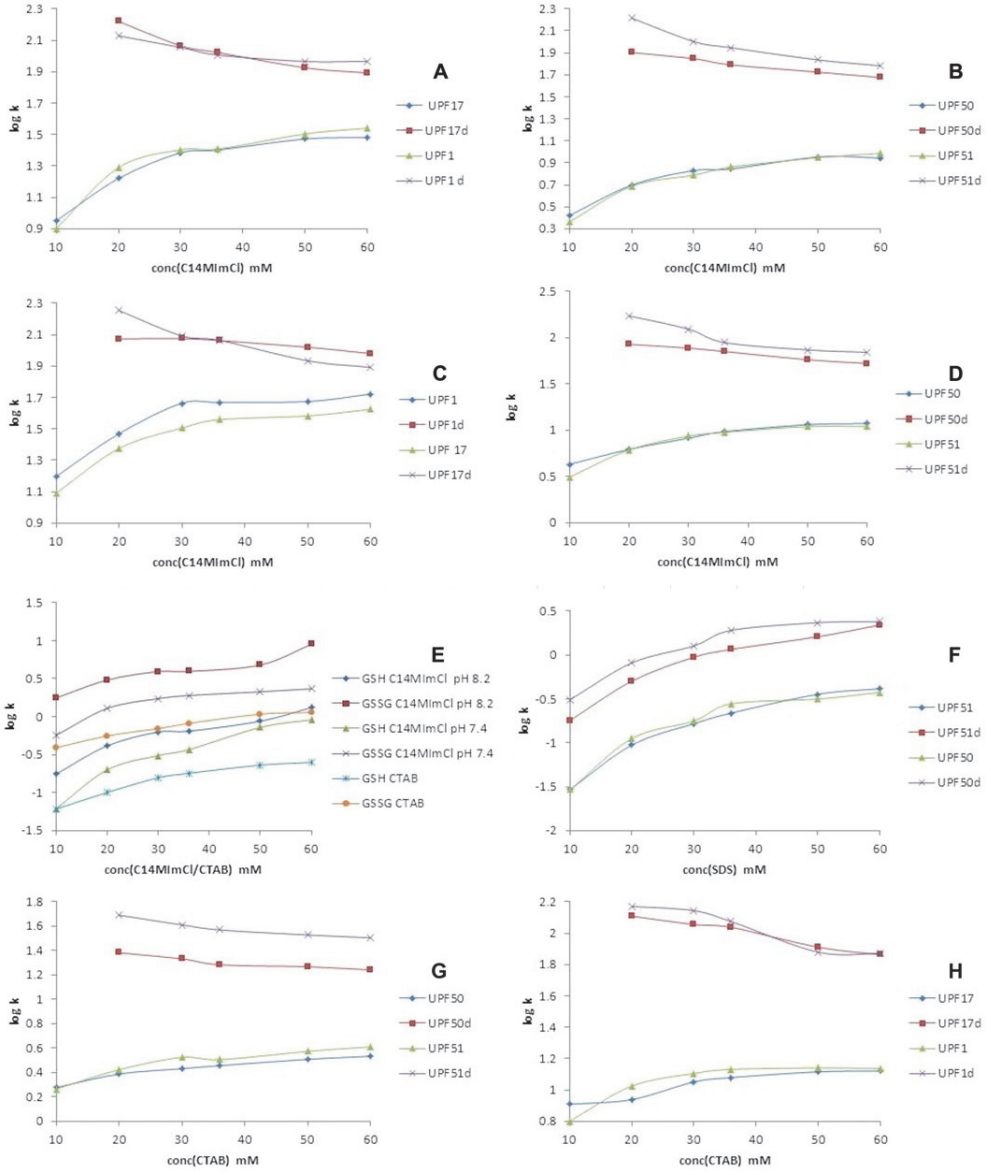

Figure 11. Retention factors of glutathione and its analogues (reduced and oxidized forms) plotted against the concentration of C_{14}MImCl, CTAB and SDS.
MEKC conditions: refer to Fig. 8.
(A, B) phosphate buffer (pH 7.4); (C, D) phosphate buffer (pH 8.2); (E) phosphate buffer (pH 7.4 and 8.2); (F) borate buffer (pH 8.2); (G, H) phosphate buffer (pH 7.4).

3.4 Determination of metal content in SODs by CE (Publication IV)

3.4.1 BGE optimization

For the determination of metal content of superoxide dismutase enzymes a novel BGE composed of pyridine-2,6-dicarboxylic acid (PDC) and

1-tetradecyl-3-methylimidazolium chloride (C_{14}MImCl) was selected. Before optimizing BGE (pH and concentration) the dynamic wall coating must be tuned. C_{14}MImCl was tested in a 0.5−2.5 mM concentration range. A stable dynamic coating with fewer fluctuations of the baseline as well as optimal selectivity was achieved when 1 mM C_{14}MImCl was used. The next step was the optimization of the pH of BGE. As PDC is an ionizable compound (pK_{a1} = 2.1, pK_{a2} = 4.4 at 25 °C [66]), its ligand concentration is pH dependable: more charged ligands are formed with higher pH values of the PDC solution resulting in increased levels of metal complexation. Fig. 12A shows that the corrected peak areas (ratio of peak area to migration time) of the complexed metals increased slightly when the pH of BGE was changed from 3.6 to 4.0. This effect is attributable to an increase in PDC^{2-} concentration that favors the formation of metal complexes: $[Fe(PDC)_2]^{2-}$, $[Fe(PDC)_2]^{-}$, $[Zn(PDC)_2]^{2-}$, $[Mn(PDC)_2]^{2-}$. When pH was increased further until 5, the peak areas decreased (with the exception for manganese), which may be ascribed to metal hydroxide precipitation [65]. Eventually, pH = 3.8 was selected (from the 3.6−4.0 pH range) for the subsequent studies of metals as with this pH value the most stable baseline was obtained. Following the selection of the pH value of BGE, the optimal concentration of PDC needed to be established. The PDC concentration was varied from 5 to 20 mM and the corrected peak areas of the complexed metals were calculated (Fig. 12B). The high concentration of PDC^{2-} supports the formation of metal complexes at the expense of sensitivity (with the exception for manganese), though. This decrease in sensitivity with increased PDC concentration may be caused by the high molar absorptivity of pyridine-2,6-dicarboxylic acid [66]. The $[Mn(PDC)_2]^{2-}$ complex is more favorably formed with a higher PDC concentration, though. For Fe the corrected peak areas changed negligibly with varying PDC concentration. Ultimately, BGE consisting of 10 mM PDC was selected as it provided the optimal complexation and separation of Cu, Zn, Fe and Mn.

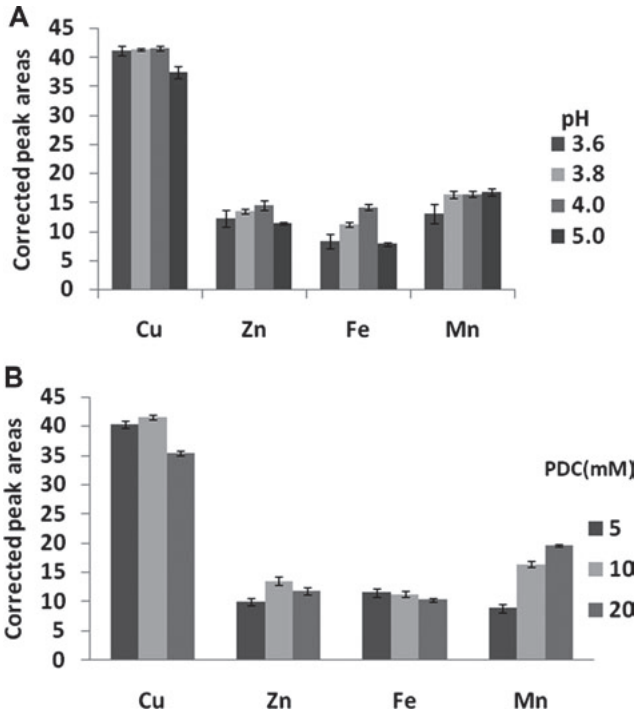

Figure 12. Dependence of the corrected peak areas on the pH of BGE (A) and the concentration of PDC (B).
(A) 10 mM PDC, 1 mM C_{14}MImCl as BGE; (B) 5, 10 and 20 mM PDC with 1 mM C_{14}MImCl at pH 3.8 as BGE.

3.4.2 Analytical performance of the CE method

Validation of the method was carried out in order to apply it to qualitative and quantitative analysis of metal ion content in superoxide dismutase proteins. Taking into account all the requirements for the complexation, separation and determination of metals, BGE containing 10 mM PDC and 1 mM C_{14}MImCl at pH 3.8 was used for subsequent analyses.

Before real sample analysis it was necessary to check for the possible interference of other metal cations that could be present in SOD solutions. Laboratory-purified SODs are stored in buffer solutions of specified pH and ionic concentrations for the optimal stability and activity of enzymes. Generally the buffers used are Tris-HCl and/or KH_2PO_4/K_2HPO_4 which also contain contaminating salts that produce cations like K^+ , Na^+ , Ca^{2+} , Mg^{2+} which potentially may interfere with detection of the metals under investigation. Other components of the buffer like Cl^- , HPO_4^{2-} and $H_2PO_4^-$ usually do not disturb the CE analysis. Tris-HCl, a common buffer used in microbiology was also checked. (Fig. 13A). Possible interferences of the unresolved peaks of amino acids and/or peptides that may have remained after acid/hydrogen peroxide treatment were also checked. The CE analysis of apo-FeSOD and apo-MnSOD (metal-free SODs) was performed and it was showed that the unresolved peaks

do not affect the determination of the iron and manganese content in FeSOD and MnSOD samples, respectively (Appendix 2).

Monovalent cations like K^+ , Na^+ were not checked for interference, as they do not form complexes with PDC. Mg^{2+} has a low complexation constant with PDC and therefore was not detected [66]. The possible interference of Ca^{2+} with the metal ions under investigation was tested. The Ca^{2+} peak appeared last on the electropherogram and was separated from Cu^{2+}, Zn^{2+}, Fe^{3+} and Mn^{2+} peaks (Fig. 13B), thus showing no interference. The migration order of the complexes of Cu^{2+}, Zn^{2+}, Fe^{3+}, Mn^{2+} and Ca^{2+} reflects the charge to size differences of anionic metal complexes. The peaks of the mentioned complexes were identified using a standard addition method. Moreover, the baseline separation of Cu^{2+}, Zn^{2+} and Fe^{2+}, Fe^{3+} has also been achieved when using BGE composed of 10 mM PDC + 1 mM C_{14}MImCl, pH 3.8 (Figs 13B–C).

Calibration curves were obtained by plotting the corrected peak areas of each analyte against concentration. Calibration equations, correlation coefficients (R^2), LODs (S/N = 3) and RSDs of the corrected peak areas and migration times are presented in Appendix 3. The calibration curves exhibit good linearities (R^2 is 0.992–0.999 in a concentration range of 2.5–100 μg/mL) with detection limits of 0.3 μg/mL for Cu^{2+}, 1.0 μg/mL for Zn^{2+}, 0.5 μg/mL for Mn^{2+} and 1.2 μg/mL for Fe^{3+}.

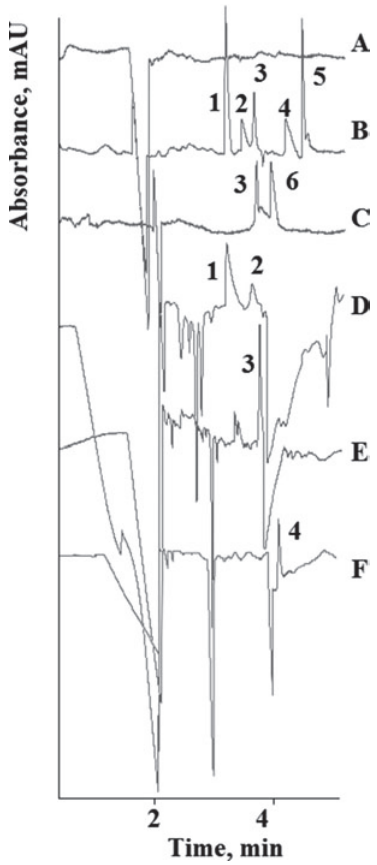

Figure 13. Electropherograms of 10 mM Tris-HCl (A), standard metal mixture (B), Fe^{2+} and Fe^{3+} mixture (C), CuZnSOD (D), FeSOD (E), MnSOD (F).
Peak identification: 1–Cu^{2+} , 2–Zn^{2+} , 3–Fe^{3+} , 4–Mn^{2+} , 5–Ca^{2+}, 6–Fe^{2+}.
CE conditions: standards concentration 15 µg/mL (B), 30 µg/mL (C), 10 mM PDC with 1 mM C_{14}MImCl at pH 3.8 as BGE, capillary length 60 cm (51.5 cm to detector), detection at 214 nm, injection pressure 50 mbar for 6 s, capillary temperature 30 °C, applied voltage -20 kV.

3.4.3 Sample analysis

In order to obtain an accurate measurement of the content of Cu^{2+}, Zn^{2+}, Fe^{3+}, Mn^{2+} ions of metalloenzymes by employing the proposed CE method, the bound metal ions must be released into solution. First, the freeze-dried protein was treated with HNO_3 and H_2O_2 however, this distorted subsequent CE analysis probably due to the molar absorptivity of nitric acid. Alternatively, the lyophilized protein samples were digested with cHCl and H_2O_2. In Figs. 13D–F the electropherograms of CuZnSOD, FeSOD and MnSOD are presented, whereas in Fig. 13D the electropherogram of CuZnSOD has two positive peaks (marked 1 and 2) that belong to Cu^{2+} and Zn^{2+}, respectively, and negative peaks, which immediately follow the Zn^{2+} peak, to the amino acids that may have remained in the solution even after acid hydrolysis. Because the stability of CuZnSOD to high temperatures, pH extremes and detergents is generally higher than those of FeSOD and MnSOD, the negative dip (peak of comigrating amino acids/peptides) is larger compared to that of Mn- or FeSOD (Fig. 13E, F). The negative peak that follows the Fe^{3+} peak (Fig. 13E) may have interfered with the determination of Fe^{2+} (Fig. 13C) but as sample preparation was carried out in

aerobic and acidic conditions only, the amount of Fe^{3+} in FeSOD was actually measured. The metal content of the corresponding SOD enzymes measured by CE and GF/FAAS methods is presented in Table 3 where the metal concentration is given as μg metal per 1 mg of protein. As also seen from Table 3, the manganese content of Mn(Fe)SOD (Fe-substituted MnSOD, which means that naturally occurring Mn is replaced with Fe) was only measured by AAS. The reason is the insufficient amount of manganese in laboratory-purified enzyme to be detected by CE. Nevertheless, the results obtained from CE were in good agreement and highly correlated with the AAS outcomes (R^2>0.99).

Table 3. Metal ion content in laboratory-purified SOD enzymes obtained by CE and AAS (n = 3).

SOD	Metal ion	CE μg metal/mg protein (± SD)	AAS μg metal/mg protein (± SD)
CuZnSOD	Cu^{2+}	3.01 ± 0.09	2.858 ± 0.003
	Zn^{2+}	3.1 ± 0.2	3.000 ± 0.004
Mn(Fe)SOD	Fe^{3+}	0.92 ± 0.09	0.820 ± 0.003
	Mn^{2+}	N.D.	0.375 ± 0.004
MnSOD	Mn^{2+}	1.30 ± 0.05	1.190 ± 0.004
FeSOD	Fe^{3+}	1.8 ± 0.2	1.600 ± 0.003

N.D. – not detected

4 CONCLUSIONS

The aims of the present research were to show the diverse opportunities that capillary electrophoresis techniques open for the investigation of endogenous antioxidants and their synthetic analogues as possible drugs for the preclinical investigations as well as study of metal content in superoxide dismutase enzymes. The summarized results from individual studies are as follows:

- A CE protocol was developed to separate reduced glutathione and its four novel analogues UPF1 (Tyr(Me)-γ-Glu-Cys-Gly), UPF17 (Tyr(Me)-α-Glu-Cys-Gly), UPF50 (β-Ala-His-Tyr(Me)-γ-Glu-Cys-Gly), UPF51 (β-Ala-His-Tyr(Me)-α-Glu-Cys-Gly) as well as their homo- and heterodimers by varying the concentration and/or pH of different BGEs. The separability of peptides was investigated in a broad pH range (7.40–10.0), using inorganic buffers (phosphate and boric) and zwitterionic buffers (CHES, TES and MOPS) at different concentrations (50 to 250 mM). The results revealed that borate (200 mM, pH 8.45) was the best medium for separation of the peptides under investigation.
- Capillary zone electrophoresis proved to be a suitable and useful method for the simultaneous determination of pK_a values of imidazolyl, thiol and amino moieties in newly synthesized GSH analogues as well as their homo- and heterodimers. Effective electrophoretic mobilities of analytes were measured in the pH range 5.50–10.00, using optimized BGEs (CHES, TES, MOPS and acetate buffers) with an ionic strength of 50 mM at 25°C that allowed determination of the pK_a values for imidazolyl, amino and thiol moieties of the analyzed peptides, being in the range of 5.94–6.29, 8.81–9.10, and 7.86–8.13, respectively. Although the borate buffer showed the best separability of GSH analogues, it was not used for the pK_a determination due to its possible interaction with the analytes.
- The retention factors of negatively charged GSH analogues under physiological pH were determined using C_{14}MImCl, CTAB and SDS-based surfactants by micellar electrokinetic chromatography. The retention factor values of GSH analogues were in the range of 0.36–2.22 for glutathione analogues and from -1.21 to 0.37 for glutathione when 1-tetradecyl-3-methylimidazolium chloride was used. When cetyltrimethylammonium bromide was employed, the retention factor values were in the range of 0.27–2.17 for glutathione analogues and from -1.22 to 0.06 for glutathione. If sodium dodecyl sulfate was used, the retention factor values of glutathione analogues with carnosine moiety (UPF50/51) were in the range of -1.54–0.38.

The curves of hydrophilic GSH analogues partitioning into net positively charged micelles converged to a limiting value with increasing concentration of PSP. In general, the strength of monomeric UPF peptide-micelle interactions increased more with increasing pH and micelle concentration. The retention factors obtained when C_{14}MImCl was used as PSP were higher than those obtained with CTAB as PSP, due to the higher number of interaction sites provided by the imidazolium cation. The obtained results suggested that

hydrophobic interactions between monomeric UPF peptides and cationic micelles were weaker than electrostatic ones that are considered primarily responsible for the retention of monomeric GSH analogues. It was revealed that hydrophobic methoxy-tyrosine moieties of UPF1 and UPF17 homodimers and histidine residues in addition to methoxy tyrosine moieties of UPF50 and UPF51 homodimers induced a unique peptide conformation that did not have a sufficiently strong hydrophobic surface to interact with charged micelles. Moreover, additional steric effects may have hindered the complexation between the homodimers of UPF peptides and cationic micelles. At the same time, the hydrophobic interaction between negatively charged reduced and oxidized forms of UPF50/51 and SDS micelles overcame the electrostatic repulsion between them, in contrast to GSH, UPF1/17 and their corresponding homodimers.

- Altogether, the obtained results of MEKC experiments under physiological conditions using different PSPs enable better understanding of the molecular interactions that contribute to the overall retention of the studied GSH analogues and provide extra information about the possible diverse interactions between complex biological membranes and ionized compounds like UPF peptides as potential drugs.

On the whole, though CE is considered less reproducible than established HPLC methods, from a practical point of view this "drawback" should not limit the application of capillary electrophoresis methods based to migration or mobility measurements like pK_a or log k as these parameters are more robust and reproducible compared to concentration quantification.

- A possible aggregation of phosphate and ionic liquid (C_{14}MImCl) based BGEs during MEKC experiments for investigation of the interaction between GSH analogues and 1-tetradecyl-3-methylimidazolium chloride was discovered. After a certain transit period, the aggregates appeared as a random sequence of spikes on a UV detector signal. The observation suggested that MEKC is a simple and easy technique for micelle aggregation studies.
- A fast, simple and cost-efficient CZE protocol for a simultaneous determination of metal ion (Cu^{2+}, Zn^{2+}, Fe^{3+} and Mn^{2+}) content in superoxide dismutase enzymes was developed. It demonstrated that on-column complexation could be used for separation and quantification of metal ions in a novel electrolyte containing PDC and 1 mM C_{14}MImCl at pH 3.8. The results revealed that LODs were higher than those obtained by other methods. Nevertheless, CE with dynamic coating still may be used as an alternative or complimentary technique for analysis of metal ions present in sufficient amount in laboratory-purified enzymes.

REFERENCES

[1] Chaudiere, J., Ferrari–Iliou, R. Intracellular antioxidants: from chemical to biochemical mechanisms. – *Food Chem Toxicol*, 1999, 37, 949–962.

[2] Jacob, R.A., Burri, B.J. Oxidative damage and defense. – *Am. J. Clin. Nutr*, 1996, 63(6), 985–990.

[3] Aquilano, K., Baldelli, S., Ciriolo, M. R. Glutathione is a crucial guardian of protein integrity in the brain upon nitric oxide imbalance. – *Commun Integr Biol,* 2011, 4, 477–479.

[4] Biswas, S., Chida, A. S., Rahman, I. Redox modifications of protein-thiols: emerging roles in cell signaling. – *Biochem. Pharmacol,* 2006, 71, 551–564.

[5] Filomeni, G., Rotilio, G., Ciriolo, M. R. Cell signaling and the glutathione redox system. – *Biochem. Pharmacol,* 2002, 64, 1057–1064.

[6] Fratelli, M., Goodwin, L. O., Ørom, U. A. Gene expression profiling reveals a signaling role of glutathione in redox regulation. – *Proc Natl Acad Sci USA,* 2005, 102, 13998–14003.

[7] Pastore, A., Federici, G., Bertini, E., Piemonte, F. Analysis of glutathione: implication in redox and detoxification**.** – *Clin Chim Acta,* 2003, 333, 19–39.

[8] Kwon, Y. W., Masutani, H., Nakamura, H., Ishii, Y., Yodoi, J. Redox regulation of cell growth and cell death. – *Biol Chem*, 2003, 384, 991–996.

[9] Schafer, F.Q., Buettner, G. R. Redox environment of the cell as viewed through the redox state of the glutathione disulfide/glutathione couple**.** – Free Radic Biol Med, 2001, 30, 1191–1212.

[10] Ehrlich, K., Viirlaid, S., Mahlapuu, R., Saar, K., Kullisaar, T., Zilmer, M., Langel, U., Soomets, U. Design, synthesis and properties of novel powerful antioxidants, glutathione analogues. – *Free Radic Res*, 2007, 41, 779–787.

[11] Kubáń, P., Timerbaev, A.R. Inorganic analysis using CE: Advanced methodologies to face old challenges. – *Electrophoresis*, 2014, 35, 225–233.

[12] Vaher, M., Viirlaid, S., Ehrlich, K., Mahlapuu, R., Jarvet, J., Soomets, U., Kaljurand, M. Characterization of the antioxidative activity of novel nontoxic neuropeptides by using capillary electrophoresis. – *Electrophoresis*, 2006, 27, 2582–2589.

[13] Whittaker, J.W. Metal uptake by manganese superoxide dismutase. – *Biochim Biophys Acta*, 2010, 1804, 298–307.

[14] Salvemini, D., Muscoli, C., Riley, D.P., Cuzzorea, S. Superoxide dismutase mimetics. – *Pulm Pharmacol Ther,* 2002, 15(5), 439–447.

[15] Chaudiere, J., Ferrari-Iliou, R. Intracellular antioxidants: from chemical to biochemical mechanisms. – *Food Chem Toxicol*, 1999, 37(9-10), 949–962.

[16] Lushchak, V.I. Glutathione homeostasis and functions: potential targets for medical interventions. – *J Amino Acids*, 2012, 2012, 26 pages.

[17] Kannan, K., Jain, S.K. Oxidative stress and apoptosis. – *Pathophysiology,* 2000, 7, 153–163.

[18] Mytilineou, C., Kramer, B.C., Yabut, J.A. Glutathione depletion and oxidative stress. – *Parkinsonism Relat Disord*, 2002, 8(6), 385–387.

[19] Emerit, J., Edeas, M., Bricaire, F. Neurodegenerative diseases and oxidative stress. – *Biomed Pharmacother*, 2004, 58(1), 39–46.

[20] Wu, J.H., Batist, G. Glutathione and glutathione analogues; therapeutic potentials. – *Biochim Biophys Acta*, 2013, 1830, 3350–3353.
[21] De Flora, S., Izzotti, A., D'Agostini, F. Balansky, R.M. Mechanisms of N-acetylcysteine in the prevention of DNA damage and cancer, with special reference to smoking-related end-points. – *Carcinogenesis*, 2001, 22(7), 999–1013.
[22] Kairane, C., Mahlapuu, R., Ehrlich, K., Kilk, K., Zilmer, M., Soomets, U. Diverse effects of gluatathione and UPF peptides on antioxidant defense system in human erythroleukemia cells K562. – *Int J Pept*, 2012, 2012, 5 pages
[23] Kals, J., Starkopf, J., Zilmer, M., et al. Antioxidant UPF1 attenuates myocardial stunning in isolated rat hearts. – *Int J Cardiol*, 2008, 125(1), 133–135.
[24] Põder, P., Zilmer, M., Starkopf, J., et al. An antioxidant tetrapeptide UPF1 in rats has a neuroprotective effect in transient global brain ischemia. – *Neurosci Lett*, 2004, 370(1), 45–50.
[25] Boldyrev, A. A., Aldini, G., Derave, W. Physiology and pathophysiology of carnosine. – *Physiol Rev*, 2013, 93, 1803–1845.
[26] Bellia, F., Vecchio, G., Rizzarelli, E. Carnosinases, Their Substrates and Diseases. – *Molecules*, 2014, 19, 2299–2329.
[27] Di Paola, R., Impellizzeri, D., Trovato Salinaro, A., et al. Administration of carnosine in the treatment of acute spinal cord injury. – *Biochem Pharmacol*, 2011, 82(10), 1478-1489.
[28] Fridovich, I. Superoxide anion radical ($O_2^{\bullet -}$), superoxide dismutases and related matters. – *J Biol Chem*, 1997, 272(30), 18515–18517.
[29] Fukai, T., Ushio-Fukai, M., Superoxide dismutases: role in redox signaling, vascular function, and diseases. – *Antioxid Redox Signal*, 2011, 15(6), 1583–1606.
[30] Whittaker, J.W. The irony of manganese superoxide dismutase. – *Biochem Soc Trans*, 2003, 6, 1318–1321.
[31] Culotta, V.C., Yang, M., O'Halloran, T.V. Activation of superoxide dismutases: putting the metal to the pedal. – *Biochim Biophys Acta*, 2006, 1763(7), 747–758.
[32] Miller, A.F. Superoxide dismutases: ancient enzymes and new insights. – *FEBS Lett*, 2012, 586(5), 585–595.
[33] Holzgrabe, U., Brinz, D., Kopec, S., Weber, Ch., Bitar, Y. Why not using capillary electrophoresis for drug analysis? – *Electrophoresis*, 2006, 27, 2283–2292.
[34] Dovichi, N.J., Zhang, J. How capillary electrophoresis sequenced human genome. – *Angew Chem Int Ed Engl,* 2000, 39, 4463–4468.
[35] Sekhon, B.S. An overview of capillary electrophoresis: pharmaceutical, biopharmaceutical and biotechnology applications. – *J Pharm Educ Res*, 2011, 2 (2), 36 pages.
[36] Yao, X., Wang, Y., Chen, G. Simultaneous determination of aminothiols, ascorbic acid and uric acid in biological samples by capillary electrophoresis with electrochemical detection. – *Biomed Chromatogr*, 2007, 520–526.

[37] Gorbatsova, J., Lõugas, T., Vokk, R., Kaljurand, M. Comparison of the contents of various antioxidants of sea buckthorn berries using CE. – *Electrophoresis*, 2007, 28, 4136–4142.
[38] Olędzka, I., Kaźmierska, K., Plenis, A., Kamińska, B., Bączek, T. Capillary electromigration techniques as tools for assessing the status of vitamins A, C and E in patients with cystic fibrosis. – *J Pharm Biomed Anal*, 2015,102, 45–53.
[39] Pang, H., Kenseth, J., Coldiron, Sh. High-throughput multiplexed capillary electrophoresis in drug discovery. – *Drug Discov Today*, 2004, 9, 1072–1080.
[40] Introduction to pharmaceutical bioinformatics. / ed. J. E.S. Wikberg. Stockholm: Oakleaf Academic, 2011.
[41] Modern analytical chemistry. / ed. D. Harvey. United States of America: McGraw-Hill, 2000.
[42] High performance capillary electrophoresis. / eds. Lauer, H. H., Rozing, G.P. Germany: Agilent Technologies, 2014.
[43] Wan, H., Holmen, A.G., Wang, Y. et al. High-throughput screening of pK_a values of pharmaceuticals by pressure-assisted capillary electrophoresis and mass-spectrometry. – *Rapid Commun Mass Spectrom*, 2003, 17, 2639–2648.
[44] Wan, H., Thompson, R.A. Capillary electrophoresis technologies for screening in drug discovery. – *Drug Discov Today*, 2005, 2(2), 171–178.
[45] Poole, S.K., Patel, S., Dehring, K., et al. Determination of acid dissociation constants by capillary electrophoresis. – *J Chromatogr A*, 2004, 1037(1-2), 445–454.
[46] Kibbey, C.E., Poole, S.K., Robinson, B., Jackson, J.D., Durham, D.J. An integrated process for measuring the physicochemical properties of drug candidates in a preclinical discovery environment. – *Pharm Sci*, 2001, 90, 1164–1175.
[47] Liškova, A., Krivánková, L. Determination of dissociation constants of compounds with potential cognition enhancing activity by capillary zone electrophoresis. – *Electrophoresis*, 2005, *26,* 4429–4439.
[48] Terabe, Sh. Capillary Separation: Micellar Electrokinetic Chromatography. – *Annu. Rev Anal Chem,* 2009, 2, 99–120.
[49] Rageh, A.H., Pyell, U. Imidazolium-based ionic liquid-type surfactant as pseudostationary phase in micellar electrokinetic chromatography of highly hydrophilic urinary nucleosides. – *J Chromatogr A*, 2013, 1316, 135–146.
[50] Borissova, M., Palk, K., Koel, M. Micellar electrophoresis using ionic liquids. – *J Chromatogr A*, 2008, 1183, 192–195.
[51] Luczak, J., Hupka, J., Thöming, J., Jungnickel, Ch. Self-organization of imidazolium ionic liquids in aqueous solution. – *Physicochem Eng Aspects*, 2008, 329, 125–133.
[52] Wiedmer, S.K., Lokajová, J. Capillary electromigration techniques for studying interactions between analytes and lipid dispersions. – *J Sep Sci*, 2013, 36, 37–51.
[53] Razak, J.L., Cutak, B.J., Larive, C.K., Lunte, C.E. Correlation of the capacity factor in vesicular electrokinetic chromatography with the octanol:water partition coefficient for charged and neutral analytes. – *Pharm Res*, 2001, 18, 104–111

[54] Barbato, F., Grumetto, L., Carpentiero, C., Rocco, A., Fanali, S., Capillary electrochromatography as a new tool to assess drug affinity for membrane phospholipids. – *J Pharm Biomed Anal*, 2011, 54, 893– 899.
[55] Poole, S.K., Durham, D., Kibbet, C. Rapid method for estimating the octanol-water partition coefficient ($logP_{ow}$) by microemulsion electrokinetic chromatography**.** – *J Chromatogr B, Biomed Sci Appl*, 2000, 745(1), 117– 126.
[56] Lucangioli, S.E., Carducci, C.N., Tripodi, V.P., Kenndler, E.K. Retention of bile salts in micellar electrokinetic chromatography: relation of capacity factor to octanol-water partition coefficient and critical micellar concentration. – *J Chromatogr B*, 2001, 765(2), 113–120.
[57] Orientaite, I., Maruška, A., Pyell, U. Regulation of the retention factor for weak acids in micellar electrokinetic chromatography with cationic surfactant via variation of the chloride concentration. – *Electrophoresis*, 2011, 32, 604–613.
[58] Sheng, Y., Abreu, I.A., Cabelli, D.E. Superoxide Dismutases and Superoxide Reductases. – *Chem Rev*, 2014, 114(7), 3854–3918.
[59] Schaumlöffel, D. Capillary liquid separation techniques with ICP MS detection. – *Anal Bioanal Chem*, 2004, 379(3), 351–354.
[60] Montes-Bayón, M., DeNicola, K., Caruso, J.A. Liquid chromatography-inductively coupled plasma mass spectrometry. – *J Chromatogr A*, 2003, 1000(1-2), 457–476.
[61] Timerbaev, A. R., Element speciation analysis by capillary electrophoresis. – *Talanta*, 52(4), 573–606.
[62] Olšauskaite, V., Paliulionyte, V., Padarauskas, A. Rapid analysis of cation constituents of urine by capillary electrophoresis. – *Clin Chim Acta*, 2000, 293, 181–186.
[63] Sarazin, C., Delaunay, N., Costanza, C., Eudes, V., Gareil, P. Capillary electrophoresis analysis of inorganic cations in post-blast residue extracts applying a guanidinium-based electrolyte and bilayer-coated capillaries. – *Electrophoresis*, 2011, 32, 1282–1291.
[64] Pozdniakova, S., Padarauskas, A. Speciation of metals in different oxidation states by capillary electrophoresis using pre-capillary complexation with complexones. – *Analyst,* 1998, 123, 1497–1500.
[65] Chen, Z.L., Naidu, R. On-column complexation of metal ions using 2,6-pyridinedicarboxylic acid and separation of their anionic complexes by capillary electrophoresis with direct UV detection. – *J Chromatogr A*, 2002, 966, 245–251.
[66] Sarazin, C., Delaunay, N., Verenne, A., Costanza, Ch., Eudes, V., Gareil, P. Simultaneous capillary electrophoretic analysis of inorganic anions and cations in post-blast extracts of acid-aluminum mixtures. – *J Sep Sci*, 2010, 33, 3177–3183.
[67] Soga, T., Ross, G.A. Simultaneous determination of inorganic anions, organic acids and metal cations by capillary electrophoresis. – *J Chromatogr A*, 1999, 834, 65–71.

[68] Zhou, L., Danielson, N.D. The ionic liquid isopropylammonium formate as a mobile phase modifier to improve protein stability during reversed phase liquid chromatography. – *J Chromatogr B*, 2013, 940, 112–120.
[69] Shashkov, M.V., Sidelnikov, V.N. Properties of columns with several pyridinium and imidazolium ionic liquid stationary phases. – *J Chromatogr A*, 2013, 1309, 56–63.
[70] Dertinger, J.J., Walker, A.V. Ionic liquid matrix-enhanced secondary ion mass spectrometry: the role of proton transfer. – *J Am Soc Mass Spectrom*, 2013, 24, 348–355.
[71] Vaher, M., Koel, M., Kazarjan, J., Kaljurand, M. Capillary electrophoretic analysis of neutral carbohydrates using ionic liquids as background electrolytes. – *Electrophoresis*, 2011, 32, 1068 –1073.
[72] Borissova, M., Gorbatsova, J., Ebber, A., Kaljurand, M., Koel, M., Vaher, M. Nonaqueous CE using contactless conductivity detection and ionic liquids as BGEs in ACN. – *Electrophoresis*, 2007, 28, 3600–3605.
[73] Hunter, G.J., Hunter, T. GroESL protects superoxide dismutase (SOD)—Deficient cells against oxidative stress and is a chaperone for SOD. – *Health*, 2013, 5, 1719–1729.
[74] Trinh, C.H., Hunter, T., Stewart, E.E., Phillips, S.E.V., Hunter, G.J. Purification, crystallization and X-ray structures of the two manganese superoxide dismutases from *Caenorhabditis elegans.* – *Acta Crystallogr Sect F Struct Biol Cryst Commun*, 2008, 64, 1110–1114.
[75] Fuguet, E., Reta, M., Gibert, C., et al. Critical evaluation of buffering solutions for pK_a determination by capillary electrophoresis. – *Electrophoresis*, 2008, 29, 2841–2581.
[76] Goldberg, R. N., Kishore, N., Lennen, R. M. Thermodynamic Quantities for the Ionization Reactions of Buffers. – *J Phys Chem Ref Data,* 2002, 31, 231–370.
[77] Wiedmer, S.K., Lokajová, J., Riekkola, M. - L., Marker compounds for the determination of retention factors in EKC. – *J Sep Sci*, 2010, 33, 394–409.
[78] Vanyúr, R., Biczók, L., Miskolczy, Z. Micelle formation of 1-alkyl-3-methylimidazolium bromide ionic liquids in aqueous solution. – *Colloids Surf A Physicochem Eng Asp*, 2007, 299, 256–260.
[79] Fuguet, E., Ráfols, C., Rosés, M., Bosch, E. Critical micelle concentration of surfactants in aqueous buffered and unbuffered systems. – *Anal Chim Acta*, 2005, 548, 95–100.
[80] Qui, H., Mallik, A.K., Takafuji, M., et al. A new imidazolium-embedded C18 stationary phase with enhanced performance in reversed-phase liquid chromatography. – *Anal Chim Acta*, 2012, 738, 95–101.
[81] Singh, S.K., Kundu, A., Kishore, N. Interactions of some amino acids and glycine peptides with aqueous sodium dodecyl sulfate and cetyltrimethylammonium bromide at T=298.15 K: a volumetric approach. – *J Chem Thermodyn*, 2004, 36, 7–16.
[82] Moore, D.S. Amino acid and peptide net charges: A simple calculational procedure. – *Biochem Educ*, 1985, 1, 10–11.

[83] Carrozine, J.M., Khaledi, M.G. Effects on Drug Interactions with Lipid Bilayers by Liposome Electrokinetic Chromatography. – *J Chromatogr A*, 2005, 1079, 307–316.

[84] Khaledi, M.G., Rodgers, A.H. Micellar mediated shifts of ionization constants of amino acids and peptides. – *Anal Chim Acta*, 1990, 239, 121–128.

[85] Fürtös-Matei, A., Li, J., Waldbron, K.C. Micellar electrokinetic chromatographic study of the interaction between enkephalin peptide analogs and charged micelles. – *J Chromatogr B*, 1997, 695, 39–47.

APPENDICES

Appendix 1

Equations describing the dissociation, possible complexation and association equilibria of UPF peptides with borate and/ or charged PSP.

1a $P \leftrightarrow P - O^- + H^+$

1b $P + B^- \leftrightarrow [BP]^-$

1c $\mathrm{P}\text{–}O^- + B^- \leftrightarrow [\mathrm{BP}\text{–}O^-]^{2-}$

1d $P + M^{x+} \leftrightarrow [PM^{x+}]$

1e $P - O^- + M^{x+} \leftrightarrow [(P - O^-)M^{x+}]$

1f $[BP]^- + M^{x+} \leftrightarrow [(BP)^- M^{x+}]$

1g $[BP - O^-]^{2-} + M^{x+} \leftrightarrow [(BP - O^-)^{2-} M^{x+}]$

$$k = \frac{conc_{aq}(P)}{conc_{aq}(P)+conc_{aq}(P-O^-)+conc_{aq}(BP)^-+conc_{aq}(BP-\mathrm{O}^-)^{2-}} k_P + \frac{conc_{aq}(P-O^-)}{conc_{aq}(P)+conc_{aq}(P-O^-)+conc_{aq}(BP)^-+conc_{aq}(BP-O^-)^{2-}} k_{(P-O^-)} + \frac{conc_{aq}(BP)^-}{conc_{aq}(P)+conc_{aq}(P-O^-)+conc_{aq}(BP)^-+conc_{aq}(BP-O^-)^{2-}} k_{(BP)^-} + \frac{conc_{aq}(BP-O^-)^{2-}}{conc_{aq}(P)+conc_{aq}(P-O^-)+conc_{aq}(BP)^-+conc_{aq}(BP-O^-)^{2-}} k_{(BP-O^-)^{2-}}$$

$$k = \frac{conc_{aq}(BP)^-}{conc_{aq}(BP)^-+conc_{aq}(BP-O^-)^{2-}} k_{(BP)^-} + \frac{conc_{aq}(BP-O^-)^{2-}}{conc_{aq}(BP)^-+conc_{aq}(BP-O^-)^{2-}} k_{(BP-O^-)^{2-}}$$

where P denotes (UPF) peptide, B^- is tetrahydroxyborate anion, $[BP]^-$ is the complexed form of the peptide, $P\text{–}O^-$ symbolizes the deprotonated form of the peptide, $[BP\text{–}O^-]^{2-}$ denotes the complexed deprotonated form of the peptide, x designates an effective charge number, M^{x+} micelle, $conc_{aq}(P)$ is the molar concentration of the neutral form in the micellar BGE, $conc_{aq}$ $(P\text{–}O^-)$ is the molar concentration of the deprotonated form in the micellar BGE, $conc_{aq}(BP)^-$ is the molar concentration of the complexed form in the micellar BGE, $conc_{aq}$ $(BP\text{–}O^-)^{2-}$ is the molar concentration of the complexed deprotonated form in the micellar BGE , k_P is the retention factor of protonated form, $k_{(P\text{–}O^-)}$ is the retention factor of the deprotonated form, $k_{(BP)^-}$ is the retention factor of complexed form, $k_{(BP\text{–}O^-)^{2-}}$ is the retention factor of the complexed deprotonated form.

Electropherograms of apo-FeSOD (A), apo-FeSOD with added Fe^{3+} (B), apo-MnSOD with added Mn^{2+} (C), apo-MnSOD (D)
Peak identification: *3- Fe^{3+}, 4- Mn^{2+}*

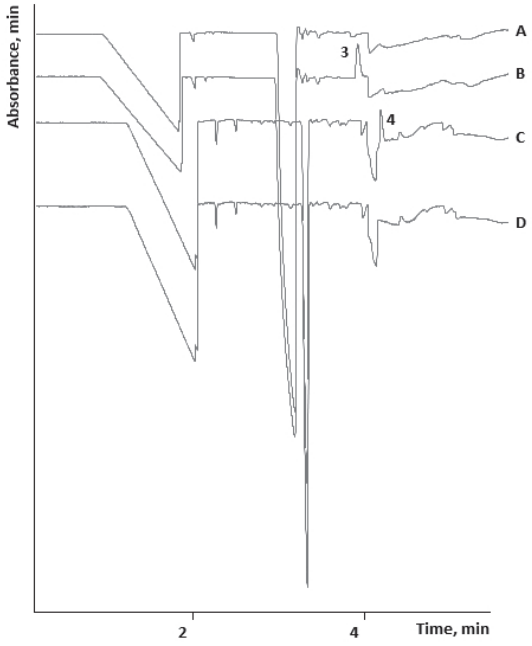

Appendix 3

Analytical parameters of the developed CE method (n=4)

	Calibration equation	R^2	LOD µg/ mL	Corrected peak area RSD%	Migration time RSD%
Cu^{2+}	y = 1.4005x - 0.2242	0.9992	0.3	1.32	1.46
Zn^{2+}	y = 0.568x - 0.8354	0.9922	1.0	5.38	2.67
Mn^{2+}	y = 0.5018x + 0.2798	0.9976	0.5	1.89	4.94
Fe^{3+}	y = 0.5034x - 1.5792	0.9959	1.2	0.96	2.29

Electropherogram showing the effect of C_{14}MImCl concentration on the interaction between monomeric and homodimeric forms of UPF50 and the corresponding micelles.

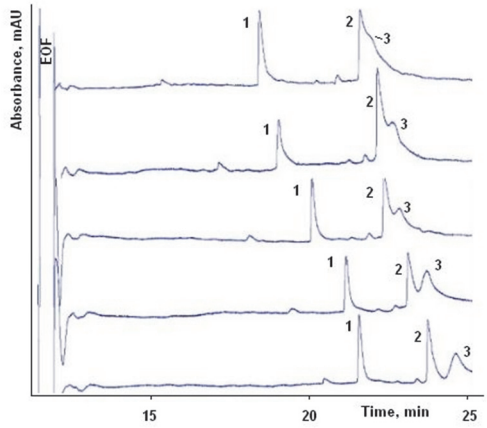

CE and MEKC conditions: fused-silica capillary 60/51.5cm (L_{tot}/L_{eff}), id 50 µm, detection 200 nm and 230 nm, capillary temperature 25 °C, applied voltage -10 kV (micellar BGE with C_{14}MImCl and CTAB) and +10 kV (non-micellar BGE and micellar BGE with SDS).
1-tetradecyl-3 methylimidazolium chloride concentration increases from top to bottom of the electropherogram.
The ionic strength of all buffers was held constant at 35 mM.

1- UPF50 monomer
2- UPF50 homodimer
3- dodecylbenzene

Log *k* values of the retention factors of the reduced and oxidized forms of GSH analogues.

The log *k* values of the retention factors of monomeric and dimeric forms of GSH analogues were in the range of 0.95–2.22 (RSD% 1.10–8.87) for UPF17, 0.90–2.13 (RSD% 2.82–8.10) for UPF1, 0.36–2.22 (RSD% 1.92–8.43) for UPF51, 0.42–1.90 (RSD% 2.90–8.60) for UPF50, -1.21–0.37 (RSD% 2.24–6.38) for GSH when C_{14}MImCl was used as a pseudostationary phase (PSP).
When CTAB was employed as PSP for determination of the retention factors of monomeric and dimeric forms of UPF peptides, the log *k* values were in the range of 0.91–2.11 (RSD% 4.90–9.94) for UPF17, 0.80–2.17 (RSD% 2.34–9.40) for UPF1, 0.27–1.69 (RSD% 2.50–11.70) for UPF51, 0.28–1.38 (RSD% 1.64–9.21) for UPF50, -1.22–0.06 (RSD% 1.60–10.30) for GSH.

ACKNOWLEDGEMENTS

This research was carried out at the Chair of Analytical Chemistry of the Department of Chemistry at Tallinn University of Technology (TUT).
There are quite a number of persons whom I would like to thank for all the support and help offered to me throughout my research. I am indebted forever to my committed supervisors- Dr. Merike Vaher for her unrelenting support throughout this research and Professor Mihkel Kaljurand for his valuable guidance and assistance during my Ph.D. studies.
I thank my colleagues at TUT who kindly shared their experinces: Dr. Mihkel Koel, Dr. Jelena Gorbatšova, Dr. Maria Kuhtinskaja, Dr. Maria Kulp and Aini Vaarmann. I wish to convey my warm thanks to Tiina Ait and Piret Saar-Reismaa for their sincere willingness to help. I thank all my labmates at TUT: Maria Fomitšenko, Ekaterina Mazina, Heidi Lees, Piia Jõul and Eeva-Gerda Kobrin, who in some way or another were helpful during my Ph.D. studies. I also thank the colleagues from the University of Tartu who were involved in this research.
I am grateful to Professor Gary James Hunter and Dr. Thérèse Hunter from the Department of Physiology and Biochemistry, University of Malta (UoM) for giving me the opportunity to work in their research group. I am also thankful to Dr. Rosalin Bonetta and Ms. Marita Vella for their invaluable guidance and help during my stay at UoM.
Last but not least, this work was supported by the Estonian Science Foundation, the Ministry of Education and Research, and the European Union through the European Regional Development Fund. This work was also partly supported by the Graduate School “Functional materials and technologies”. The international programme DoRa activity 6 “Development of international cooperation networks by supporting the mobility of Estonian doctoral” and activity 8 “Participation of Young Researchers in the International Circulation” are acknowledged as well.
Most importantly of all, I would like to express my heartfelt thanks to every member of my family, including my closest friend Dr. Jelena Suhhova for their unremitting encouragement and support.

ABSTRACT

This thesis describes the development of capillary electrophoretic techniques for investigation of endogenous antioxidants (glutathione, superoxide dismutase enzymes) and their synthetic analogues (glutathione analogues aka UPF peptides). These antioxidant defensive systems contribute to the biodiversity of mechanisms for the removal of reactive oxygen species (ROS) and ultimately, SOD and GSH work synergically against free radical damage. Under certain diseased conditions, GSH pool depletion occurs leading to ROS/antioxidant imbalance and, as a result, an oxidative stress is developed. Administrating GSH directly to overcome this problem is complicated due to the low bioavailability of the latter. Therefore there is a need to design GSH analogues as potential pharmaceuticals that will possess similar antioxidative properties like glutathione but have a higher chance to penetrate through the membranes. When the passive absorption of compounds across anisotropic and charged biomembranes is under question, the knowledge of the acid dissociation (pK_a) constants of compounds and partitioning mechanisms (log k) of ionized compounds like UPF peptides are of vital importance and should be determined in the first place. Thereby, the constant search for new potential drugs has caused an increased demand for the development of fast, accurate and sensitive analytical techniques that can overcome problems of low quantities, impurities and unstable nature of compounds of interest during the early stages of the drug development process and exploratory studies. Special attention is devoted to the capillary electrophoresis (CE) method – an important analytical tool that has prominent benefits such as high speed of separation, low background electrolyte and sample requirements, ease of operation and automation. Besides, an often-required step in sample preparation for CE analysis is dilution only. This all makes capillary electrophoresis a promising analytical method for clinical chemists in the early stages of drug development processes. Diverse applications of CE techniques include not only estimation of pK_a and log k values for physicochemical profiling in early drug (UPF peptide) discovery stages, but also metal cofactor determination in superoxide dismutase enzymes, which is an essential step in the characterization of SOD. Different metal cofactors present in various forms of SOD enzymes ensure redox cycling resulting in the disproportionation of the superoxide radical into molecular oxygen and hydrogen peroxide. The SOD activity depends on the effective metal ion acquisition and the degree of metalation, therefore measurement of metal content is crucial in characterizing enzyme biological activity. Therefore, a capillary electrophoresis protocol was developed for the simultaneous determination of transition metal content in superoxide dismutase enzymes as an important step in understanding the SOD activity.

KOKKUVÕTE

Antud töö on pühendatud kapillaarelektroforeetiliste metoodikate väljatöötamisele endogeensete antioksüdantide [glutatioon (GSH), superoksiiddismutaas (SOD)] ja nende sünteetiliste analoogide (glutatiooni analoogide ehk UPF-peptiidide) uurimiseks. Need antioksüdantsed kaitsesüsteemid toetavad mitmesuguste bioloogiliste kaitsemehhanismide toimimist, eemaldamaks aktiivset hapnikku sisaldavaid osakesi (ROS), kusjuures SOD ja GSH toimivad sünergiliselt vabaradikaalse kahjustuse vältimiseks. Teatud haiguste korral ilmneb GSH varude kahanemine, põhjustades ROS/antioksüdant tasakaalu rikkumist ning seega oksüdatiivse stressi tekkimist. Madala omastatavuse tõttu on GSH otsene manustamine selle probleemi ületamiseks raskendatud. Seetõttu kerkib esile vajadus välja arendada (disainida) GSH analoogid, et luua glutatiooni-taoliste antioksüdatiivsete omadustega, kuid kõrgema membraaniläbimisvõimega potentsiaalseid ravimeid. Tingimustes, mil ühendite passiivne absorptsioon läbi anisotroopsete ja laetud biomembraanide on küsitav, võib ioniseeritud ühendite (nt UPF-peptiidide) happelise dissotsiatsiooni konstandi (pK_a) ja jaotuskonstandi ($log\ k$) teadmine olla eluliselt oluline ning nende määramine esmatähtis. Seega, vajadus konstantide määramiseks uute potentsiaalsete ravimite loomisel põhjustab kasvava nõudluse kiirete, täpsete ja tundlike analüüsimetoodikate järele, mis võimaldaksid ületada väikeste määratavate koguste, rohkete lisandite ning ühendite labiilsusega seotud probleeme juba ravimi uurimusliku ja arendusliku etapi varajastes staadiumites.

SOD-ensüümides esinevad metall-kofaktorid, mis tagavad redokstsükliseerumise, mille tulemuseks on superoksiidradikaali disproportsioneerumine hapnikuks ja vesinikperoksiidiks. Kuna SOD-i aktiivsus sõltub efektiivse metalliiooni kättesaadavusest ja metallisisalduse määrast, siis on metallisisalduse mõõtmine ensüümi bioloogilise aktiivsuse iseloomustamisel keskse tähtsusega.

Käesolevas töös on metoodikate arendamisel pööratud erilist tähelepanu kapillaarelektroforeesile (CE) ja tema alaliigile mitsellaarsele elektrokineetilisele kromatograafiale (MEKC), analüüsimeetodile, millel on sellised olulised eelised nagu suur lahutuskiirus, efektiivsus, madalad nõudmised taustelektrolüüdi ja proovi osas, käitlemise lihtsus ning automatiseerimise võimalus.

Järgnevalt on esitatud töö põhitulemused:

Arendati välja kapillaarelektroforeesi protokollid glutatiooni ja selle analoogide üheaegseks lahutamiseks ning seejärel nende peptiidide dissotsiatsioonikonstantide määramiseks. Peptiidide lahutuvust uuriti laias pH vahemikus (7,40–10,00), kasutades erinevate kontsentratsiooniga (50–250 mM) anorgaanilisi (fosfaat ja boraat) ning tsvitterioonseid (CHES, TES and MOPS) puhvreid/taustelektrolüüte. Dissotsiatsioonikonstantide määramiseks mõõdeti peptiidide efektiivsed elektroforeetilised mobiilsused pH vahemikus 5,50–10,00, kasutades optimeeritud taustelektrolüüte (CHES, TES, MOPS ja atsetaati) ioontugevusega 50 mM. Uuriti UPF-peptiidide ja nende homodimeeride vahelisi interaktsioone sõltuvalt ioonsete pindaktiivsete ainete tüüpidest ja kontsentratsioonist, kasutades MEKC meetodikat. Füsioloogilise pH juures mõõdeti negatiivselt laetud GSH

analoogide jaotuskonstandid, kasutades nii katioonseid (C_{14}MImCl, CTAB) kui ka anioonseid (SDS) mitsellaarseid süsteeme. Leiti, et peptiid-mitsell interaktsioonid kasvavad nii pH kui ka pindaktiivse aine kontsentratsiooni kasvuga. Katioonsete mitsellide puhul täheldati tugevamaid interaktsioone C_{14}MImCl-ga, mis võib olla tingitud suurema arvu interaktsioonisaitide olemasolust imidazooliumi ioonis. Hüdrofoobsed interaktsioonid monomeersete UPF-peptiidide ja katioonsete mitsellide vahel on nõrgemad kui elektrostaatilised mõjud.

Määrati siirdemetallide sisaldus superoksiiddismutaasides, millel on oluline osa selle ensüümi aktiivsuse mõistmisel. Selleks töötati välja ja valideeriti kiire, lihtne ning kuluefektiivne CE protokoll, mis võimaldas Cu^{2+}, Zn^{2+}, Fe^{3+} and Mn^{2+} üheaegset määramist.

Kokkuvõtteks – kapillaarelektroforees on sobiv meetod erinevate aineklasside füsikokeemiliste parameetrite mõõtmisteks.

ORIGINAL PUBLICATIONS

Publication I

Kazarjan, J., Vaher, M., Mahlapuu, R., Hansen, M., Soomets, U., Kaljurand. M. Separation of glutathione and its novel analogues and determination of their dissociation constants by capillary electrophoresis. – *Electrophoresis,* 2013, 34, 1820-1827.

Jana Kazarjan[1]
Merike Vaher[1]
Riina Mahlapuu[2]
Mats Hansen[2]
Ursel Soomets[2]
Mihkel Kaljurand[1]

[1]Department of Chemistry, Tallinn University of Technology, Tallinn, Estonia
[2]The Centre of Excellence for Translational Medicine, Faculty of Medicine, Department of Biochemistry, University of Tartu, Tartu, Estonia

Received May 24, 2012
Revised February 16, 2013
Accepted February 17, 2013

Research Article

Separation of glutathione and its novel analogues and determination of their dissociation constants by capillary electrophoresis

A CE protocol was developed to separate reduced glutathione and its four novel analogues UPF1 (Tyr(Me)-γ-Glu-Cys-Gly), UPF17 (Tyr(Me)-α-Glu-Cys-Gly), UPF50 (β-Ala-His-Tyr(Me)-γ-Glu-Cys-Gly), and UPF51 (β-Ala-His-Tyr(Me)-α-Glu-Cys-Gly), and their homo- and heterodimers by varying the ionic strength and/or pH of different BGEs. For the determination of dissociation constants (pK_a) of the above-mentioned peptides the CE method was used. Effective electrophoretic mobilities of analytes were measured in the pH range 5.50–10.00 using optimized BGE with an ionic strength of 50 mM at 25°C. pK_a values were calculated by fitting the experimental points to a suitable model with correlation coefficients higher than 0.99. The pK_a values for imidazolyl, amino and thiol moieties of the analyzed peptides were in the range 5.94–6.29, 8.81–9.10, and 7.86–8.13, respectively.

Keywords:
Capillary electrophoresis / pK_a Determination / Separation of GSH analogues
DOI 10.1002/elps.201200611

1 Introduction

1.1 General

Glutathione (GSH) is the most abundant intracellular low molecular weight nonenzymatic thiol-containing compound in cells and has many important biological functions such as direct scavenging of free radicals, detoxification, and many regulatory roles, etc. [1]. After the scavenging of oxyradicals, an oxidized glutathione disulfide (GSSG) is formed. Maintaining the GSH/GSSG ratio is a vital cellular mechanism to ensure intracellular homeostasis. The reducing environment within the cells is very important for redox enzyme regulation, cell cycle progression, transcription of antioxidant response elements, and regulation of many other cellular processes [2–7].

Cells under stress and in many diseased states commonly experience GSH pool depletion. However, the administration of GSH directly to alleviate this problem is complicated by excessive extracellular degradation and poor cellular uptake of the compound. Thus, there is a high interest to design GSH analogues as possible new bioactive compounds for pharmacological applications. In an effort toward this goal, new tetrapeptide analogues of GSH called UPFs, have been synthesized [8]. Among them, UPF1 and UPF17 are of biological interest because they possess antioxidative activities [9]. Their effect on different isolated cells has also been investigated [10–12].

The physiochemical properties of these new compounds must be precisely determined prior to pharmaceutical use. Knowledge of pK_a values also aids in the biological studies of their metabolism, biological transport, chemical reactivity, adsorption, etc. Traditional techniques to determine pK_a values, such as potentiometric titration or spectroscopic methods, typically require large amounts of material with high purity. However, it is often prohibitively difficult to obtain compounds in this form, especially at early stages in process development and in exploratory studies. Thus, development of alternative methods is a necessary and useful scientific pursuit.

CE is widely used in the determination and separation of GSH and its oxidation products [13, 14]. Besides CE, it is possible to determine both GSH and GSSG by HPLC, although sensitivity may need to be improved using fluorescent derivatizing or electrochemical detection [15, 16]. GSH separation may also be accomplished in real time using thermospray LC-MS [17]. Occasionally, HPLC suffers from low selectivity when applied to solve particular problems. Furthermore, a long time is required to separate GSH from its

Correspondence: Jana Kazarjan, Department of Chemistry, Tallinn University of Technology, Akadeemia tee 15, 12618 Tallinn, Estonia
E-mail: jana.kazarjan@gmail.com
Fax: +372-620-43-25

Abbreviations: GSH, glutathione; **GSSG**, glutathione disulfide; **TES**, 2-[[1,3-dihydroxy-2-(hydroxymethyl)propan-2-yl]amino]ethanesulfonic acid

Colour Online: See the article online to view Figs. 2, 4 and 5 in colour.

oxidation products. In comparison with other techniques the CE method has remarkable benefits such as high speed of separation and low consumption of both the sample and buffer. Hence, CE is extensively used in the separation of proteins and peptides under various conditions [18, 19]. CE has several benefits compared to other methods: it requires a very small quantity of material, which may be relatively unstable and impurities do not disturb the measurements [20].

CE has been extensively used for the determination of pK_a values for different analytes such as amino acids and peptides in both aqueous and hydro-organic conditions [21–24]. The determination of pK_a by CE is based on the measurement of variation of migration times of the analyte as a function of pH of the background electrolyte.

The main goal of the present study was to develop a suitable separation protocol for GSH and its four newly synthesized analogues: UPF1 (Tyr(Me)-γ-Glu-Cys-Gly), UPF17 (Tyr(Me)-α-Glu-Cys-Gly), UPF50 (β-Ala-His-Tyr(Me)-γ-Glu-Cys-Gly), and UPF51 (β-Ala-His-Tyr(Me)-α-Glu-Cys-Gly), as well as their homo- and heterodimers and to determine the pK_a values of compounds.

In this work peptides UPF50 and UPF51 were synthesized by us and described for the first time ever.

In the determination of optimal CE separation conditions (composition and pH of BGE, additives to support peptide solubility, change/ improve selectivity, etc.) of the above-mentioned peptides, we followed the main rules for a rational selection of experimental conditions for peptides in general [25–28].

1.2 Theoretical background

If an acid HA deprotonates, then the effective mobility in a predefined BGE is given as $\mu_e = \beta \cdot \mu_{A^-}$, where μ_{A^-} is the ionic mobility of the fully deprotonated substance (A^-) and β is the fraction of the ionized analyte. The relationship between effective mobility, μ_e, pH of BGE, and p*K*a of an analyte for diluted solutions can be expressed as follows:

$$\mu_e = \frac{\mu_{A^-}}{1 + 10^{(pH - pK_a)}}. \quad (1)$$

The effective mobility of an ion was calculated as follows:

$$\mu_e = \frac{L_{tot} \cdot L_{eff}}{V}\left(\frac{1}{t_{app}} - \frac{1}{t_{EOF}}\right), \quad (2)$$

where L_{eff} is the distance between the injection point and the detector, L_{tot} is the total capillary length, t_{app} is the migration time of an analyte, t_{EOF} is the migration time of a neutral marker compound, v_{app} is the apparent velocity, and V is the applied voltage.

Experimentally, pK_a values are measured on the basis of migration times of analytes and the neutral marker in the background electrolyte of constant ionic strength at a given temperature and by varying the pH over a certain range.

From the relationship between the calculated effective mobilities and the pH of the electrolyte, a curve identical to a Boltzmann sigmoid [29] (Eq. (1)) is obtained for each analyte.

The curve can be fitted with the nonlinear regression model where two unknowns—the mobility of the fully ionized species and pK_a (depends on the number of the ionizable groups)—are regression parameters. For concentrated solutions, the pK_a values should be corrected for the ionic strength of the BGE according to the well-known Debye–Hückel theory.

2 Materials and methods

2.1 Synthesis of GSH analogues

All Fmoc-L-amino acids were purchased from Novabiochem (Merck-Millipore, Hohenbrunn, Germany), except Fmoc-L-Tyr(Me)-OH, which was sourced from CBL Patras (Patras, Greece). All the other reagents used to synthesize peptides were purchased from Merck Chemicals (Merck-Millipore).

Peptides UPF1 (Tyr(Me)-γ-Glu-Cys-Gly), UPF17 (Tyr(Me)-α-Glu-Cys-Gly), UPF50 (β-Ala-His-Tyr(Me)-γ-Glu-Cys-Gly), and UPF51 (β-Ala-His-Tyr(Me)-α-Glu-Cys-Gly) were synthesized by us on a Fmoc-Gly-Wang resin from Novabiochem (Merck-Millipore), utilizing a standard Fmoc solid-phase peptide synthesis [10].

In order to enhance the antioxidant properties and bioavailability of GSH analogues UPF1 and UPF17, two novel analogues with additional carnosine (β-Ala-His) dipeptides in the N-termini of the peptides were designed. We named these UPF50 and UPF51, respectively (Fig. 1).

2.2 Reagents and chemicals

Peptides GSH and GSSG, disodium hydrogen phosphate, sodium dihydrogen phosphate, CHES, MOPS, 2-[[1,3-dihydroxy-2-(hydroxymethyl)propan-2-yl] amino] ethanesulfonic acid (TES), and ammonium acetate, as well as 2, 5- dihydroxybensoic acid used as the MALDI matrix, were obtained from Sigma-Aldrich (Steinheim, Germany). Sodium hydroxide and boric and acetic acids were purchased from Riedel-de Haën (Germany).

Milli-Q water (MilliQ, Millipore S. A. Molsheim, France) was used for all solutions of standards, preparation of BGEs, dilution of samples and preparation of stock solutions of GSH, and its four analogues UPF1, UPF17, UPF50, and UPF51. All stock solutions were stored at −18°C.

BGEs used in CE where boric acid (stock 500 mM), Na_2HPO_4/NaH_2PO_4 buffer (stock 100 mM), CHES (stock 500 mM), MOPS (stock 500 mM), TES (stock 500 mM), and acetic acid (stock 100 mM) with pH adjusted to the respective pH level by 1 M sodium hydroxide or 1 M ammonium hydroxide. All running buffers were filtered through a 0.45 μm syringe filter (Millipore, Bedford, MA, USA) and

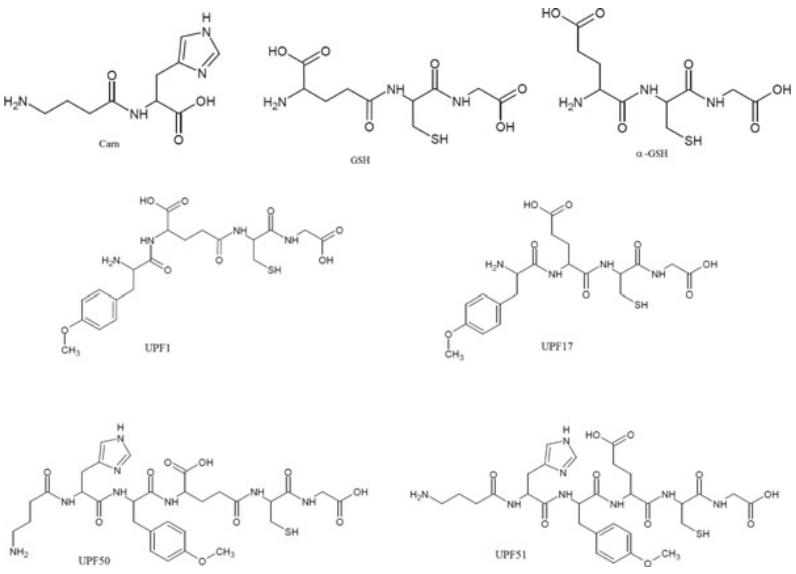

Figure 1. General structure of UPF peptides and their fragments.

stored at 8°C until used, except ammonium acetate that was made freshly just before analysis.

The following chemicals used as neutral markers, that is mesityl oxide, benzene, acetone, DMSO and DMF, were obtained from Lachema (Brno, Czech Republic).

All reagents and chemicals used in all experiments were of analytical reagent grade.

2.3 Instrumentation

An Agilent 3D instrument (Agilent Technologies, Waldbronn, Germany) equipped with a UV/Vis DAD was used for the separation and determination of pK_a values of peptides.

A fused-silica capillary (Polymicro Technologies, Phoenix, AZ, USA) with an internal diameter of 50 μm and a length of 51.5/60 cm (L_{eff}/L_{tot}) was employed in the experiments. The separation voltage was +20/+25 kV. The analytes were detected by DAD at 195 nm. Sample solutions were introduced at the anionic end of the capillary with 50 mbar pressure for 10 s. The temperature of the capillary was set at 25°C. All electropherograms were recorded and integrated with Agilent ChemStation software. In order to minimize the hysteresis effect and/or equilibrate the capillary wall, it was preconditioned prior to performing measurements by sequentially rinsing it with 1 M sodium hydroxide and Milli-Q water.

Between runs, the capillary was rinsed with 1 M sodium hydroxide for 5 min, Milli-Q water for 3 min, and the BGE solution for 5 min.

The pH value of the electrolyte solution was measured with a Metrohm 744 pH meter equipped with a combination electrode (Metrohm, Herisau, Switzerland) that had been calibrated with commercial buffers at pH 7.00 (±0.01), pH 10.00 (±0.01), and pH 12.00 (±0.01) (Sigma-Aldrich).

MALDI-TOF-MS analysis was carried out in the delayed extraction (20–100 ns) positive-ion reflection mode on a Bruker Autoflex II mass spectrometer (Bruker Daltonics, Denmark) equipped with a nitrogen laser (337 nm). The laser power was set to obtain a good S/N (approx. 50%), and the mass range of 250–1650 m/z was scanned.

3 Results and discussion

3.1 Choice of electroosmotic marker

A neutral marker was added to the BGE to determine EOF mobility. Mesityl oxide, benzene, DMSO, acetone, and DMF were tested by varying their concentrations. Eventually, DMF was chosen as a neutral marker in order to perform CE separation of the above-mentioned peptides and to calculate the effective mobilities of the analytes. DMF gives a high absorbance and good peak symmetry and it does not interact with these analytes.

3.2 Separation and identification of peptides

The CE method presented here is optimized for simultaneous separation and identification, and, as a further step, for

determination of the pK_a values of UPF1/17 and UPF50/51 peptides as well as their homo- and heterodimers.

The separability of peptides was inspected in a broad pH range (5.50–10.00) and the results were in agreement with the rule of thumb, which states that the separation of peptides is most likely to be achieved in BGEs of pH around the pK_a values of analytes. The pK_a values of the peptides under study were expected to be around 9, according to that of the reduced GSH.

3.2.1 Inorganic buffers

At first the separation of both mixtures consisting of UPF1, UPF50, GSH or UPF17, UPF51, GSH and their homo- and heterodimers was performed using 50 mM phosphate buffers (pH 7.40, 7.80, and 8.20), but no baseline separation of peptides was achieved.

In order to improve the peak shape and separation selectivity boric acid at different concentrations (50–250 mM) and pH values (7.40–10.00) was investigated.

Efficiency and selectivity improved when buffer ionic strength was increased; migration times and resolution increased with increasing borate concentration. At higher boric acid concentrations (250 mM and higher) and pH values (>9), the heat dissipation was insufficient. This destabilized the current and the signal was corrupted due to baseline fluctuation. On the other hand, at boric acid concentrations lower than 200 mM, the heat dissipation problem was solved even at high pH values, however, the separation of some peptides was poor and baseline separation was not achieved.

The pH of BGE plays a dual role in CE: it influences not only the magnitude of the EOF generated but also the amount of the ionizable species.

Figure 2 shows that at the boric acid concentration of 200 mM the optimal pH for the separation of one of the peptide mixtures (UPF51, UPF17, and GSH) was 8.45.

The separation of UPF1, UPF17, UPF50, and UPF51, as well as their homo- and heterodimers mixture was not achieved because of the same molecular weight of the analytes.

At greater or smaller pH values than the optimal pH of 8.45, the total selectivity decreased and the baseline separation of some peaks was not achieved. The CE analysis of the peptide mixture (UPF51, UPF17, and GSH) with pH values 8.45 and 7.40 was performed at different times, thus the formation of homo- and heterodimers increased in time (pH 7.40); hence, peak intensities increased compared to those obtained at pH 8.45.

The peaks of peptides in each electropherogram (Fig. 2) were identified using the standard addition method and comparing their UV spectra.

First, to identify a homodimer, a solution of the corresponding individual peptide was kept at room temperature for 24 h in order to allow peptide to dimerize. The formed homodimer was confirmed by MALDI-TOF-MS (data not shown). Then the CE separation of the dimerized sample

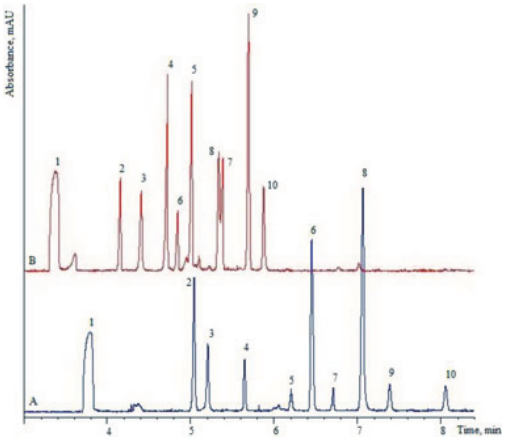

Figure 2. Electropherograms of UPF51, UPF17, and GSH and their homo- and heterodimers at different pH values. CE conditions: 200 mM boric acid as BGE, capillary length 60 cm (51.5 cm to detector), detection at 195 nm, capillary temperature 25°C, injection pressure 50 mbar for 10 s, applied voltage 25 kV. (A) pH 8.45 and (B) pH 7.40. Peak identification: 1—DMF, 2—UPF51, 3—UPF51 homodimer, 4—UPF51 – GSH heterodimer, 5—UPF51 – UPF17 heterodimer, 6—GSH, 7—GSSG, 8—UPF17, 9—UPF17 – GSH heterodimer, 10—UPF17 homodimer.

was carried out and the recorded electropherogram with one peak corresponding to the homodimer was compared with the electropherogram of the unreacted standard that had two peaks, one corresponding to the reduced form of the peptide and the other to its oxidized form (homodimer). Similarly, the solution of two different peptides was allowed to form homo- and heterodimers.

The combination of pairs was as follows: UPF51 + UPF 17, UPF51 + GSH, UPF17 + GSH and UPF50 + UPF 1, UPF50 + GSH, UPF1 + GSH.

The CE separation of the mixture of two peptides afforded five peaks on the electropherogram whose two peaks corresponded to the reduced form of peptides, two to their oxidized form—homodimers, and one extra peak that was associated with the corresponding mixed dimer–heterodimer. The peaks were also confirmed using MALDI-TOF-MS (data not shown).

The mixture consisting of UPF51, GSH, and UPF17 was made and kept at room temperature for 24 h in order to let homo- and heterodimers of the mentioned peptides form. Then the reaction mixture was subjected to MALDI-TOF-MS analysis and mass spectra of the reaction products of oxidation of the UPF51, GSH, and UPF17 mixture were obtained (Fig. 3). Shortly, the CE separation was carried out with the same mixture and the electropherogram revealed five peaks: two belonging to homodimers and three to heterodimers, the reduced forms were absent, which means that the peptides were completely oxidized.

The migration order of peptides at pH 8.45 was as follows: UPF51, UPF51 homodimer, UPF51 – GSH heterodimer,

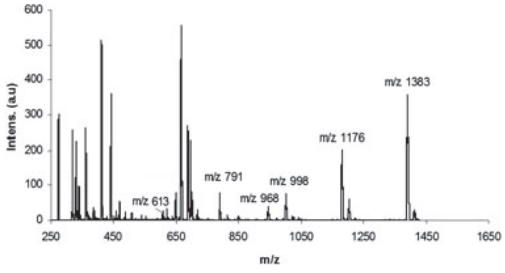

Figure 3. Mass spectra of the oxidation reaction products of the mixture of UPF51, GSH, and UPF17. GSSG—613 Da, GSH–UPF17 heterodimer—791 Da, UPF17 homodimer—968 Da, GSH–UPF51 heterodimer—998 Da, UPF51 – UPF17 heterodimer—1176 Da, UPF51 homodimer—1383 Da.

UPF51 – UPF17 heterodimer, GSH, GSSG, UPF17, UPF17 – GSH heterodimer, with the last migrating species being the UPF17 homodimer. Compared to pH 7.40, the migration order of UPF51 and UPF17 heterodimer, GSH, UPF17, and GSSG peptides had changed, indicating that in this case, the migration behavior does not depend clearly on the pK_a value only, but maybe also on specific interactions between the peptides being analyzed and the $B(OH)_3/B(OH)_4^-$ buffer used [30, 31].

The same procedures were performed with the mixture of UPF50, UPF1, and GSH peptides and the results obtained were in agreement with the above.

3.2.2 Zwitterionic buffers

For the separation of a mixture consisting of UPF1/17, UPF50/51, and GSH peptides, zwitterionic buffers (CHES/CHES$^-$, TES/TES$^-$, MOPS/MOPS$^-$) with concentrations of from 50 to 200 mM and pH indicated in Table 1, were also tested.

CHES/CHES$^-$ (pK_a = 9.39) and $B(OH)_3/B(OH)_4^-$ (pK_a = 9.24) buffers were tested for the ability to separate the above-mentioned mixture of peptides by varying the concentrations from 50 to 200 mM and pH from 8.45 to 10.00 and the results were compared. The optimal pH for the separation of peptides was the same for both the CHES/CHES$^-$ buffer and the $B(OH)_3/B(OH)_4^-$ buffer (pH 8.45). The selectivities for different concentrations (50–200 mM) of CHES/CHES$^-$ and $B(OH)_3/B(OH)_4^-$ buffers with fixed pH of 8.45 remained in the range of 1.02–1.27. No significant differences in selectivity between the buffers of different concentrations were noted. The CHES/CHES$^-$ buffer had a slightly higher selectivity at 50 mM and the $B(OH)_3/B(OH)_4^-$ buffer at 200 mM.

In addition to selectivity, the number of theoretical plates (50–200 mM) at pH 8.45 for CHES/CHES$^-$ and $B(OH)_3/B(OH)_4^-$ buffers was calculated. For both buffers the average efficiency was more than one million.

The migration order of peptides (CHES/CHES$^-$ buffer at pH 8.45) was as follows: UPF51 peptide, UPF51 homodimer, UPF51 – GSH heterodimer, GSH, UPF51 – UPF17 heterodimer, GSSG, UPF17, UPF17 – GSH heterodimer, with the last migrating species being the UPF17 homodimer (Fig. 4A). Compared to the $B(OH)_3/B(OH)_4^-$ buffer at the same pH of 8.45, the migration order of GSH and UPF51 – UPF17 heterodimer had changed.

The TES/TES$^-$ buffer at pH 8.45 (50 mM) was also tested. The migration order of the analytes was identical with that in case of the CHES/CHES$^-$ buffer at the same pH of 8.45 (50 mM). Compared to pH 8.45, at pH 7.80 (TES/TES$^-$, 50 mM) the migration order of UPF17 and GSSG had changed (Fig. 4B).

The migration order variations can also be observed when 50 mM CHES/CHES $^-$ buffer is used at different pHs (e.g. 8.45, 8.70, and 9.55).

These variations are probably due to the differences in the distribution order of pK_a values of individual ionogenic groups between GSH and UPF51 – UPF17 heterodimer and UPF17 and GSSG.

The MOPS/MOPS$^-$ buffer showed analogous results. The same procedures were performed with the mixture of UPF50, UPF1, and GSH peptides and the results were in conformity with those obtained with other buffers.

In general, an inorganic buffer $B(OH)_3/B(OH)_4^-$ and zwitterionic buffers like CHES/CHES$^-$, TES/TES$^-$, and MOPS/MOPS$^-$ showed good separability within the pH range from 7.40 to 9.05 at pH close to the pK_a values of analytes Thus, they can be used in separation of the mixture consisting of UPF1/17, UPF50/51, and GSH peptides and their homo- and heterodimers. For separation of the above-mentioned peptides, the $B(OH)_3/B(OH)_4^-$ buffer may be preferred because of the high transparency of boric acid in the UV light compared to CHES/CHES$^-$, TES/TES$^-$, and MOPS/MOPS$^-$ buffers.

Table 1. Composition of BGEs

pH range covered	Buffer constituents	pK_a[a)]
8.45–10.00	$B(OH)_3/B(OH)_4^-$	9.24
7.40–8.20	$H_2PO_4^-/HPO_4^{2-}$	7.21
6.10–5.50	CH_3COOH/CH_3COO^-	4.76
8.45–10.00	CHES/CHES$^-$	9.39
7.80–8.45	TES/TES$^-$	7.55
7.40–7.80	MOPS/MOPS$^-$	7.18

a) pK_a values are from [30, 32].

3.3 Determination of acidity constants

Because most biological reactions take place at or near neutral/basic pH between 6 and 8, the pK_a values of imidazolyl, thiol (if present in the molecule) and/or amino groups were measured.

Generally, in order to measure the pK_a value of an unknown substance, it is necessary to cover a wide pH range. In this work, we employed buffers that covered the pH range from 5.50 to 10.00 (Table 1).

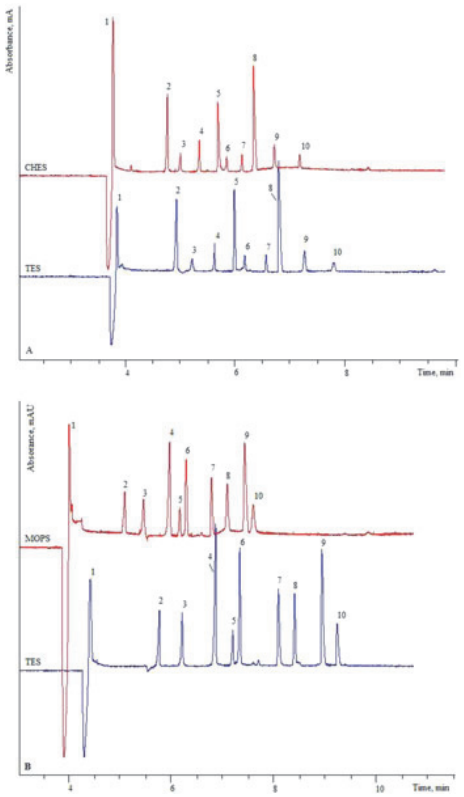

Figure 4. Separation of peptides using CHES/CHES$^-$, TES/TES$^-$, and MOPS/MOPS$^-$ buffers. CE conditions: ionic strength 50 mM, other conditions as in Fig. 2. (A) CHES/CHES$^-$, TES/TES$^-$ buffers at pH 8.45, (B) TES/TES$^-$ and MOPS/MOPS$^-$ buffers at pH 7.80. Peak identification (A): 1—DMF, 2—UPF51, 3—UPF51 homodimer, 4—UPF51 – GSH heterodimer, 5—GSH, 6—UPF51 – UPF17 heterodimer, 7—GSSG, 8—UPF17, 9—UPF17 – GSH heterodimer, 10—UPF17 homodimer. Peak identification (B): 1—DMF, 2—UPF51, 3—UPF51 homodimer, 4—UPF51 – GSH heterodimer, 5—GSH, 6—UPF51 – UPF17 heterodimer, 7—UPF17, 8—GSSG, 9—UPF17 – GSH heterodimer, 10—UPF17 homodimer.

The baseline separation was achieved in the 7–9 pH range, which allowed the peptides UPF1/17, UPF50/51, and GSH to be injected as mixture. If baseline separation was not achieved, the peptides were analyzed in pairs: UPF51 + UPF 17, UPF51 + GSH, UPF17 + GSH and UPF50 + UPF 1, UPF50 + GSH, UPF1 + GSH, with a view to obtain the pK_a values for the corresponding mixture of dimers.

In order to get an exact pH value, the stock solutions used were mixed in an appropriate way and diluted to obtain the desired ionic strength. As the determination of pK_a depends on the ionic strength of the background electrolyte, this strength must be held constant throughout the buffer series. The constituents of running buffers were selected to achieve a compromise between buffering capacity, effective

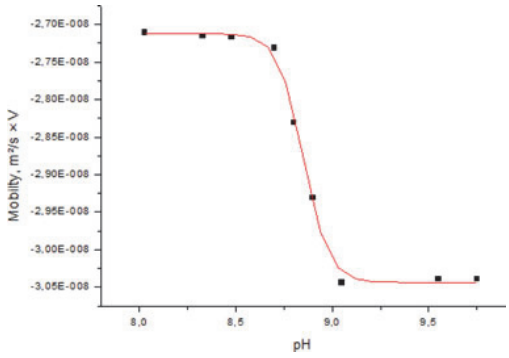

Figure 5. Dependence of the mobility of UPF17 homodimer on pH. Conditions are the same as in Fig. 2, except that 50 mM buffers were used and borate buffer was not used. The inflexion point of the sigmoidal curve corresponds to the pK_a value of the amino group of the UPF17 homodimer.

stacking of analytes, low Joule heating, small temperature gradients, and viscosity differences. Taking into account all requirements for buffer for correct pK_a determination, an ionic strength of 50 mM was chosen. The buffers used for pK_a determination were CHES/CHES$^-$, TES/TES$^-$, and MOPS/MOPS$^-$ and CH_3COOH/CH_3COO^- (used for determination of pK_a of the imidazolyl group). As already mentioned, $B(OH)_3/B(OH)_4^-$ may interact with the analytes, therefore this buffer was not employed to determine pK_a.

For the determination of dissociation constants, the effective mobility of each analyte was presented as a function of pH. The plots (Fig. 5) obtained were resolved using statistical software SigmaPlot 11.0.

The pK_a values obtained are shown in Table 2. Among the thiol groups, the pK_a value of the UPF17 peptide is the lowest (7.86 ± 0.03), while that of GSH is the highest (8.12 ± 0.4). Among the amino groups, the pK_a value of the UPF50 – UPF1 heterodimer is the highest (9.10 ± 0.07). The pK_a value of the UPF51 – UPF17 heterodimer (6.29 ± 0.04) is the highest in the imidazolyl group, the UPF50 homodimer having the lowest (5.94 ± 0.03). Some differences in pK_a between the peptides may be observed when determined by CE and other methods [12].

4 Concluding remarks

This study showed that for the separation of GSH analogues, the CE method is suitable, being relatively fast and easy. It was found that the pH and composition of BGE are of importance, affecting the selectivity of separation.

A borate seems to be the best medium for the separation of the peptides under analysis, but due to the possible interaction with analytes it is not suitable for the determination of pK_a. So, other buffers like CHES/CHES$^-$, TES/TES$^-$, MOPS/MOPS$^-$, and CH_3COOH/CH_3COO^- should be used.

Table 2. Determined pK_a values of some GSH analogues measured by CE ($I = 50$ mM)

Peptide	p$K_a \pm$ SD		
	Imidazolyl	Amino	Thiol
UPF1		8.91 ± 0.05	$8.03 \pm 0.02/9.3 \pm 0.1$[a)]
UPF17		8.83 ± 0.07	$7.86 \pm 0.03/9.4 \pm 0.2$[a)]
UPF50	6.21 ± 0.05	9.06 ± 0.11	7.89 ± 0.12
UPF51	6.24 ± 0.07	9.00 ± 0.10	7.99 ± 0.10
UPF1 homodimer		9.03 ± 0.08	
UPF17 homodimer		8.84 ± 0.01	
UPF50 homodimer	5.94 ± 0.03	8.95 ± 0.03	
UPF51 homodimer	6.05 ± 0.04	9.01 ± 0.04	
UPF1 – GSH heterodimer		8.90 ± 0.02	
UPF17 – GSH heterodimer		8.96 ± 0.04	
UPF50 – GSH heterodimer	6.19 ± 0.06	8.81 ± 0.04	
UPF51 – GSH heterodimer	6.01 ± 0.02	9.03 ± 0.06	
UPF50 – UPF1 heterodimer	6.20 ± 0.07	9.10 ± 0.07	
UPF51 – UPF17 heterodimer	6.29 ± 0.04	8.93 ± 0.06	
GSH		8.93 ± 0.06	$8.13 \pm 0.4/9.0 \pm 0.3$[a)]
GSSG		9.05 ± 0.04	

a) Measured pK_a values of thiol groups in GSH, UPF1, and UPF17 by titration [12].

CE proved to be a suitable and useful method for the determination of pK_a values of newly synthesized GSH analogues. Unlike many other methods, CE allows one to simultaneously determine the pK_a of several GSH-based peptides that readily form dimers under basic conditions. The effective mobilities measured in the range of 5.50–10.00 allowed us to determine the pK_a values of imidazolyl, thiol, and amino moieties in UPF peptides, as well as in their homo- and heterodimers. The baseline separation of peptides of similar molecular weights, such as UPF50 and UPF51, as well as UPF1 and UPF17 and their homo-and heteropeptides, was not achieved.

This work was supported by the Estonian Science Foundation grants SF0140023s08, ETF9106 and ETF7856, ETF9167, the European Social Fund programme "Moblitas" postdoctoral research grant MJD12, and by the European Union through the European Regional Development Fund. This work has been partially supported by graduate school "Functional materials and technologies" that received funding from the European Social Fund under project 1.2.0401.09–0079 in Estonia.

The authors have declared no conflict of interest.

5 References

[1] Aquilano, K., Baldelli, S., Ciriolo, M. R., *Commun. Integr. Biol.* 2011, *4*, 477–479.

[2] Biswas, S., Chida, A. S., Rahman, I., *Biochem. Pharmacol.* 2006, *71*, 551–564.

[3] Filomeni, G., Rotilio, G., Ciriolo, M. R., *Biochem. Pharmacol.* 2002, *64*, 1057–1064.

[4] Fratelli, M., Goodwin, L. O., Ørom, U. A, *Proc. Natl. Acad. Sci. USA* 2005, *102*, 13998–14003.

[5] Pastore, A., Federici, G., Bertini, E., Piemonte, F., *Clin. Chim. Acta* 2003, *333*, 19–39.

[6] Kwon, Y. W., Masutani, H., Nakamura, H., Ishii, Y., Yodoi, J., *Biol. Chem.* 2003, *384*, 991–996.

[7] Schafer, F. Q., Buettner, G. R., *Free Radic. Biol. Med.* 2001, *30*, 1191–1212.

[8] Ehrlich, K., Viirlaid, S., Mahlapuu, Saar, K., Kullisaar, T., Zilmer, M., Langel, Ü., Soomets, U., *Free Radic. Res.* 2007, *41*, 779–787.

[9] Vaher, M., Viirlaid, S., Ehrilch, K., Mahlapuu, R., Jarvet, J., Soomets, U., Kaljurand, M., *Electrophoresis* 2006, *27*, 2582–2589.

[10] Põder, P., Zilmer, M., Starkopf, J., Kals, J. A., Talonpoika, A., Pulges, A., Langel, U., Kullisaar, T., Viirlaid, S., Mahlapuu, R., Zarkovski, A., Arend, A., Soomets, U., *Neurosci. Lett.* 2004, *370*, 45–50.

[11] Mahlapuu, R., Vaher, M., Ehrlich, K., Kaljurand, M., Soomets, U., *J. Pept. Sci.* 2006, *12*, 796–799.

[12] Kairane, C., Mahlapuu, R., Ehrlich, K., Kilk, K., Zilmer, M., Soomets, U., *Int. J. Pept.* 2012, *2012*, 124163.

[13] Maeso, N., García-Martínez, D., Rupérez, F. J., Cifuentes, A., Barbas, C, *J. Chromatogr. B* 2005, *822*, 61–69.

[14] Carru, C., Zinellu, A., Sotgia, S., Marongiu, Farina, M. G., Usai, M. F., Pes, G. M., Tadolini, B., Deiana, L., *J. Chromatogr. A* 2003, *1017*, 233–238.

[15] Cereser, C., Guichard, J., Drai, J., Bannier, E., Garcia, I., Boget, S., Parvaz, P., Revol, A., *J. Chromatogr. A* 2001, *752*, 123–132.

[16] Zhang, W., Wan, F., Zhu, W., Xu, H., Ye, X, *J. Chromatogr. A* 2005, *818*, 227–232.

[17] Deutsch, J. C., Santosh-Kumar, C. R., Kolhouse, J. F., *J. Chromatogr. A* 1999, *862*, 161–168.

[18] Kašička, V., *Electrophoresis* 2006, *27*, 142–175.

[19] Mikšik, I., Deyl, Z., *J. Chromatogr. A* 1999, *852*, 325–336.

[20] Caliaro, A. C., Herbots, C.A., *J. Pharm. Biomed. Anal.* 2001, *26*, 427–434.

[21] Yang, L., Yuan, Z., *Electrophoresis* 1999, *20*, 2877–2883.

[22] Sanz-Nebot, V., Benavente, F., Toro, I., Barbosa J., *J. Chromatogr. A* 2001, *22*, 4333–4340.

[23] Sanz-Nebot, V., Toro, I., Benavente, F., Barbosa, J., *J. Chromatogr. A* 2002, *942*, 145–156.

[24] Sanz-Nebot, V., Benavente, F., Toro, I., Barbosa, J., *J. Chromatogr. A* 2001, *921*, 69–79.

[25] Kašička, V., Prusík, Z., in: Parvez, H., Caudy, P., Parvez, S., Roland-Gosselin, P. (Eds.), *Capillary Electrophoresis in Biotechnology and Environmental Analysis*, VSP, Utrecht 1997, pp. 173–197.

[26] Kašička, V., in: Aboul-Enein, H. Y. (Ed.), *Analytical and Preparative Separation Methods of Biomacromolecules*, Marcel Dekker, New York 1999, pp. 39–97.

[27] Castagnola, M., Messana, I., Rosetti, D. V., in: Righetti, P. G. (Ed.), *Capillary Electrophoresis in Analytical Biotechnology*, CRC Press, Boca Raton, FL 1996, pp. 239–275.

[28] Arakawa, H., Maeda, M., Hanai, T., in: Deyl, Z. (Ed.), *Advanced Chromatographic and Electromigration Methods in BioSciences*, Elsevier, Amsterdam 1998.

[29] Liškova, A., Křivánková, L., *Electrophoresis* 2005, *26*, 4429–4439.

[30] Fuguet, E., Reta, M., Gibert, C., Roses, M., Bosch, E., Rafols, C., *Electrophoresis* 2008, *29*, 2841–2581.

[31] Köse, D. A., Zümreoglu-Karan, B., *Chem. Pap.* 2012, *66*, 54–60.

[32] Goldberg, R., Kishore, N., Lennen, R., *J. Phys. Chem. Ref. Data* 2002, *31*, 231–370.

Publication II

Kazarjan, J., Vaher, M., Mahlapuu, R., Hansen, M., Soomets, U., Kaljurand. M. Investigation of the surfactant type and concentration effect on the retention factors of glutathione and its analogues by micellar electrokinetic chromatography. – *J. Sep. Sci*., 2015, 38, 1042-1045.

Jana Kazarjan[1]
Riina Mahlapuu[2]
Mats Hansen[2]
Ursel Soomets[2]
Mihkel Kaljurand[1]
Merike Vaher[1]

[1]Department of Chemistry, Tallinn University of Technology, Tallinn, Estonia
[2]Institute of Biomedicine and Translational Medicine, Department of Biochemistry, Centre of Excellence for Translational Medicine, University of Tartu, Tartu, Estonia

Received May 31, 2015
Revised July 9, 2015
Accepted July 11, 2015

Research Article

Investigation of the surfactant type and concentration effect on the retention factors of glutathione and its analogues by micellar electrokinetic chromatography

In the present study, a micellar electrokinetic chromatographic method was used to determine the retention factors of hydrophilic monomeric and homodimeric forms of glutathione analogues. Ionic-liquid-based surfactant, 1-tetradecyl-3-methylimidazolium chloride, as well as cetyltrimethylammonium bromide and phosphate buffer (pH 7.4) were employed in the experiments. Since the studied peptides possess a negative charge under physiological conditions, it is expected that the peptides interact with the oppositely charged 1-tetradecyl-3-methylimidazolium chloride and cetyltrimethylammonium bromide micelles via hydrophobically assisted electrostatic forces. The dependence of the retention factor on the micellar concentration of 1-tetradecyl-3-methylimidazolium chloride and cetyltrimethylammonium bromide is nonlinear and the obtained curves converge to a limiting value. The retention factor values of GSH analogues were in the range of 0.36–2.22 for glutathione analogues and –1.21 to 0.37 for glutathione when 1-tetradecyl-3-methylimidazolium chloride was used. When cetyltrimethylammonium bromide was employed, the retention factor values were in the range of 0.27–2.17 for glutathione analogues and –1.22 to 0.06 for glutathione. If sodium dodecyl sulfate was used, the retention factor values of glutathione analogues with carnosine moiety were in the range of –1.54 to 0.38.

Keywords: Glutathione analogues / Ionic-liquid-based surfactants / Micellar electrokinetic chromatography / Retention factors / UPF peptides
DOI 10.1002/jssc.201500567

Additional supporting information may be found in the online version of this article at the publisher's web-site

1 Introduction

Glutathione (GSH) is the most abundant intracellular low-molecular-weight antioxidant that has many vital roles such as direct scavenging of free radicals, regulation of cellular redox homeostasis, drug detoxification and elimination. Reduction in GSH level is associated with many pathological states like cancer, neurologic degeneration, pulmonary and inflammatory diseases [1]. Exogenous administration of GSH to overcome the glutathione pool depletion problem is complicated because of its excessive extracellular degradation and poor transport into the cells [2]. Thus, there is a high pharmacoclinical interest in designing GSH analogues that could mimic glutathione's biological activity and have higher hydrophobicity. Lately, new tetrapeptic GSH analogues referred to as UPF peptides (Supporting Information Fig. S1) have been synthesized. Two of them, UPF1 and UPF17, have antioxidative activity and their effect on different isolated cells has been investigated [2–4].

In addition to biological effects, the physicochemical properties of new GSH analogues should be known before pharmaceutical use. Amongst these properties are ionization (pK_a) and hydrophobicity. Recently, the pK_a values of UPF1, UPF17, UPF50, and UPF51 have been determined [5]. Hydrophobicity, which is related to the interaction of a drug (peptide) with biomembranes, is traditionally referred to as the octanol-water partition coefficient (log *P*). However, GSH (and presumably UPFs) are under physiological conditions (pH 7.4) not neutral but ionized, and biomembranes are charged and anisotropic. Thus, not only hydrophobic interactions but also ionic bonds and charge transfers play an essential role in the interactions between biological membranes and ionized compounds [6].

Possible ways to measure partition coefficients of ionized compounds by CE modes involve using artificial

Correspondence: Ms. Jana Kazarjan, Department of Chemistry, Tallinn University of Technology, Akadeemia tee 15, 12618 Tallinn, Estonia
E-mail: jana.kazarjan@gmail.com
Fax: +372-620-43-25

Abbreviations: C_{14}MImCl, 1-tetradecyl-3-methylimidazolium chloride; **CTAB**, cetyltrimethylammonium bromide; **GSH**, glutathione; **GSSG**, glutathione disulfide; **I**, ionic strength; **IL**, ionic liquid; **PSP**, pseudostationary phase

membranes, i.e. liposomes [7], vesicles [8], immobilized artificial membranes (IAM) [9], microemulsions [10], and micelles [11, 12]. The preparation of liposomes, vesicles, IAMs, and microemulsions that are used to monitor partition coefficients of ionized compounds is tedious and time-consuming. On the other hand, the use of micelles in MEKC allows an optimal modeling of intermolecular interactions present in biological systems by a simple change of the surfactant type of the micellar pseudo-stationary phase (PSP). Moreover, the use of micelles is cost-effective compared to artificial membranes. Micelles are amphiphilic aggregates of surfactants that provide anisotropic microenvironments with hydrophobic and polar site interactions. Anionic SDS is the most widely employed surfactant to generate micelles in MEKC as it has several advantages, such as high solubilization capability, low UV absorbance and easy availability. Another popular surfactant used in MEKC is cationic cetyltrimethylammonium bromide (CTAB) that adsorbs on the capillary wall and reverses the direction of the EOF [13]. Along with these conventional surfactants, ionic liquid (IL) type surfactants, namely alkylimidazolium-based ILs, are gaining popularity as PSPs in MEKC [14, 15]. In general, IL is a salt that is liquid below 100°C. The most remarkable properties of ILs are negligible vapor pressure, miscibility with water and many organic solvents, as well as prominent catalytic properties. Analysis of the structure-activity relationship of a typical imidazolium IL showed that ILs possess surface active properties that are similar to those of surfactants and, as a result, in aqueous solution micelles are formed. This property makes ILs a possible new class of surface-active agents that have the properties of classical cationic surfactants. Compared to traditional PSPs, IL-type surfactants with alkyl chains longer than four behave as amphiphilic compounds that offer versatile interaction types like electrostatic, ion–dipole, π–π, van der Waals, hydrogen-bonding interactions with the imidazolium cation head and hydrophobic interactions because of the long alkyl tail [16].

In the present work, an alkylimidazolium-based surfactant, namely, 1-tetradecyl-3-methylimidazoilium chloride (C_{14}MImCl), was used as PSP in MEKC experiments for the determination of the retention factors of UPF peptides. According to our knowledge, the MEKC analysis of UPF peptides has not been reported so far. The retention factors of UPF peptides under physiological (pH 7.4) obtained with the use of positive C_{14}MImCl micelles were compared to those exhibited by a conventional cationic surfactant (CTAB). Moreover, an anionic surfactant (SDS) was also employed in the retention factor determination of UPF peptides. Though UPF peptides are negatively charged at pH 7.4 and SDS micelles are negative as well, the anionic SDS is of particular interest since about 10% of plasma membranes are negatively charged [6].

On the whole, the main goal of this work was to investigate the effects of the surfactant type and concentration on the retention factors of the mentioned UPF peptides and glutathione in reduced and oxidized forms under physiological conditions (pH 7.4) using MEKC to get extra information about possible molecular forces responsible for the interaction of ionized compounds like UPF peptides and biological membranes.

According to our knowledge, this is also for the first time when MEKC was applied to analysis of GSH analogues employing IL-type surfactants.

2 Materials and methods

2.1 Chemicals and BGEs

Peptides GSH and GSSG, methanol, disodium hydrogen phosphate, sodium dihydrogen phosphate, 3-morpholinopropane-1-sulfonic acid (MOPS), 2-[[1,3-dihydroxy-2-(hydroxymethyl)propan-2-yl] amino] ethanesulfonic acid (TES) and 2-[4-(2-hydroxyethyl)piperazin-1-yl]ethanesulfonic acid (HEPES) were obtained from Sigma–Aldrich (Steinheim, Germany). UPF1, UPF17, UPF50, and UPF51 peptides were synthesized by us (for more details refer to Supporting Information). An aqueous solution of each peptide was prepared at a concentration of 1 mM. Each peptide was injected into the capillary individually at a concentration of 200 μM.

Sodium hydroxide, boric acid, phosphoric acid and hydrochloric acid were purchased from Riedel-de Haën (Germany). SDS, CTAB were from Sigma–Aldrich (Steinheim, Germany) and C_{14}MImCl was supplied by IoLiTec Ionic Liquids Technologies (Heilbronn, Germany).

Milli-Q water (MilliQ, Millipore Molsheim, France) was used for the preparation of all solutions of standards, preparation of BGEs, dilution of samples and preparation of stock solutions of GSH, and its four analogues: UPF1, UPF17, UPF50, and UPF51. All stock solutions were stored at −18°C.

Buffers used in the experiments were $H_2PO_4^-$/HPO_4^{2-}(stock 100 mM, pH 7.4 and 8.2), $B(OH)_3$/$B(OH)_4^-$ (stock 500 mM, pH 8.2), MOPS/$MOPS^-$, TES/TES^-, HEPES/$HEPES^-$ (stock 500 mM, pH 7.4). The pH of the solutions was adjusted to the respective pH level by 1 M sodium hydroxide, 1 M phosphoric acid, or 1 M hydrochloric acid.

Micellar BGEs were (i) phosphate buffer (pH 7.4) containing 10, 20, 30, 36, 50, or 60 mM C_{14}MImCl or (ii) phosphate buffer (pH 7.4) containing 10, 20, 30, 36, 50, or 60 mM CTAB or (iii) phosphate buffer (pH 8.2) containing 10, 20, 30, 36, 50, or 60 mM C_{14}MImCl or (iv) borate buffer (pH 8.2) containing 10, 20, 30, 36, 50, or 60 mM SDS. Despite the different buffer compositions employed in CZE/MEKC experiments, the ionic strength (I) of all buffers was held constant and equal to 35 mM. All BGEs were freshly prepared and filtered through a 0.45 μm syringe filter (Millipore, Bedford, MA, USA).

The pH value of the electrolyte solutions was measured with a Metrohm 744 pH meter equipped with a combination electrode (Metrohm, Herisau, Switzerland) that had been

calibrated with commercial buffers at pH 7.00 (±0.01) and pH 10.00 (±0.01) (Sigma–Aldrich).

In CZE experiments, the electrophoretic hold-up time t_0 was measured using DMF (Lachema, Brno, Czech Republic). Dodecanophenone, α-tocopherol, vitamin K1, and dodecylbenzene (Sigma–Aldrich, Steinheim, Germany) dissolved in methanol were used as micellar markers.

All the reagents and chemicals used in all experiments were of analytical reagent grade.

2.2 CE methods

All CZE and MEKC experiments were performed on an Agilent 3D instrument (Agilent Technologies, Waldbronn, Germany) equipped with a UV/Vis DAD detector set at 200 and 230 nm, the latter being used for glutathione detection when CTAB was used as PSP [17].

A fused-silica capillary (Polymicro Technologies, Phoenix, AZ, USA) with an internal diameter of 50 μm and a length of 51.5/60 cm (L_{eff}/L_{tot} effective capillary length/total capillary length) was employed in the experiments. The separations were performed under an applied voltage of –10 and +10 kV. The injection pressure was set to 50 mbar for 10 s. The temperature was kept at 25°C. All electropherograms were recorded and integrated with Agilent ChemStation software.

New capillaries were conditioned by flushing them first with 1 M NaOH solution for 30 min, MilliQ water for 15 min and BGE for 5 min. Between runs, the capillary was rinsed with 1 M sodium hydroxide for 2 min, MilliQ water for 2 min, methanol for 2 min, MilliQ water for 2 min and finally with the BGE solution for 5 min.

For amphoteric compounds like UPF peptides the overall retention factor is the weighted sum of the retention factors of all species present [14]. The UPF peptides can interact with positively charged micelles (C_{14}MImCl and CTAB) by electrostatic interaction due to the negative net charges acquired by dissociation and possible complexation (borate buffer, pH 8.2 [5]). As seen from the equations in Supporting Information Table S1, the described dissociation (Eq. 1a), possible complexation (Eqs. 1b–c) and association (Eqs. 1d–g) equilibria have to be considered in the overall retention factor determination of UPF peptides. It can be predicted that for cationic micelles (C_{14}MImCl, CTAB) and negatively charged UPF peptides a strong electrostatic interaction takes place and an electrostatic repulsion is expected to occur with anionic micelles (SDS).

The impact of equilibria described by Eqs. 1(f)–(g) (Supporting Information Table S1) is negligible as the possible complexation of UPF peptides with a tetrahyhydroxyborate anion is considered to be very low, due to absence of vicinal hydroxyl groups. Additionally, SDS as a negatively charged micelle-forming surfactant with borate buffer (pH 8.2, I = 35 mM) was used to determine the retention factors of negatively charged peptides. Thus, it is expected that $k_{(PN)^-}$ and $k_{(PN-O)^{2-}}$ will be very small (Supporting Information Table S1).

To calculate the retention factors of UPF peptides the following equation can be employed [14, 18]:

$$\mu = \frac{1}{k+1}\mu_{eff} + \frac{k}{1+k}\mu_{mc} \quad (1)$$

where μ is the pseudoeffective electrophoretic mobility of the UPF peptide in micellar BGE, k is the overall retention factor of the UPF peptide, μ_{eff} is the effective electrophoretic mobility of the UPF peptide in micelle-free BGE and μ_{mc} is the electrophoretic mobility of the micelles in micellar BGE. From Eq. (1) the following expression can be derived, which allows calculation of the true retention factor k in MEKC from the mobilities μ, μ_{eff}, and μ_{mc}:

$$k = \frac{\mu - \mu_{eff}}{\mu_{mc} - \mu} \quad (2)$$

The mentioned mobilities have to be determined in separate measurements: μ and μ_{mc} are determined in the presence of micelles (MEKC condition) and μ_{eff} is determined in the absence of surfactant (CZE condition). All CZE and MEKC peptide mobility and retention factor values are the average of four measurements.

3 Results and discussion

3.1 Choice of micelle marker

At the beginning of the investigation different compounds—dodecanophenone, α tocopherol, vitamin K1, and dodecylbenzene—were employed as possible micellar markers [19]. Dodecanophenone, α tocopherol, and vitamin K1 did not give reproducible migration times of micelle when using BGE composed of phosphate buffer (pH 7.4) and different surfactants (C_{14}MImCl, CMC 2.5 mM/3.5 mM in 25 mM phosphate/water, respectively [20]), CTAB, SDS (CMC 3.27 mM in 20 mM phosphate buffer, pH 7.0 [21]) probably due to the strong absorption on the capillary wall and high methanol content needed in the marker sample solution [14, 18]. Replacing the phosphate buffer (pH 7.4) with MOPS, TES, and HEPES buffers (pH 7.4) to improve the migration time reproducibility of the mentioned markers did not give any positive results with the same surfactants (C_{14}MImCl, CTAB, SDS).

Dodecylbenzene proved to give reproducible migration times (t_{mc} RSD <10%) of micelles when BGE composed of phosphate buffer (pH 7.4), C_{14}MImCl, and CTAB was used.

The migration time of SDS micelles was still not improved with BGE composed of

phosphate, MOPS, TES or HEPES buffer (pH 7.4) when dodecylbenzene was used as a marker, though. A positive effect on the migration time of SDS micelle (t_{mc} RSD <10%) was obtained when dodecylbenzene was used as a marker in BGE composed of borate buffer (pH 8.2). The RSD% of the migration time of C_{14}MImCl micelles was 10.38 and of CTAB

micelles 6.91 (RSD% of the migration time of micelles was calculated on the basis of all UPF peptides).

For MEKC experiments dodecylbenzene was dissolved in MeOH at a concentration of *ca.* 2 mg/mL.

3.2 Effect of surfactant concentration

As discussed above, the studied UPF peptides are hydrophilic analytes with pK_a values of imidazolyl, amino and thiol moieties in the range of 5.94–6.29, 8.81–9.10, and 7.86–8.13, respectively [5]. Thus, it is expected that these GSH analogues are negatively charged at physiological pH and electrostatic interactions between these analytes and micelles (C_{14}MImCl, CTAB, and SDS) should contribute to the overall retention factors. Presumably, UPF peptides exist in two forms in an aqueous solution: reduced, monomeric peptide, and oxidized, homodimeric peptide (Supporting Information).

In Fig. 1 the pseudoeffective electrophoretic mobility μ of the investigated UPF peptides and glutathione (reduced and oxidized forms) is plotted against the concentration of the surfactant (conc(C_{14}MImCl, CTAB, and/or SDS)) ranging from 10 to 60 mM with conc(surfactant) increments of 10 mM. A detailed study of Fig. 1 shows that surfactant concentration of 36 mM has been used instead of 40 mM. The reason for that is the micelle aggregation of BGE composed of phosphate buffer (pH 7.4) and 40 mM 1-tetradecyl-3-methylimidazolium chloride during MEKC. This aggregation is seen as spikes on the output electropherogram and therefore the identification of analytes is hindered. To avoid the aggregation of micellar BGE, the concentration of C_{14}MImCl was gradually lowered and 36 mM 1-tetradecyl-3-methylimidazolium chloride was chosen [22]. To match the concentrations used in MEKC experiments for C_{14}MImCl, the same range of CTAB and SDS concentrations was employed.

Figures 1A–D further show that μ values obtained in MEKC experiments are positive unlike the effective mobility μ_{eff} measured in BGE without surfactant due to the interaction of negatively charged peptides with positively charged micelles (C_{14}MImCl, CTAB). A slight increase in the μ values of the reduced and oxidized forms of UPF peptides with increasing PSP concentration is obtained. These curves confirm that the mode of interaction between these UPF peptides and cationic micelles is not purely electrostatic interaction but hydrophobically assisted electrostatic interaction. The obtained results differ from those reported in case of charged analytes where a plateau curve is obtained when μ is plotted against surfactant concentration [14]. The contribution of the hydrophobic interaction between UPF1 and UPF17 (and their corresponding homodimers) and cationic micelles is lower compared to that between UPF50 and UPF51 as can be seen from Figs. 1A–D depicting more 'plateau like' gently sloping curves. This can be explained by the carnosine moiety present in UPF50 and UPF 51 peptides. Compared to UPF peptides the μ of GSH and GSSG significantly increases with c(C_{14}MImCl/CTAB) ranging from 0 to 60 mM, indicating that these analytes have a relatively strong interaction with micelles (Fig. 1E). GSSG has a more powerful interaction with both with C_{14}MImCl and CTAB than GSH, being stronger when 1-tetradecyl-3-methylimidazolium chloride is used. It is also clear from Figs. 1A–D that the resolution between UPF peptides is slightly better in the case of CTAB as PSP than in the case of C_{14}MImCl. For GSH and GSSG the resolution is better when C_{14}MImCl was used as PSP (Fig. 1E). In general, in case of UPF peptides the extent of micelle complexation for C_{14}MImCl was higher than that for CTAB. For example, doubling the surfactant concentration from 30–60 mM increased the pseudoeffective electrophoretic mobility μ by 12.7% with C_{14}MImCl versus 6.7% with CTAB for UPF17 and by 10.8% with C_{14}MImCl versus 3.1% with CTAB for UPF17 homodimer. This can be ascribed to the versatile interaction sites provided by the polar imidazolium functional group of C_{14}MImCl. In addition to the electrostatic interaction induced by the imidazolium cation, which is comparable to the one exerted by the ammonium group, the hydrophobic interaction with the long alkyl tail of C_{14}MImCl is also possible. The imidazolium moiety can also give rise to ion-dipole interactions, and the hydrogen bonding with the C-2 hydrogen of the imidazolium cation is possible as well [23].

In addition to C_{14}MImCl and CTAB, the pseudoeffective electrophoretic mobility of UPF peptides (as well as GSH and GSSG) was plotted against the concentration of SDS (Figs. 1F–H). The BGE used in Figs. 1F–H was composed of borate buffer (pH 8.2) and SDS from 0–60 mM. All μ values, including the μ_{eff} measured in BGE without a surfactant, are negative due to the absence of the interaction between the negatively charged peptides and negatively charged micelles.

As can be seen from Figs. 1F–G, μ increases (becomes more positive) with increasing PSP in the case of GSH, GSSG, UPF1 and UPF17 (monomer and homodimer) due to the absence of the interaction between the mentioned peptides and SDS micelles. Fig. 1H shows the decrease in μ (becomes more negative) with increasing PSP in the case of UPF50 (monomer and homodimer) and UPF51 (monomer and homodimer) due to the complexation of the corresponding peptides with SDS micelles. Presumably, the interaction between UPF50, UPF51 (and their corresponding homodimers) and SDS micelles is a hydrophobic interaction as the peptides under study are negatively charged and electrostatic repulsion exists between these peptides and negative SDS micelles. As mentioned above, the carnosine moiety has an impact on the hydrophobic interaction of UPF50 and UPF51 peptides (and the corresponding homodimers) and SDS micelles. BGE composed of phosphate buffer (pH 8.2) and C_{14}MImCl/CTAB with the concentration range 0–60 mM was also employed. The results obtained were similar to those obtained with phosphate buffer (pH 7.4) with the pseudoeffective mobility values being slightly higher when pH 8.2 was used (data not shown).

The reproducibility of the migration times (Figs. 1A–H) of peptides ranged from 0.061% to 1.49% in the case of CTAB, from 0.045% to 1.15% in the case of C_{14}MImCl and from 0.068% to 1.96% in the case of SDS. The differences in RSD% values obtained with different concentrations of surfactants

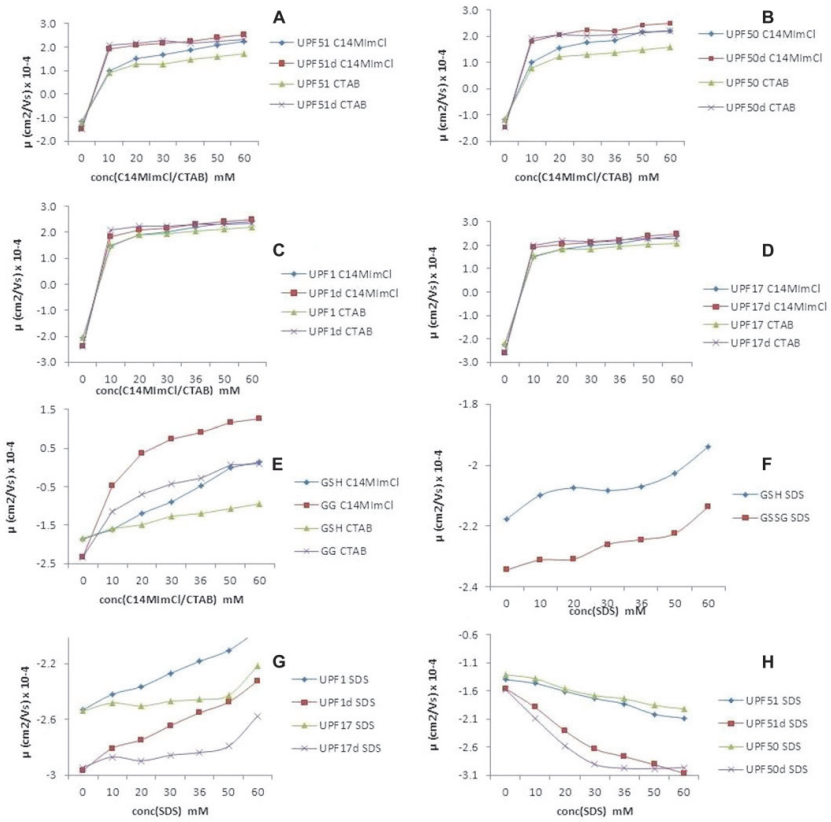

Figure 1. Effect of the concentration of 1-tetradecyl-3-methylimidazolium chloride, cetyltrimethylammonium bromide and SDS on the pseudoeffective mobility of peptides. A–E phosphate buffer (pH 7.4) and 0–60 mM C_{14}MImCl/CTAB F–H borate buffer (pH 8.2) and 0–60 SDS CE and MEKC conditions: fused-silica capillary 60/51.5 cm (L_{tot}/L_{eff}), id 50 μm, detection 200 nm and 230 nm, capillary temperature 25°C, applied voltage –10 kV (micellar BGE with C_{14}MImCl and CTAB) and +10 kV (non-micellar BGE and micellar BGE with SDS) The ionic strength of all buffers was held constant at 35 mM. *d* represents homodimer.

can be ascribed to the unique micelle structures of PSPs and the dynamic coating of the capillary of cationic surfactants [14, 24].

3.3 Retention factors of the UPF peptides

As mentioned above, under physiological conditions (pH 7.4) the studied analytes are negatively charged [24]. Their separation in MEKC is based on chromatographic as well as electrophoretic principles. The overall retention factor of peptides will be the weighted average of the retention factors of all species (neutral and charged) present in the solution. The retention factors were calculated according to Eq. 1. To use Eq. 1 several assumptions are made: the influence of PSP on the ionic strength, viscosity and dielectric constant of BGE is very low and the interaction of the peptide with surfactant monomers is neglected.

The true retention factor k in MEKC was calculated from the mobilities μ, μ_{eff}, and μ_{mc}, which have to be determined in different CE modes under the same conditions: μ and μ_{mc} were measured in the MEKC mode and μ_{eff} in the CZE mode.

The dependence of the retention factors of reduced and oxidized forms of UPF peptides and glutathione on the concentration of the surfactant (C_{14}MImCl, CTAB, and SDS) is shown in Fig. 2. As seen from Figs. 2A–D, G, and H the retention factors of monomeric UPF peptides increase and that of dimeric UPF peptides decrease with increasing surfactant concentration. The dependence of the retention factor on the C_{14}MImCl and CTAB micelle concentration is non-linear and the obtained curves converge to a limiting value. The absorption of monomeric UPF peptides in micelles

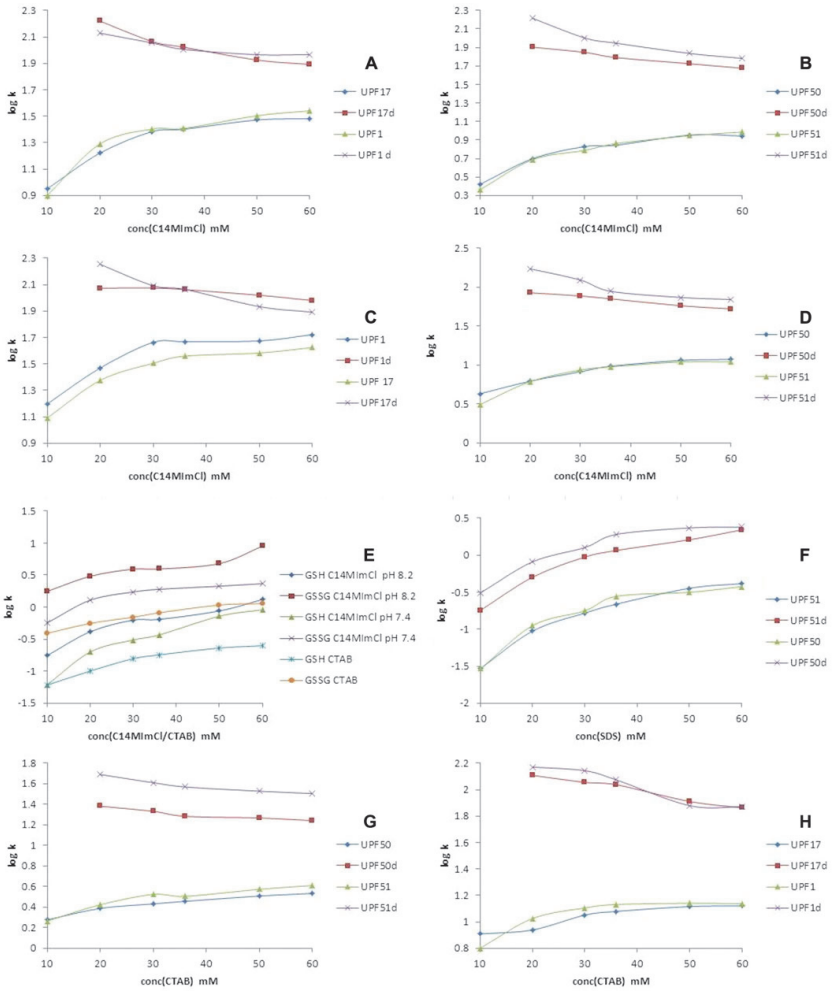

Figure 2. Retention factors of glutathione and glutathione analogues (reduced and oxidized forms) dependent on the concentration of 1-tetradecyl-3-methylimidazolium chloride, cetyltrimethylammonium bromide and SDS. MEKC conditions: refer to Fig. 1 A, B phosphate buffer (pH 7.4) C, D phosphate buffer (pH 8.2) E phosphate buffer (pH 7.4 and 8.2) F borate buffer (pH 8.2) G, H phosphate buffer (pH 7.4)

achieves saturation approximately when the concentration of C_{14}MImCl/CTAB reaches 36 mM. Afterwards, the increase of the C_{14}MImCl/CTAB concentration only performs the function of "dilution" (and a more "plateau-like" curve is obtained, see Figs. 2A–D, G, and H).

The retention factors of monomeric UPF peptides increase when the pH of the phosphate buffer is set at 8.2 (Figs. 2C,D), unlike those obtained when pH is 7.4 (Figs. 2A,B), probably due to the higher net negative charge of peptides at pH 8.2. Negative monomeric UPF peptides interact more strongly with oppositely charged micelles (C_{14}MImCl and CTAB) mainly by electrostatic interaction. Unlike UPF peptides, the retention factors of GSH and GSSG increase with increasing surfactant concentration (C_{14}MImCl, CTAB). Compared to CTAB, the retention factors of GSH and GSSG are higher when C_{14}MImCl is employed as PSP. When the pH of the phosphate buffer was increased from 7.4 to 8.2, the retention factors of GSH and GSSG were increased as well (Fig. 2E). In general, when C_{14}MImCl was used as a surfactant, the retention factors of UPF peptides, GSH and GSSG were higher compared to that of CTAB, which can be ascribed to the versatility of interaction sites provided by the imidazolium cation.

The homodimeric forms of UPF peptides should have a greater net negative charge compared to their corresponding monomeric forms [25] and thus, have a more pronounced

electrostatic interaction with oppositely charged micelles. Surprisingly, for homodimeric forms of UPF peptides with the increase of PSP concentration (C_{14}MImCl and CTAB) the retention factors decreased (Figs. 2A–D, G, and H). One possible explanation for this phenomenon is that the pK_a [26,27] of the homodimers of GSH analogues shifts that is caused by their interaction with cationic micelles. This micellar-mediated shift in ionization constants can lead to a change in the net charge of peptides from negative to neutral. As GSH analogues under investigation are hydrophilic, the interaction of the neutral homodimeric forms of peptides with charged micelles are considered to be very weak. Thus, by increasing the concentration of PSP, the homodimers of UPF peptides acquire a more positive charge and the interaction between peptides and micelles weakens, resulting in lower retention factors.

Another explanation may be the influence of peptide conformation that can be stabilized by intermolecular hydrogen bonds. A bend in the homodimers backbone may again induce a change in pK_a. At the same time, the hydrophobicity of the neighboring amino acids may also have an influence on peptide ionization constants [28]. The homodimers of UPF1 and UPF17 have hydrophobic methoxy-tyrosine moieties, while UPF50 and UPF51 have histidine residues in addition to methoxy-tyrosine moieties that may change the pK_a values of the neighboring amino acids and thus alter the backbone stereochemistry and hinder the complex formation with the micelle. Consequently, the electrostatic interaction between the micelles and homodimers of UPF peptides is decreased. Indeed, as seen from Supporting Information Fig. S2, a stronger interaction between the UPF50 homodimer and C_{14}MImCl micelle is observed when the concentration of 1-tetradecyl-3-methylimidazolium chloride is lower.

Another possible explanation for the reduced retention factors of the homodimers of UPF peptides with increasing concentration of cationic surfactants is that the shape of micellar associates changes, suggesting that the homodimers of UPF1, UPF17, UPF50 and UPF51 preferably bind to C_{14}MImCl and/or CTAB of a specific shape [24]. When SDS was employed as PSP, only reduced and oxidized forms of UPF50 and UPF51 interacted with SDS micelles. The retention factors of the mentioned GSH analogues increase with increasing PSP concentration for both forms of UPF50 and UPF51 peptides (Fig. 2F).

The log k values of the retention factors of monomeric and dimeric forms of GSH analogues are presented in the supplementary material.

4 Concluding remarks

The retention factors of negatively charged GSH analogues under physiological pH have been determined using C_{14}MImCl, CTAB and SDS-based surfactants. The curves of hydrophilic GSH analogues partitioning into net positively charged micelles converge to a limiting value with increasing concentration of PSP. In general, the strength of monomeric UPF peptide micelle interactions increased more with increasing pH and micelle concentration. The retention factors obtained when C_{14}MImCl was used as PSP were higher than those obtained with CTAB as PSP, due to the higher number of interaction sites provided by the imidazolium cation. The obtained results suggest that hydrophobic interactions between monomeric UPF peptides and cationic micelles are weaker than electrostatic ones that are primarily responsible for the retention of monomeric GSH analogues. It is also clear that hydrophobic methoxy-tyrosine moieties of UPF1 and UPF17 homodimers and histidine residues in addition to methoxy-tyrosine moieties of UPF50 and UPF51 homodimers induce a unique peptide conformation that does not have a sufficiently strong hydrophobic surface to interact with charged micelles. Moreover, additional steric effects may hinder the complexation between the homodimers of UPF peptides and cationic micelles. At the same time, the hydrophobic interaction between negatively charged reduced and oxidized forms of UPF51/51 and SDS micelles overcomes the electrostatic repulsion between them, in contrast to GSH, UPF1/17 and their corresponding homodimers.

On the whole, the obtained results of MEKC experiments under physiological conditions using different PSPs can help better understand the molecular interactions that contribute to the overall retention of the studied GSH analogues and provide extra information about the possible diverse interactions between complex biological membranes and ionized compounds like UPF peptides as potential drugs.

This work was supported by the Estonian Science Foundation (grant no. 9167), by the Ministry of Education and Science through targeted financings IUT 33-20 and IUT 20-42 and by the European Union through the European Regional Development Fund.

The authors have declared no conflict of interest.

5 References

[1] Wu, J.H., Batist, G., Biochim, *Biophys. Acta* 2013, *1830 (5)*, 3350–3353.

[2] Kairane, C., Mahlapuu, R., Ehrlich, K., Kilk, K., Zilmer, M., Soomets, U., *Int. J. Pept.* 2012, *2012*, 5

[3] Põder, P., Zilmer, M., Starkopf, J., Kals, J.A., Talonpoika, A., Pulges, A., Langel, U., Kullisaar, T., Viirlaid, S., Mahlapuu, R., Zarkovski, A., Arend, A., Sommets, U., *Neurosci. Lett.* 2004, *370*, 45–50.

[4] Vaher, M., Viirlaid, S., Ehrlich, K., Mahlapuu, R., Jarvet, J., Soomets, U., Kaljurand, M., *Electrophoresis* 2006, *27*, 2582–2589.

[5] Kazarjan, J., Vaher, M., Mahlapuu, R., Hansen, M., Soomets, U., Kaljurand, M., *Electrophoresis* 2013, *34*, 1820–1827.

[6] Taillardat-Bertschinger, A., Carrupt, P.-A., Testa, B., *J. Pharm. Sci.* 2002, *15*, 225–234.

[7] Wiedmer, S. K., Lokajová, J., *J. Sep. Sci.* 2013, *36*, 37–51.

[8] Razak, J. L., Cutak, B. J., Larive, C. K., Lunte, C. E., *Pharm. Res.* 2001, *18*, 104–111.

[9] Barbato, F., Grumetto, L., Carpentiero, C., Rocco, A., Fanali, S., *J. Pharm. Biomed. Anal.* 2011, *54*, 893–899.

[10] Liu, J., Sun, J., Wang, Y., Li, H., Sui, X., Li, Y., He, Z., *Asian J. Pharm. Sci.* 2008, *3 (4)*, 158–167.

[11] Lucangioli, S. E., Carducci, C. N., Tripodi, V. P., Kenndler, E. K., *J. Chromatogr. B* 2001, *765*, 113–120.

[12] Quirino, J.P., Kato, M., *J. Sep. Sci.* 2014, *37*, 2613–2617.

[13] Terabe, Sh., *Annu. Rev. Anal. Chem.* 2009, *2*, 99–120.

[14] Rageh, A. H., Pyell, U., *J. Chromatogr. A* 2013, *1316*, 135–146.

[15] Borissova, M., Palk, K., Koel, M., *J. Chromatogr. A* 2008, *1183*, 192–195.

[16] Luczak, J., Hupka, J., Thöming, J., Jungnickel, Ch., *Physicochem. Eng. Aspects* 2008, *329*, 125–133.

[17] Lindkvist, B., Weinander, R., Engman, L., Koetse, M., Engberts, J.B.F.N., Morgenstern, R., *J. Biochem.* 1997, *323*, 39–43.

[18] Orentaite, I., Maruška, A., Pyell, U., *Electrophoresis* 2011, *32*, 604–613.

[19] Wiedmer, S. K., Lokajová, J., Riekkola, M. -L., *J. Sep. Sci.* 2010, *33*, 394–409.

[20] Vanyúr, R., Biczók, L., Miskolczy, Z., *Physicochem. Eng. Aspects* 2007, *299*, 256–260.

[21] Fuguet, E., Ráfols, C., Rosés, M., Bosch, E., *Anal. Chim. Acta* 2005, *548*, 95–100.

[22] Kazarjan, J., Vaher, M., Kaljurand, M., *Electrophoresis* 2015, *36*, 1040–1042.

[23] Qui, H., Mallik, A. K., Takafuji, M., Liu, X., Jiang, S., Ihara, H., *Anal. Chim. Acta* 2012, *738*, 95–101.

[24] Singh, S. K., Kundu, A., Kishore, N., *J. Chem. Thermodyn.* 2004, *36*, 7–16.

[25] Moore, D. S., *Biochem. Educ.* 1985, *1*, 10–11.

[26] Carrozzino, J.M., Khaledi, M.G., *J. Chromatogr. A* 2005, *1079*, 307–316.

[27] Khaledi, M. G., Rodgers, A. H., *Anal. Chim. Acta* 1990, *239*, 121–128.

[28] Fürtös-Matei, A., Li, J., Waldron, K. C., *J. Chromatogr. B* 1997, *695*, 39–47.

Publication III

Kazarjan, J., Vaher, M., Kaljurand, M. Aggregation of phosphate and 1-tetradecyl-3-methylimidazolium chloride background electrolytes during micellar electrokinetic chromatography. – *Electrophoresis,* 2015, 36, 1040-1042.

Electrophoresis 2015, *36*, 1040–1042

Jana Kazarjan
Merike Vaher
Mihkel Kaljurand

Department of Chemistry, Tallinn University of Technology, Tallinn, Estonia

Received September 19, 2014
Revised December 29, 2014
Accepted January 2, 2015

Short Communication

Aggregation of phosphate and 1-tetradecyl-3-methylimidazolium chloride background electrolytes during micellar electrokinetic chromatography

We report the possible aggregation of phosphate and ionic liquid (1-tetradecyl-3-methylimidazolium chloride) based BGEs during MEKC. After a certain transit period, the aggregates appear as a random sequence of spikes on a UV detector signal. Root mean square values of the spikes and aggregation time (T_a) were plotted against BGE concentrations. The observation suggests that MEKC is a simple and easy technique for micelle aggregation studies.

Keywords:
Aggregation / Ionic liquids / Micellar electrokinetic chromatography

DOI 10.1002/elps.201400448

Aggregation of different substances under electric field is a well-known phenomenon and thus it should be frequently encountered in CE as well. According to Magnúsdóttir et al. [1], the use of CE to study the formation of aggregates was originally proposed by Hjerten [2]. The most prominent theories explaining aggregation during CE were proposed by Armstrong and co-workers [3, 4]. Several investigators have found aggregation to be useful phenomenon to study bacterial interactions [5, 6]. Ubner et al. [7] have reported possible aggregation of humic substances. However, there are no reports concerning studies of micelle aggregation.

Usually aggregation of micellar BGE appears as a random sequence of spikes of detector signal (in the case of optical detectors due to the possible blocking of the optical path of the detector window). The phenomenon may be interpreted as a failure of the electrophoretic run and not studied further. On the other hand MEKC may be an excellent technique for micelle aggregation studies. In this communication, we would like to report the possible formation of aggregates composed of phosphate buffer and 1-tetradecyl-3-methylimidazolium chloride (C_{14}MImCl, CMC 2.5 mM/3.5 mM in 25 mM phosphate/water, respectively [8]).

An Agilent 3D instrument (Agilent Technologies, Waldbronn, Germany) equipped with a DAD UV/Vis was used for MEKC experiments. A fused-silica capillary (Polymicro Technologies, Phoenix, AZ, USA) with an internal diameter of 50 μm and a length of 51.5/60 cm (L_{eff}/L_{tot}, where L_{eff} is effective capillary length, length to detector and L_{tot} is total capillary length) was employed in the experiments. The separation voltage was set to −5, −10, and −15 kV. The aggregates were detected at a wavelength of 200 nm. The micellar BGEs used were 5, 10, 15, 20, 25, 30, 35, and 45 mM phosphate buffers, each containing 30, 36, 38, 40, 45, 50, 55, and 60 mM C_{14}MImCl (pH 7.4). The temperature of the capillary was set at 25°C. All the electropherograms were recorded with the Agilent Chemstation software. Between runs the capillary was rinsed with methanol 2 min, water 2 min, NaOH (1 M) 2 min, water 2 min, and finally with micellar BGE for 5 min.

In our experiments, the capillary was entirely filled with micellar BGE at known concentrations and the response of the UV detector was monitored as a function of time directly after the application of the field. Since the field is applied over a homogeneous solution, the only source of variations in the detector output (other than the noise) should originate from formation of micelle aggregates that block the light path of the detector. The aggregation could only be observed when the electric field was applied, no spiking was observed if the BGE was pumped through capillary under pressure.

An example of electropherograms obtained in such conditions is presented in Fig. 1. In the beginning, the signal from the detector remains constant, as expected for a homogeneous and stable micellar BGE solution. However, the spiking in the signal starts to increase significantly after a few minutes, indicating the appearance of heterogeneities in the solution, which can be attributed to the progressive formation of aggregates and to their passage in front of the detector. The height of spikes grows progressively, reflecting the increase in the average size (and/or density) of the aggregates. After

Correspondence: Jana Kazarjan, Department of Chemistry, Tallinn University of Technology Akadeemia tee 15, 12618 Tallinn, Estonia
E-mail: jana.kazarjan@gmail.com
Fax: +372-620-4325

Abbreviations: C_{14}MImCl, 1-tetradecyl-3-methylimidazolium chloride; **RMS**, root mean square

Colour online: See the article online to view Figs. 1–3 in colour.

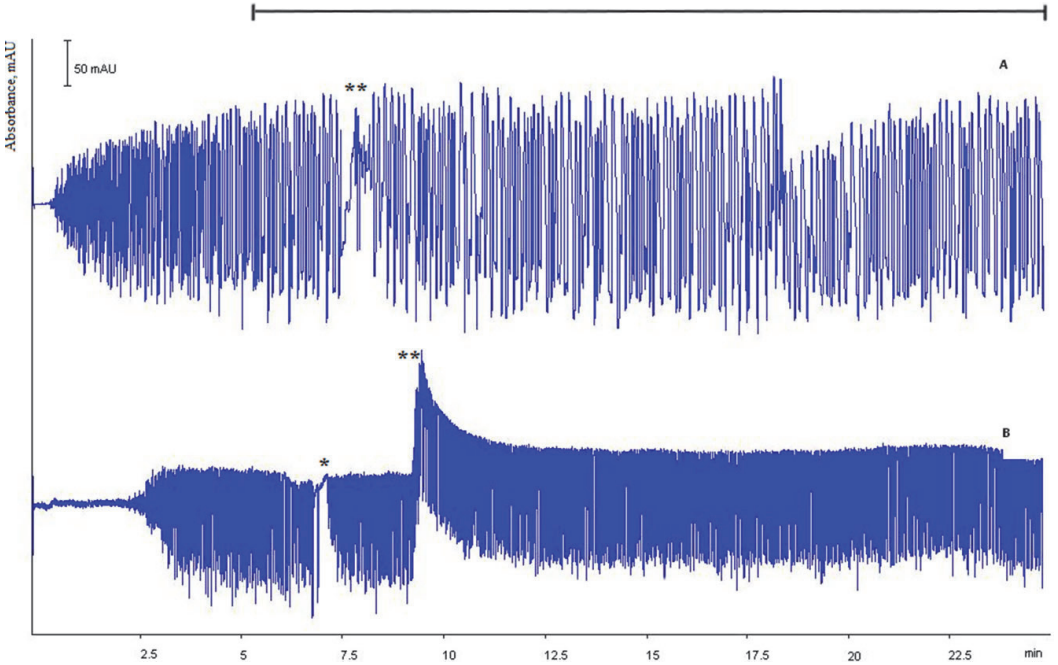

Figure 1. The evolution of the UV detector response at the capillary window from the time the high voltage of −10 kV was applied. MEKC conditions: fused-silica capillary (id 50 μm, total length 60 cm, length to detector 51.5 cm), detection at 200 nm, capillary temperature 25°C, applied voltage −10 kV. (A) 10 mM phosphate buffer and 30 mM C_{14}MImCl-based BGE (pH 7.4). (B) 25 mM phosphate buffer and 45 mM C_{14}MImCl-based BGE (pH 7.4). The ├─┤ represents an apparent stationary state.

approximately 5 min (Fig. 1A), the aggregates formation has come to an apparent stationary state, and the pattern of spikes stabilizes. This may correspond to the situation in which the aggregates have reached the size comparable to that of the capillary (the micelle aggregates do not become larger).

For comparison of the aggregation potential of BGE of different concentrations, we measured the root mean square (RMS) of the signal fluctuation over the stationary area (e.g., area of constant fluctuation size, see Fig. 1A and B) as a reproducible and unique criterion for all BGE concentrations. RMS as a function of BGE concentration and different voltages (−5, −10, −15 kV) is plotted in Fig. 2A and B.

As can be seen from Fig. 2A with the application of −5, −10, and −15 kV, the RMS is more intensive when 10 and 15 mM phosphate buffers are used with the highest RMS belonging to −10 kV. The lowest RMS corresponds to 5 and 45 mM phosphate buffers with application of −5, −10, and −15 kV. On the whole, −10 kV produces the highest and −5 kV the lowest RMS values (Fig. 2A). In Fig. 2B, the highest RMS value corresponds to 50 mM C_{14}MImCl when −15 kV was applied, the lowest one to 45 mM C_{14}MimCl with application of −5 kV. In general, when −10 kV was applied, the RMS values were high, being the greatest with 40 and 45 mM C_{14}MimCl (Fig. 2B).

When the voltage was set to −10 kV and the phosphate buffer concentration was kept constant at 10 mM with the ionic liquid concentration varied from 30 to 60 mM, the pattern of spikes on the electropherograms appeared from 30 to 45 mM C_{14}MImCl and the aggregation time was shorter as the BGE became more diluted. At the same time, when the phosphate buffer concentration was set to 15 mM and the ionic liquid concentration was varied over the same range, the pattern of spikes on the electropherograms appeared from 40 to 60 mM C_{14}MImCl and the aggregation time was longer as the BGE became more diluted (Fig. 3). With the application of −5 and −15 kV, the aggregation time was constant regardless of phosphate buffer and C_{14}MImCl concentrations in BGEs.

So it follows from our results that the appearance of the aggregates depends on the concentration of BGE components: micelle aggregates appear at a certain threshold concentration of BGE components (phosphate and C_{14}MImCl) and cease to appear at higher BGE concentrations.

There are reports that aggregation can be observed beyond a certain field threshold, which is probably due to the finite size of the capillary [1]. Nevertheless, we do not attempt to give a theoretical explanation of the observed spikes appearance phenomenon and leave this matter for further studies.

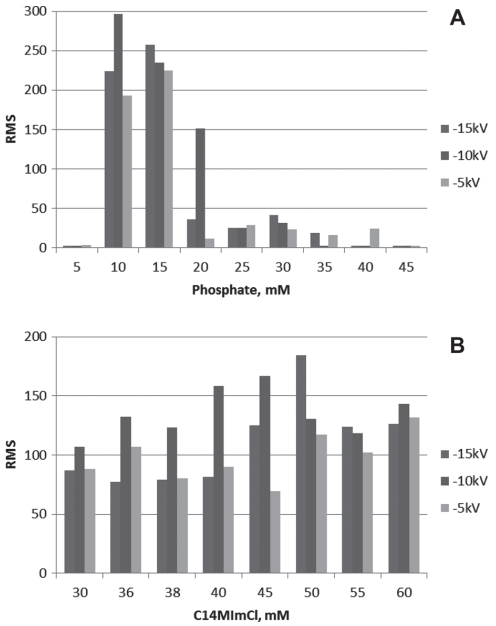

Figure 2. RMS of spikes as a function of phosphate buffer (pH 7.4) concentration (A) and C_{14}MImCl concentration (B). Experimental conditions: applied voltage −5, −10, and −15 kV, other conditions as in Fig. 1.

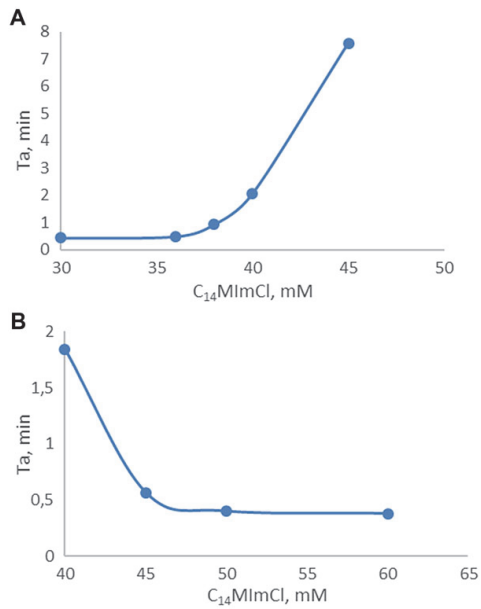

Figure 3. Aggregation time T_a as a function of C_{14}MImCl concentration. Experimental conditions: (A) 10 mM phosphate buffer, pH 7.4; (B) 15 mM phosphate buffer, pH 7.4, other conditions as in Fig. 1.

It seems that the aggregation is a much more widely spread fact than presently anticipated and should emerge in many common BGE systems. Obviously, it is a disturbing factor if CE is considered as an analytical method. On the other hand, CE could be a good platform for study of aggregation of different substances.

The authors have declared no conflict of interest.

References

[1] Magnúsdottir, S., Isambert, H., Heller, Ch., Viovy, J.-L., *Biopolymers* 1999, *49*, 385–401.

[2] Hjerten, S., Srichaiyo, T., Elenbring, K., *Abstract Presented at HPCE '91*, San Diego, CA 1991, pp. 3–6.

[3] Schneiderheinze, J. M., Armstrong, D. W., Schukte, G., Westenberg, D. J., *FEMS Microbiol. Lett.* 2000, *189*, 39–44.

[4] Armstrong, D. W., Girod, M., He, L., Rodriguez, M. A., Wei, W., Zheng, J., Yeung, E. S., *Anal. Chem.* 2002, *74*, 5523–5530.

[5] Zheng, J., Yeung, E. S., *Anal. Chem.* 2003, *75*, 818–824.

[6] Dziubakiewicz, E., Buszewski, B., *Electrophoresis* 2014, *35*, 1160–1164.

[7] Übner, M., Lepane, V., Lopp, M., Kaljurand, M., *J. Chromatogr. A* 2004, *1045*, 253–258.

[8] Vanyúr, R., Biczók, L., Miskolczy, Z., *Physicochem. Eng. Aspects* 2007, *299*, 256–260.

Publication IV

Kazarjan, J., Vaher, M., Hunter, T., Kulp, M., Hunter, G.J., Bonetta, R., Farrugia, D., Kaljurand, M. Determination of metal content in superoxide dismutase enzymes by capillary electrophoresis. – *J. Sep. Sci*., 2015, 38, 1042-1045.

Jana Kazarjan[1]
Merike Vaher[1]
Thérèse Hunter[2]
Maria Kulp[1]
Gary James Hunter[2]
Rosalin Bonetta[2]
Diane Farrugia[2]
Mihkel Kaljurand[1]

[1]Department of Chemistry, Tallinn University of Technology, Tallinn, Estonia
[2]Department of Physiology and Biochemistry, University of Malta, Msida, Malta

Received August 22, 2014
Revised December 23, 2014
Accepted December 26, 2014

Short Communication

Determination of metal content in superoxide dismutase enzymes by capillary electrophoresis†

Superoxide dismutases are antioxidant scavenger enzymes that contain a metal cofactor (copper, zinc, iron, and manganese) in their active site. Metal content measurement is one of the essential steps to characterize enzyme biological activity. We have developed a capillary electrophoretic protocol for the determination of the metal content in superoxide dismutase enzymes. The background electrolyte containing 10 mM pyridine-2,6-dicarboxylic acid and 1 mM 1-methyl-3-tetradecylimidazolium chloride at pH 3.8 was optimized for on-column complexation of the above-mentioned metals. The minimum detectable levels of metals ranged from 0.3 to 1.2 μg/mL. The reliability of the method was checked by parallel quantitative determination of the metal content in superoxide dismutase enzymes by graphite furnace or flame atomic absorption spectrophotometry methods.

Keywords: Capillary electrophoresis / On-column complexation / Quantitative metal analysis / Superoxide dismutase
DOI 10.1002/jssc.201400925

Additional supporting information may be found in the online version of this article at the publisher's web-site

1 Introduction

Superoxide dismutases (SOD) are metalloenzymes that protect cells against oxidative damage caused by superoxide radicals that are unavoidably formed by aerobic respiration. Three forms of SOD have been identified, each having different metal cofactors at their active site: CuZnSOD, FeSOD, and MnSOD. These metal cofactors are necessary for the redox cycling that results in the disproportionation of the superoxide radical into molecular oxygen and hydrogen peroxide. SOD activity, therefore, depends on the degree of metalation [1–3]. Currently, there are several methods to measure the metal content in proteins. The most common ones are graphite furnace or flame atomic absorption spectrophotometry (GFAAS or FAAS) and inductively coupled plasma with atomic emission spectrophotometry [4, 5]. Compared to these techniques, CE is a fast and simple method that has advantages such as high separation ability of mixtures of ions, small sample, and BGE consumption and ease of automation [6]. Moreover, CE has been used for the general characterization of SODs [7, 8].

CE has been extensively used for the determination of metal ions in different matrices [9, 10]. In general, there are two possible ways to measure metals by CE [11]. The First one is the precolumn complexation, where an excess of ligand is added to the sample to ensure the complete complex formation [12]. The second approach is on-column complexation, which allows direct injection of sample to CZE where a rapid complexation reaction between metal ions and ligand(s) occurs [13]. On-column complexation of metal ions with direct UV detection is possible when using pyridine-2,6-dicarboxylic acid (PDC) as a ligand that chelates metal ions producing anionic complexes [14, 15]. To get a fast CE separation of the anionic metal complexes, addition of a cationic surfactant is necessary. An ionic liquid (IL), 1-methyl-3-tetradecylimidazolium chloride (C_{14}MImCl), which has a long alkyl chain on the cation, was used in this work as an additive in the BGE to reverse the direction of the EOF, and detection of the chelated metals was performed in reverse polarity separation mode. Nowadays ILs have numerous chemical applications and are used in various analytical techniques including HPLC, GC, and MS [16–18]. ILs also serve as BGE additives in CE in the analysis of different samples [19, 20].

Correspondence: Jana Kazarjan, Department of Chemistry, Tallinn, University of Technology, Akadeemia tee 15, 12618 Tallinn, Estonia
E-mail: jana.kazarjan@gmail.com
Fax: +372-620-43-25

Abbreviations: AAS, atomic absorption spectrophotometry; **C_{14}MImCl**, 1-methyl-3-tetradecylimidazolium chloride; **GF/FAAS**, graphite furnace/flame atomic emission spectrophotometry; **IL**, ionic liquid; **PDC**, pyridine-2,6-dicarboxylic acid; **SOD**, superoxide dismutase

†This paper is included in the virtual special issue on Amino acids, proteins and peptides available at the Journal of Separation Science website.

The main objective of the present study is to develop a CE protocol for the separation, identification and quantification of Cu, Zn, Mn, and Fe contentin SOD enzymes using novel PDC and C_{14}MImCl-based BGE. To our knowledge, this is the first report of metal-content determination in SOD enzymes by CE.

2 Materials and methods

2.1 Chemicals

All chemicals were of analytical grade and were used as received. Pyridine-2,6-dicarboxylic acid was purchased from Merck (Darmstadt, Germany), 1-methyl-3-tetradecylimidazolium chloride was supplied by Queen's University Ionic Liquid Laboratories (Belfast, UK).

The metal standard solutions were prepared by dissolving appropriate amounts of metal sulfate or chloride salts in deionized water (Milli-Q, Millipore, USA, resistivity >18 MΩ·cm) MilliQ water at a final concentration of 500 μg/mL and then filtered through a 0.45 μm membrane filter before use. MilliQ water was also used for the preparation of BGEs and dilution of samples.

2.2 Instrumentation

Capillary electrophoretic analyses were performed using an Agilent 3D instrument (Agilent Technologies, Waldbronn, Germany) equipped with a diode array UV/Vis detector. A fused-silica capillary (Polymicro Technologies, Phoenix, USA) with an internal diameter of 75 μm and a length of 51.5/60 cm (L_{eff}/L_{tot}, effective capillary length (length to detector)/total capillary length, respectively) was used in the experiments. The separation voltage was –20 kV. The analytes were detected at a wavelength of 214 nm. The injection pressure was set to 50 mbar for 6 s. The temperature of the capillary was set at 30°C. All electropherograms were recorded and integrated with Agilent ChemStation software. Between runs, the capillary was rinsed with MilliQ water for 2 min and BGE solution for 5 min (for more details see Supporting Information).

2.3 Sample preparation

The analyzed protein samples include Bovine CuZnSOD, *Escherichia coli* FeSOD, *Caenorhabditis elegans* MnSOD all of which were purified to more than 95% purity based on SDS-PAGE analysis (Supporting Information). For CE analysis of metals SOD stocks were (0.44–1.62 mg, 200–976 μL) lyophilized under vacuum at 50°C. The residues were resuspended in 35% HCl (1:1) and the hydrolysis was performed overnight at 100°C. Then hydrogen peroxide was added (1:1) and the mixture was incubated for 5 h at 85°C in a water bath. Finally, the mixture was dried under reduced pressure and then dissolved in appropriate amount (100–200 μL) of MilliQ water. For GF/FAAS analysis the proteins were treated with concentrated nitric acid (1:1) in a water bath at 85°C for 2 h. After cooling, the samples were diluted with MilliQ water.

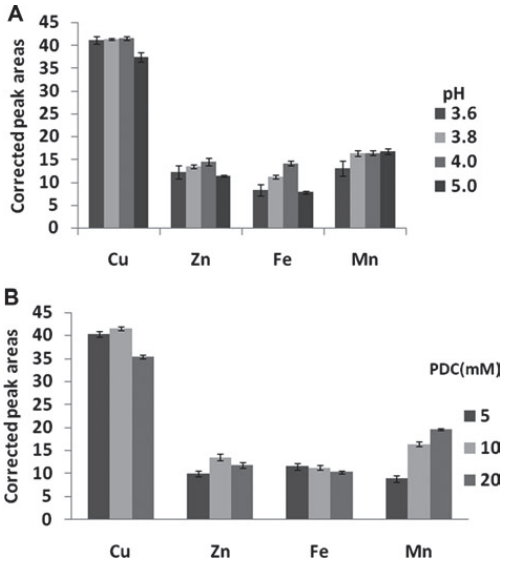

Figure 1. Dependence of the corrected peak areas on the pH of the BGE (A) and the concentration of the PDC (B). (A) 10 mM PDC, 1 mM C_{14}MImCl as BGE (B) 5, 10, and 20 mM PDC with 1 mM C_{14}MImCl at pH 3.8 as BGE.

3 Results and discussion

3.1 Capillary coating

Before optimizing the pH of BGE and PDC concentration the dynamic wall coating with 1-methyl-3-tetradecylimidazolium chloride was tested in a concentration range 0.5–2.5 mM. A final concentration of 1 mM of C_{14}MImCl was selected as it provided stable dynamic coating and optimal selectivity.

3.2 pH of the BGE

PDC is an ionizable compound ($pK_{a1} = 2.1$, $pK_{a2} = 4.4$ at 25°C [15]), therefore, its ligand concentration depends on the pH: the higher the pH of the solution, the more charged ligand is formed and more metals are complexed. When the pH of the BGE was increased from 3.6 to 4.0 (Fig. 1A), the peak areas of the complexed metals increased slightly. This is probably due to an increase in the PDC^{2-} concentration that, in turn, favors the formation of the complex ($[Fe(PDC)_2]^{2-}$, $[Fe(PDC)_2]^{-}$, $[Zn(PDC)_2]^{2-}$, $[Mn(PDC)_2]^{2-}$). With the exception of manganese, with the further increase in pH until 5 a slight reduction in the peak areas was observed, probably attributable to precipitation of the metal hydroxide [21].

Although the peak areas were slightly higher at pH 4.0, a pH of 3.8 was selected for the subsequent studies of the metals because of the more stable baseline.

3.3 PDC concentration

The concentration of PDC was varied from 5 to 20 mM (Fig. 1B). Although, the high concentration of PDC^{2-} supports the formation of the complex, overall the sensitivity of detection slightly decreases with the exception of the Mn ion. This decrease in sensitivity may be due to a higher background absorbance with the increase of the PDC concentration that has a high molar absorptivity [15]. In the case of manganese, the $[Mn(PDC)_2]^{2-}$ complex is more favorably formed when PDC concentration is increased. The corrected peak areas for Fe remained almost unchanged with the variation in PDC concentration. The above experiments suggest that the optimal complexation and separation for Cu, Zn, Fe, and Mn complexes can be achieved using 10 mM PDC.

3.4 Sample analysis

Real sample analysis was carried out with the optimized BGE containing 10 mM PDC and 1 mM C_{14}MImCl at pH 3.8.

Before sample analysis, it was necessary to check for the possible interference of other metal cations that may be present in the protein solutions. In general, purified proteins are stored in buffer solutions of specified pH and ionic concentrations for optimal stability and activity. These buffers (Tris-HCl and/or KH_2PO_4/K_2HPO_4) usually contain contaminating salts, so cations like K^+, Na^+, Ca^{2+}, Mg^{2+} may potentially interfere with detection of the metals under investigation. Some other components of the buffer like Cl^-, HPO_4^{2-} and $H_2PO_4^-$ usually do not disturb the CE analysis. The possible effect of Tris-HCl, which is also a common buffer used in microbiology, has been checked (Fig. 2A). Monovalent cations (K^+, Na^+) do not form complexes with PDC, thus they were not checked. Magnesium ion was not detected as it has a low complexation constant with PDC [15]. The potential interference of calcium ions with the metals ions under investigation was studied. As seen from Fig. 2B, the Ca^{2+} peak appears last on the electropherogram and is separated from Cu^{2+}, Zn^{2+}, Fe^{3+}, and Mn^{2+} peaks, thus showing no interference.

The peaks of metal complexes in Fig. 2B, C and later in the real samples were identified using standard addition method. The migration order of metal complexes in Fig. 2B is Cu^{2+}, Zn^{2+}, Fe^{3+}, Mn^{2+}, and Ca^{2+} that reflects the charge to size differences of the anionic metal complexes. Moreover, compared to previous works [15, 21], baseline separation of Cu^{2+}, Zn^{2+} and Fe^{3+}, Fe^{2+} has also been achieved (Fig. 2B, C).

Calibration curves were obtained by plotting the corrected peak areas (ratio of peak area to migration time) of each analyte against concentration. Calibration equations, correlation coefficients (R^2), LODs (S/N = 3) and RSDs of the corrected peak areas and migration times are presented in Supporting Information Table S1. The calibration curves exhibit good linearities (R^2 is 0.992–0.999 in a concentration range 2.5–100 μg/mL), the obtained detection limits are 0.3 μg/mL for Cu^{2+}, 1.0 μg/mL for Zn^{2+}, 0.5 μg/mL for Mn^{2+}, and 1.2 μg/mL for Fe^{3+}.

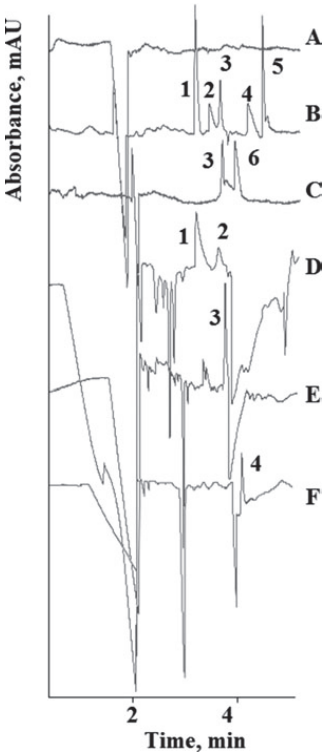

Figure 2. Electropherograms of 10 mM Tris-HCl (A), standard metal mixture (B), Fe^{2+} and Fe^{3+} mixture (C), CuZnSOD (D), FeSOD (E), MnSOD (F) Peak identification: 1–Cu^{2+}, 2–Zn^{2+}, 3–Fe^{3+}, 4–Mn^{2+}, 5–Ca^{2+}, 6–Fe^{2+}, CE conditions: standards concentration 15 μg/mL (B), 30 μg/mL (C), 10 mM PDC with 1 mM C14MImCl at pH 3,8 as BGE, capillary length 60 cm (51,5 cm to detector), detection at 214 nm, injection pressure 50 mbar for 6 s, capillary temperature 30°C, applied voltage –20 kV.

In Fig. 2D the electropherogram of CuZnSOD is given with two positive peaks (marked 1 and 2) representing Cu^{2+} and Zn^{2+}, respectively, whereas the negative peaks belong to the amino acids that may remain in the solution even after acid hydrolysis. The large negative dip that immediately follows the Zn^{2+} peak (Fig. 2D) is an unresolved peak of significant amount of amino acids. The stability of MnSODs and FeSODs to high temperatures, pH extremes, detergents is generally lower than that of CuZnSOD [22], therefore, the negative peak of comigrating amino acids of CuZnSOD is larger compared to that of FeSOD and MnSOD (Fig. 2E, F). The negative dip that follows Fe^{3+} (Fig. 2C, E) may interfere with the determination of Fe^{2+} but as sample preparation was

Table 1. Comparative metal ion content in laboratory-purified SOD enzymes obtained by CE and AAS ($n = 3$)

SOD	Metal ion	CE μg metal/mg protein (±SD)	AAS μg metal/mg protein (±SD)
CuZnSOD	Cu^{2+}	3.01 ± 0.09	2.858 ± 0.003
	Zn^{2+}	3.1 ± 0.2	3.000 ± 0.004
Mn(Fe)SOD	Fe^{3+}	0.92 ± 0.09	0.820 ± 0.003
	Mn^{2+}	N.D.	0.375 ± 0.004
MnSOD	Mn^{2+}	1.30 ± 0.05	1.190 ± 0.004
FeSOD	Fe^{3+}	1.8 ± 0.2	1.600 ± 0.003

N.D., not detected.

carried out in aerobic and acidic conditions only the amount of Fe^{3+} was measured in FeSOD.

To exclude possible interferences of unresolved peaks of amino acids, CE analysis (Supporting Information Fig. S2) of apo-FeSOD and apo-MnSOD (metal-free SOD) was performed. As seen from Supporting Information Fig. S2 the negative dip does not affect the determination of Fe^{3+} and Mn^{2+} in FeSOD and MnSOD samples, respectively.

The metal content of the protein samples was also measured by the GF/FAAS methods. The data obtained by both the CE and AAS is represented in Table 1, where the metal concentration is given as μg metal per 1 mg of protein. As it may be seen from Table 1 the result for the Mn content in Mn(Fe)SOD is given only when measured by AAS. Mn(Fe)SOD is a Fe-substituted MnSOD, which means that naturally occurring Mn is replaced with Fe. Hence the CE result is missing because of an insufficient amount of manganese to be detected by CE. In general, the results obtained from CE were in good agreement and highly correlated with the AAS results ($R^2 > 0.99$).

4 Concluding remarks

The proposed CE method allowed for the simultaneous determination of metal (Cu^{2+}, Zn^{2+}, Fe^{3+}, and Mn^{2+}) content in superoxide dismutase enzymes. It demonstrated that on-column complexation can be used for the separation and quantification of metal ions in a new electrolyte containing PDC and 1 mM C_{14}MImCl at pH 3.8. The developed CE protocol is fast, simple, and cost-efficient. Although LODs are higher when compared to other methods (Supporting Information Table S2), CE still may be used for the metal content analysis if metal ions are present in a sufficient amount in laboratory-purified enzymes.

This work was supported by the Estonian Science Foundation Grant SF0140023s08. D.F. was funded by the Strategic Educational Pathways Scholarship, Malta award, which is part-financed by the European Social Fund Operational Programme II 2007–2013. This work was also partially funded by the University of Malta research grant PHBRP02–03 awarded to T.H.

The authors have declared no conflict of interest.

5 References

[1] Whittaker, J. W., *Biochim. Biophys. Acta* 2010, *1804*, 298–307.

[2] Yang, M., Cobine, P. A, Molik, S., Naranuntarat, A., Lill, R., Winge, D. R., Culotta, V. C., *Embo. J.* 2006, *25*, 1775–1783.

[3] Van Raamsdonk, J. M., Hekimi, S., *Proc. Natl. Acad. Sci. USA* 2012, *109*, 5785–5790.

[4] Savory, J., Herman, M. M., *Ann. Clin. Lab. Sci.* 1999, *29*, 118–126.

[5] Szpunar, J., *Analyst* 2000, *125*, 963–988.

[6] Kuban, P., Timerbaev, A. R., *Electrophoresis* 2014, *35*, 225–233.

[7] Borges-Alvarez, M., Benavente, F., Barbosa, J., Sanz-Nebot, V., *Electrophoresis* 2012, *33*, 2561–2569.

[8] Borges-Alvarez, M., Benavente, F., Barbosa, J., Sanz-Nebot, V., *Mass Spectrom.* 2010, *24*, 1411–1418.

[9] Olšauskaite, V., Paliulionyte, V., Padarauskas, A., *Clin. Chim. Acta* 2000, *293*, 181–186.

[10] Sarazin, C., Delaunay, N., Costanza, C., Eudes, V., Gareil, P., *Electrophoresis* 2011, *32*, 1282–1291.

[11] Liu, B. F., Liu, L. B., Cheng, J. K., *J. Chromatogr. A* 1999, *834*, 277–308.

[12] Pozdniakova, S., Padarauskas, A., *Analyst* 1998, *123*, 1497–1500.

[13] Quirino, J. P., Haddad, P. R., *J. Sep. Sci.* 2011, *34*, 2872–2878.

[14] Soga, T., Ross, G. A., *J. Chromatogr. A* 1999, *834*, 65–71.

[15] Sarazin, C., Delaunay, N., Verenne, A., Costanza, Ch., Eudes, V., Gareil, P., *J. Sep. Sci.* 2010, *33*, 3177–3183.

[16] Zhou, L., Danielson, N. D., *J. Chromatogr. B* 2013, *940*, 112–120.

[17] Shashkov, M. V., Sidelnikov, V. N., *J. Chromatogr. A* 2013, *1309*, 56–63.

[18] Dertinger, J. J., Walker, A. V., *J. Am. Soc. Mass Spectrom.* 2013, *24*, 348–355.

[19] Vaher, M., Koel, M., Kazarjan, J., Kaljurand, M., *Electrophoresis* 2011, *32*, 1068–1073.

[20] Borissova, M., Gorbatšova, J., Ebber, A., Kaljurand, M., Koel, M., Vaher, M., *Electrophoresis* 2007, *28*, 3600–3605.

[21] Chen, Z., Naidu, R., *J. Chromatogr. A* 2002, *927*, 245–251.

[22] Grune, T. (Ed.), *Oxidants and Antioxidant Defense Systems, The Handbook of Environmental Chemistry*, Springer, Heidelberg 2005.

CURRICULUM VITAE

1. Personal data

Name	Jana Kazarjan
Date and place of birth	21.03.1985, Tallinn, Estonia
E-mail address	jana.kazarjan@gmail.com

2. Education

Educational institution	Graduation year	Education (field of study/ degree)
Tallinna Linnamäe Gümnaasium	2004	Secondary education
Tallinn University of Technology	2007	Applied Chemistry and Biotechnology/ B.Sc. (Hons)
Tallinn University of Technology	2011	Applied Chemistry and Biotechnology/ M.Sc. (Hons)

3. Language competence/ skills (fluent, average, basic skills)

Language	Level
Estonian	Fluent
English	Fluent
Russian	Fluent

4. Special Courses

Period	Educational or other organisation
2011–2014	Graduate School "Functional materials and processes", Tallinn University of Technology, Estonia
Sept 30–Oct 3, 2012	19th International Symposium, Exhibit & Workshops on Electro- and Liquid Phase-separation Techniques, Baltimore, Maryland, USA
Feb–Jun 2013	Department of Physiology and Biochemistry, University of Malta, Malta
Oct 22–23, 2013	POKE Symposium, Sustainable Chemistry and Process Technology in the Northern Baltic Sea Region, Vaasa, Finland
Dec 11–12, 2013	POKE Symposium, Sustainable Chemistry and Process Technology in the Northern Baltic Sea Region, Tallinn, Estonia
Spring 2014	Pharmaceutical Bioinformatics, online course, Uppsala Universitet, Sweden
Jan–Jun 2014	Department of Physiology and Biochemistry, University of Malta, Malta

Spring 2015	Applied Pharmaceutical Bioinformatics, online course, Uppsala Universitet, Sweden
Jun 21–25, 2015	42nd International Symposium on High Performance Liquid Phase Separations and Related Techniques, Geneva, Switzerland

5. Professional Employment

Period	Organisation	Position
2011–2013	Tallinn University of Technology	Teaching in the fields of analytical chemistry

6. Research activity

Jana Kazarjan, bachelor's degree, 2007, suprs Aini Vaarmann, Anu Viitak, Investigation of content of heavy metals and chlorides in dusts of street cleaning services, Tallinn University of Technology, Faculty of Science, Department of Chemistry, Chair of Analytical Chemistry

Jana Kazarjan, master's degree, 2011, supervisor Merike Vaher, Determination of carbohydrates by capillary electrophoresis, Tallinn University of Technology, Faculty of Science, Department of Chemistry

ELULOOKIRJELDUS

1. Isikuandmed

Ees-ja perekonnanimi	Jana Kazarjan
Sünniaeg ja -koht	21.03.1985, Tallinn, Eesti
Kodakondsus	Eesti
E-posti aadress	jana.kazarjan@gmail.com

2. Kontaktandmed

Õppeasutus (nimetus lõpetamise ajal)	Lõpetamise aeg	Haridus (eriala/ kraad)
Tallinna Linnamäe Gümnaasium	2004	Keskharidus
Tallinna Tehnikaülikool	2007	Rakenduskeemia ja Biotehnoloogia/ B.Sc. (Hons)
Tallinna Tehnikaülikool	2011	Rakenduskeemia ja Biotehnoloogia/ M.Sc. (Hons)

3. Keelteoskus (alg-, kesk- või kõrgtase)

Keel	Tase
Eesti	Kõrg
Inglise	Kõrg
Vene	Kõrg

4. Täiendusõpe

Õppimise aeg	Täiendusõppe korraldaja nimetus
2011–2014	Doktorikool "Funktsionaalsed materjalid ja tehnoloogiad", Tallinna Tehnikaülikool, Eesti
Sept 30–Oct 3, 2012	19th International Symposium, Exhibit & Workshops on Electro- and Liquid Phase-separation Techniques, Baltimore, Maryland, USA
Feb–Jun 2013	Füsioloogia ja Biokeemia instituut, Malta Ülikool, Malta
Oct 22–23, 2013	POKE Symposium, Sustainable Chemistry and Process Technology in the Northern Baltic Sea Region, Vaasa, Soome
Dec 11–12, 2013	POKE Symposium, Sustainable Chemistry and Process Technology in the Northern Baltic Sea Region, Tallinn, Eesti

Kevad 2014	Pharmaceutical Bioinformatics, online kursus, Uppsala Universitet, Rootsi
Jan–Jun 2014	Füsioloogia ja Biokeemia instituut, Malta Ülikool, Malta
Kevad 2015	Applied Pharmaceutical Bioinformatics, online course, Uppsala Universitet, Rootsi
Jun 21–25, 2015	42nd International Symposium on High Performance Liquid Phase Separations and Related Techniques, Genf, Šveits

5. Teenistuskäik

Töötamise aeg	Tööandja nimetus	Ametikoht
2011–2013	Tallinna Tehnikaülikool	Õppetöö läbiviimine analüütilise keemia alal

6. Teadustegevus

Jana Kazarjan, bakalaureusekraad, 2007, juhendajad Aini Vaarmann, AnuViitak, Raskmetallide ja kloriidide sisalduse uurimine tänavakoristusfirmade pühkmetes, Tallinna Tehnikaülikool, Matemaatika-loodusteaduskond, Keemiainstituut, Analüütilise keemia õppetool

Jana Kazarjan, magistrikraad, 2011, juhendaja Merike Vaher, Neutraalsete suhkrute määramine kapillaarelektroforeesi meetodil, Tallinna Tehnikaülikool, Maatemaatika-loodusteaduskond, Keemiainstituut, Analüütilise keemia õppetool.

DISSERTATIONS DEFENDED AT
TALLINN UNIVERSITY OF TECHNOLOGY ON
NATURAL AND EXACT SCIENCES

1. **Olav Kongas**. Nonlinear Dynamics in Modeling Cardiac Arrhytmias. 1998.
2. **Kalju Vanatalu**. Optimization of Processes of Microbial Biosynthesis of Isotopically Labeled Biomolecules and Their Complexes. 1999.
3. **Ahto Buldas**. An Algebraic Approach to the Structure of Graphs. 1999.
4. **Monika Drews**. A Metabolic Study of Insect Cells in Batch and Continuous Culture: Application of Chemostat and Turbidostat to the Production of Recombinant Proteins. 1999.
5. **Eola Valdre**. Endothelial-Specific Regulation of Vessel Formation: Role of Receptor Tyrosine Kinases. 2000.
6. **Kalju Lott**. Doping and Defect Thermodynamic Equilibrium in ZnS. 2000.
7. **Reet Koljak**. Novel Fatty Acid Dioxygenases from the Corals *Plexaura homomalla* and *Gersemia fruticosa.* 2001.
8. **Anne Paju**. Asymmetric oxidation of Prochiral and Racemic Ketones by Using Sharpless Catalyst. 2001.
9. **Marko Vendelin**. Cardiac Mechanoenergetics *in silico*. 2001.
10. **Pearu Peterson**. Multi-Soliton Interactions and the Inverse Problem of Wave Crest. 2001.
11. **Anne Menert**. Microcalorimetry of Anaerobic Digestion. 2001.
12. **Toomas Tiivel**. The Role of the Mitochondrial Outer Membrane in *in vivo* Regulation of Respiration in Normal Heart and Skeletal Muscle Cell. 2002.
13. **Olle Hints**. Ordovician Scolecodonts of Estonia and Neighbouring Areas: Taxonomy, Distribution, Palaeoecology, and Application. 2002.
14. **Jaak Nõlvak**. Chitinozoan Biostratigrapy in the Ordovician of Baltoscandia. 2002.
15. **Liivi Kluge**. On Algebraic Structure of Pre-Operad. 2002.
16. **Jaanus Lass**. Biosignal Interpretation: Study of Cardiac Arrhytmias and Electromagnetic Field Effects on Human Nervous System. 2002.
17. **Janek Peterson**. Synthesis, Structural Characterization and Modification of PAMAM Dendrimers. 2002.
18. **Merike Vaher**. Room Temperature Ionic Liquids as Background Electrolyte Additives in Capillary Electrophoresis. 2002.
19. **Valdek Mikli**. Electron Microscopy and Image Analysis Study of Powdered Hardmetal Materials and Optoelectronic Thin Films. 2003.
20. **Mart Viljus**. The Microstructure and Properties of Fine-Grained Cermets. 2003.
21. **Signe Kask**. Identification and Characterization of Dairy-Related *Lactobacillus.* 2003
22. **Tiiu-Mai Laht**. Influence of Microstructure of the Curd on Enzymatic and Microbiological Processes in Swiss-Type Cheese. 2003.
23. **Anne Kuusksalu**. 2–5A Synthetase in the Marine Sponge *Geodia cydonium*. 2003.
24. **Sergei Bereznev**. Solar Cells Based on Polycristalline Copper-Indium Chalcogenides and Conductive Polymers. 2003.

25. **Kadri Kriis**. Asymmetric Synthesis of C_2-Symmetric Bimorpholines and Their Application as Chiral Ligands in the Transfer Hydrogenation of Aromatic Ketones. 2004.
26. **Jekaterina Reut**. Polypyrrole Coatings on Conducting and Insulating Substracts. 2004.
27. **Sven Nõmm**. Realization and Identification of Discrete-Time Nonlinear Systems. 2004.
28. **Olga Kijatkina**. Deposition of Copper Indium Disulphide Films by Chemical Spray Pyrolysis. 2004.
29. **Gert Tamberg**. On Sampling Operators Defined by Rogosinski, Hann and Blackman Windows. 2004.
30. **Monika Übner**. Interaction of Humic Substances with Metal Cations. 2004.
31. **Kaarel Adamberg**. Growth Characteristics of Non-Starter Lactic Acid Bacteria from Cheese. 2004.
32. **Imre Vallikivi**. Lipase-Catalysed Reactions of Prostaglandins. 2004.
33. **Merike Peld**. Substituted Apatites as Sorbents for Heavy Metals. 2005.
34. **Vitali Syritski**. Study of Synthesis and Redox Switching of Polypyrrole and Poly(3,4-ethylenedioxythiophene) by Using *in-situ* Techniques. 2004.
35. **Lee Põllumaa**. Evaluation of Ecotoxicological Effects Related to Oil Shale Industry. 2004.
36. **Riina Aav**. Synthesis of 9,11-Secosterols Intermediates. 2005.
37. **Andres Braunbrück**. Wave Interaction in Weakly Inhomogeneous Materials. 2005.
38. **Robert Kitt**. Generalised Scale-Invariance in Financial Time Series. 2005.
39. **Juss Pavelson**. Mesoscale Physical Processes and the Related Impact on the Summer Nutrient Fields and Phytoplankton Blooms in the Western Gulf of Finland. 2005.
40. **Olari Ilison**. Solitons and Solitary Waves in Media with Higher Order Dispersive and Nonlinear Effects. 2005.
41. **Maksim Säkki**. Intermittency and Long-Range Structurization of Heart Rate. 2005.
42. **Enli Kiipli**. Modelling Seawater Chemistry of the East Baltic Basin in the Late Ordovician–Early Silurian. 2005.
43. **Igor Golovtsov**. Modification of Conductive Properties and Processability of Polyparaphenylene, Polypyrrole and polyaniline. 2005.
44. **Katrin Laos**. Interaction Between Furcellaran and the Globular Proteins (Bovine Serum Albumin β-Lactoglobulin). 2005.
45. **Arvo Mere**. Structural and Electrical Properties of Spray Deposited Copper Indium Disulphide Films for Solar Cells. 2006.
46. **Sille Ehala**. Development and Application of Various On- and Off-Line Analytical Methods for the Analysis of Bioactive Compounds. 2006.
47. **Maria Kulp**. Capillary Electrophoretic Monitoring of Biochemical Reaction Kinetics. 2006.
48. **Anu Aaspõllu.** Proteinases from *Vipera lebetina* Snake Venom Affecting Hemostasis. 2006.
49. **Lyudmila Chekulayeva**. Photosensitized Inactivation of Tumor Cells by Porphyrins and Chlorins. 2006.

50. **Merle Uudsemaa**. Quantum-Chemical Modeling of Solvated First Row Transition Metal Ions. 2006.
51. **Tagli Pitsi**. Nutrition Situation of Pre-School Children in Estonia from 1995 to 2004. 2006.
52. **Angela Ivask**. Luminescent Recombinant Sensor Bacteria for the Analysis of Bioavailable Heavy Metals. 2006.
53. **Tiina Lõugas**. Study on Physico-Chemical Properties and Some Bioactive Compounds of Sea Buckthorn (*Hippophae rhamnoides* L.). 2006.
54. **Kaja Kasemets**. Effect of Changing Environmental Conditions on the Fermentative Growth of *Saccharomyces cerevisae* S288C: Auxo-accelerostat Study. 2006.
55. **Ildar Nisamedtinov**. Application of ^{13}C and Fluorescence Labeling in Metabolic Studies of *Saccharomyces* spp. 2006.
56. **Alar Leibak**. On Additive Generalisation of Voronoï's Theory of Perfect Forms over Algebraic Number Fields. 2006.
57. **Andri Jagomägi**. Photoluminescence of Chalcopyrite Tellurides. 2006.
58. **Tõnu Martma**. Application of Carbon Isotopes to the Study of the Ordovician and Silurian of the Baltic. 2006.
59. **Marit Kauk**. Chemical Composition of $CuInSe_2$ Monograin Powders for Solar Cell Application. 2006.
60. **Julia Kois**. Electrochemical Deposition of $CuInSe_2$ Thin Films for Photovoltaic Applications. 2006.
61. **Ilona Oja Açik**. Sol-Gel Deposition of Titanium Dioxide Films. 2007.
62. **Tiia Anmann**. Integrated and Organized Cellular Bioenergetic Systems in Heart and Brain. 2007.
63. **Katrin Trummal**. Purification, Characterization and Specificity Studies of Metalloproteinases from *Vipera lebetina* Snake Venom. 2007.
64. **Gennadi Lessin**. Biochemical Definition of Coastal Zone Using Numerical Modeling and Measurement Data. 2007.
65. **Enno Pais**. Inverse problems to determine non-homogeneous degenerate memory kernels in heat flow. 2007.
66. **Maria Borissova**. Capillary Electrophoresis on Alkylimidazolium Salts. 2007.
67. **Karin Valmsen**. Prostaglandin Synthesis in the Coral *Plexaura homomalla*: Control of Prostaglandin Stereochemistry at Carbon 15 by Cyclooxygenases. 2007.
68. **Kristjan Piirimäe**. Long-Term Changes of Nutrient Fluxes in the Drainage Basin of the Gulf of Finland – Application of the PolFlow Model. 2007.
69. **Tatjana Dedova**. Chemical Spray Pyrolysis Deposition of Zinc Sulfide Thin Films and Zinc Oxide Nanostructured Layers. 2007.
70. **Katrin Tomson**. Production of Labelled Recombinant Proteins in Fed-Batch Systems in *Escherichia coli*. 2007.
71. **Cecilia Sarmiento**. Suppressors of RNA Silencing in Plants. 2008.
72. **Vilja Mardla**. Inhibition of Platelet Aggregation with Combination of Antiplatelet Agents. 2008.
73. **Maie Bachmann**. Effect of Modulated Microwave Radiation on Human Resting Electroencephalographic Signal. 2008.
74. **Dan Hüvonen**. Terahertz Spectroscopy of Low-Dimensional Spin Systems. 2008.

75. **Ly Villo**. Stereoselective Chemoenzymatic Synthesis of Deoxy Sugar Esters Involving *Candida antarctica* Lipase B. 2008.
76. **Johan Anton**. Technology of Integrated Photoelasticity for Residual Stress Measurement in Glass Articles of Axisymmetric Shape. 2008.
77. **Olga Volobujeva**. SEM Study of Selenization of Different Thin Metallic Films. 2008.
78. **Artur Jõgi**. Synthesis of 4'-Substituted 2,3'-dideoxynucleoside Analogues. 2008.
79. **Mario Kadastik**. Doubly Charged Higgs Boson Decays and Implications on Neutrino Physics. 2008.
80. **Fernando Pérez-Caballero**. Carbon Aerogels from 5-Methylresorcinol-Formaldehyde Gels. 2008.
81. **Sirje Vaask**. The Comparability, Reproducibility and Validity of Estonian Food Consumption Surveys. 2008.
82. **Anna Menaker**. Electrosynthesized Conducting Polymers, Polypyrrole and Poly(3,4-ethylenedioxythiophene), for Molecular Imprinting. 2009.
83. **Lauri Ilison**. Solitons and Solitary Waves in Hierarchical Korteweg-de Vries Type Systems. 2009.
84. **Kaia Ernits**. Study of In_2S_3 and ZnS Thin Films Deposited by Ultrasonic Spray Pyrolysis and Chemical Deposition. 2009.
85. **Veljo Sinivee**. Portable Spectrometer for Ionizing Radiation "Gammamapper". 2009.
86. **Jüri Virkepu**. On Lagrange Formalism for Lie Theory and Operadic Harmonic Oscillator in Low Dimensions. 2009.
87. **Marko Piirsoo**. Deciphering Molecular Basis of Schwann Cell Development. 2009.
88. **Kati Helmja**. Determination of Phenolic Compounds and Their Antioxidative Capability in Plant Extracts. 2010.
89. **Merike Sõmera**. Sobemoviruses: Genomic Organization, Potential for Recombination and Necessity of P1 in Systemic Infection. 2010.
90. **Kristjan Laes**. Preparation and Impedance Spectroscopy of Hybrid Structures Based on $CuIn_3Se_5$ Photoabsorber. 2010.
91. **Kristin Lippur**. Asymmetric Synthesis of 2,2'-Bimorpholine and its 5,5'-Substituted Derivatives. 2010.
92. **Merike Luman**. Dialysis Dose and Nutrition Assessment by an Optical Method. 2010.
93. **Mihhail Berezovski**. Numerical Simulation of Wave Propagation in Heterogeneous and Microstructured Materials. 2010.
94. **Tamara Aid-Pavlidis**. Structure and Regulation of BDNF Gene. 2010.
95. **Olga Bragina**. The Role of Sonic Hedgehog Pathway in Neuro- and Tumorigenesis. 2010.
96. **Merle Randrüüt**. Wave Propagation in Microstructured Solids: Solitary and Periodic Waves. 2010.
97. **Marju Laars**. Asymmetric Organocatalytic Michael and Aldol Reactions Mediated by Cyclic Amines. 2010.
98. **Maarja Grossberg**. Optical Properties of Multinary Semiconductor Compounds for Photovoltaic Applications. 2010.

99. **Alla Maloverjan**. Vertebrate Homologues of Drosophila Fused Kinase and Their Role in Sonic Hedgehog Signalling Pathway. 2010.
100. **Priit Pruunsild**. Neuronal Activity-Dependent Transcription Factors and Regulation of Human *BDNF* Gene. 2010.
101. **Tatjana Knjazeva**. New Approaches in Capillary Electrophoresis for Separation and Study of Proteins. 2011.
102. **Atanas Katerski**. Chemical Composition of Sprayed Copper Indium Disulfide Films for Nanostructured Solar Cells. 2011.
103. **Kristi Timmo.** Formation of Properties of $CuInSe_2$ and $Cu_2ZnSn(S,Se)_4$ Monograin Powders Synthesized in Molten KI. 2011.
104. **Kert Tamm**. Wave Propagation and Interaction in Mindlin-Type Microstructured Solids: Numerical Simulation. 2011.
105. **Adrian Popp**. Ordovician Proetid Trilobites in Baltoscandia and Germany. 2011.
106. **Ove Pärn**. Sea Ice Deformation Events in the Gulf of Finland and This Impact on Shipping. 2011.
107. **Germo Väli**. Numerical Experiments on Matter Transport in the Baltic Sea. 2011.
108. **Andrus Seiman**. Point-of-Care Analyser Based on Capillary Electrophoresis. 2011.
109. **Olga Katargina**. Tick-Borne Pathogens Circulating in Estonia (Tick-Borne Encephalitis Virus, *Anaplasma phagocytophilum*, *Babesia* Species): Their Prevalence and Genetic Characterization. 2011.
110. **Ingrid Sumeri**. The Study of Probiotic Bacteria in Human Gastrointestinal Tract Simulator. 2011.
111. **Kairit Zovo**. Functional Characterization of Cellular Copper Proteome. 2011.
112. **Natalja Makarytsheva**. Analysis of Organic Species in Sediments and Soil by High Performance Separation Methods. 2011.
113. **Monika Mortimer**. Evaluation of the Biological Effects of Engineered Nanoparticles on Unicellular Pro- and Eukaryotic Organisms. 2011.
114. **Kersti Tepp**. Molecular System Bioenergetics of Cardiac Cells: Quantitative Analysis of Structure-Function Relationship. 2011.
115. **Anna-Liisa Peikolainen**. Organic Aerogels Based on 5-Methylresorcinol. 2011.
116. **Leeli Amon**. Palaeoecological Reconstruction of Late-Glacial Vegetation Dynamics in Eastern Baltic Area: A View Based on Plant Macrofossil Analysis. 2011.
117. **Tanel Peets**. Dispersion Analysis of Wave Motion in Microstructured Solids. 2011.
118. **Liina Kaupmees**. Selenization of Molybdenum as Contact Material in Solar Cells. 2011.
119. **Allan Olspert**. Properties of VPg and Coat Protein of Sobemoviruses. 2011.
120. **Kadri Koppel**. Food Category Appraisal Using Sensory Methods. 2011.
121. **Jelena Gorbatšova**. Development of Methods for CE Analysis of Plant Phenolics and Vitamins. 2011.
122. **Karin Viipsi**. Impact of EDTA and Humic Substances on the Removal of Cd and Zn from Aqueous Solutions by Apatite. 2012.

123. **David Schryer**. Metabolic Flux Analysis of Compartmentalized Systems Using Dynamic Isotopologue Modeling. 2012.
124. **Ardo Illaste**. Analysis of Molecular Movements in Cardiac Myocytes. 2012.
125. **Indrek Reile**. 3-Alkylcyclopentane-1,2-Diones in Asymmetric Oxidation and Alkylation Reactions. 2012.
126. **Tatjana Tamberg**. Some Classes of Finite 2-Groups and Their Endomorphism Semigroups. 2012.
127. **Taavi Liblik**. Variability of Thermohaline Structure in the Gulf of Finland in Summer. 2012.
128. **Priidik Lagemaa**. Operational Forecasting in Estonian Marine Waters. 2012.
129. **Andrei Errapart**. Photoelastic Tomography in Linear and Non-linear Approximation. 2012.
130. **Külliki Krabbi**. Biochemical Diagnosis of Classical Galactosemia and Mucopolysaccharidoses in Estonia. 2012.
131. **Kristel Kaseleht**. Identification of Aroma Compounds in Food using SPME-GC/MS and GC-Olfactometry. 2012.
132. **Kristel Kodar**. Immunoglobulin G Glycosylation Profiling in Patients with Gastric Cancer. 2012.
133. **Kai Rosin**. Solar Radiation and Wind as Agents of the Formation of the Radiation Regime in Water Bodies. 2012.
134. **Ann Tiiman**. Interactions of Alzheimer's Amyloid-Beta Peptides with Zn(II) and Cu(II) Ions. 2012.
135. **Olga Gavrilova**. Application and Elaboration of Accounting Approaches for Sustainable Development. 2012.
136. **Olesja Bondarenko**. Development of Bacterial Biosensors and Human Stem Cell-Based *In Vitro* Assays for the Toxicological Profiling of Synthetic Nanoparticles. 2012.
137. **Katri Muska**. Study of Composition and Thermal Treatments of Quaternary Compounds for Monograin Layer Solar Cells. 2012.
138. **Ranno Nahku**. Validation of Critical Factors for the Quantitative Characterization of Bacterial Physiology in Accelerostat Cultures. 2012.
139. **Petri-Jaan Lahtvee**. Quantitative Omics-level Analysis of Growth Rate Dependent Energy Metabolism in *Lactococcus lactis*. 2012.
140. **Kerti Orumets**. Molecular Mechanisms Controlling Intracellular Glutathione Levels in Baker's Yeast *Saccharomyces cerevisiae* and its Random Mutagenized Glutathione Over-Accumulating Isolate. 2012.
141. **Loreida Timberg**. Spice-Cured Sprats Ripening, Sensory Parameters Development, and Quality Indicators. 2012.
142. **Anna Mihhalevski**. Rye Sourdough Fermentation and Bread Stability. 2012.
143. **Liisa Arike**. Quantitative Proteomics of *Escherichia coli*: From Relative to Absolute Scale. 2012.
144. **Kairi Otto**. Deposition of In_2S_3 Thin Films by Chemical Spray Pyrolysis. 2012.
145. **Mari Sepp**. Functions of the Basic Helix-Loop-Helix Transcription Factor TCF4 in Health and Disease. 2012.
146. **Anna Suhhova**. Detection of the Effect of Weak Stressors on Human Resting Electroencephalographic Signal. 2012.

147. **Aram Kazarjan**. Development and Production of Extruded Food and Feed Products Containing Probiotic Microorganisms. 2012.
148. **Rivo Uiboupin**. Application of Remote Sensing Methods for the Investigation of Spatio-Temporal Variability of Sea Surface Temperature and Chlorophyll Fields in the Gulf of Finland. 2013.
149. **Tiina Kriščiunaite**. A Study of Milk Coagulability. 2013.
150. **Tuuli Levandi**. Comparative Study of Cereal Varieties by Analytical Separation Methods and Chemometrics. 2013.
151. **Natalja Kabanova**. Development of a Microcalorimetric Method for the Study of Fermentation Processes. 2013.
152. **Himani Khanduri**. Magnetic Properties of Functional Oxides. 2013.
153. **Julia Smirnova**. Investigation of Properties and Reaction Mechanisms of Redox-Active Proteins by ESI MS. 2013.
154. **Mervi Sepp**. Estimation of Diffusion Restrictions in Cardiomyocytes Using Kinetic Measurements. 2013.
155. **Kersti Jääger**. Differentiation and Heterogeneity of Mesenchymal Stem Cells. 2013.
156. **Victor Alari**. Multi-Scale Wind Wave Modeling in the Baltic Sea. 2013.
157. **Taavi Päll**. Studies of CD44 Hyaluronan Binding Domain as Novel Angiogenesis Inhibitor. 2013.
158. **Allan Niidu**. Synthesis of Cyclopentane and Tetrahydrofuran Derivatives. 2013.
159. **Julia Geller**. Detection and Genetic Characterization of *Borrelia* Species Circulating in Tick Population in Estonia. 2013.
160. **Irina Stulova**. The Effects of Milk Composition and Treatment on the Growth of Lactic Acid Bacteria. 2013.
161. **Jana Holmar**. Optical Method for Uric Acid Removal Assessment During Dialysis. 2013.
162. **Kerti Ausmees**. Synthesis of Heterobicyclo[3.2.0]heptane Derivatives *via* Multicomponent Cascade Reaction. 2013.
163. **Minna Varikmaa**. Structural and Functional Studies of Mitochondrial Respiration Regulation in Muscle Cells. 2013.
164. **Indrek Koppel**. Transcriptional Mechanisms of BDNF Gene Regulation. 2014.
165. **Kristjan Pilt**. Optical Pulse Wave Signal Analysis for Determination of Early Arterial Ageing in Diabetic Patients. 2014.
166. **Andres Anier**. Estimation of the Complexity of the Electroencephalogram for Brain Monitoring in Intensive Care. 2014.
167. **Toivo Kallaste**. Pyroclastic Sanidine in the Lower Palaeozoic Bentonites – A Tool for Regional Geological Correlations. 2014.
168. **Erki Kärber**. Properties of ZnO-nanorod/In_2S_3/$CuInS_2$ Solar Cell and the Constituent Layers Deposited by Chemical Spray Method. 2014.
169. **Julia Lehner**. Formation of Cu_2ZnSnS_4 and $Cu_2ZnSnSe_4$ by Chalcogenisation of Electrochemically Deposited Precursor Layers. 2014.
170. **Peep Pitk**. Protein- and Lipid-rich Solid Slaughterhouse Waste Anaerobic Co-digestion: Resource Analysis and Process Optimization. 2014.
171. **Kaspar Valgepea**. Absolute Quantitative Multi-omics Characterization of Specific Growth Rate-dependent Metabolism of *Escherichia coli*. 2014.

172. **Artur Noole**. Asymmetric Organocatalytic Synthesis of 3,3'-Disubstituted Oxindoles. 2014.
173. **Robert Tsanev**. Identification and Structure-Functional Characterisation of the Gene Transcriptional Repressor Domain of Human Gli Proteins. 2014.
174. **Dmitri Kartofelev**. Nonlinear Sound Generation Mechanisms in Musical Acoustic. 2014.
175. **Sigrid Hade**. GIS Applications in the Studies of the Palaeozoic Graptolite Argillite and Landscape Change. 2014.
176. **Agne Velthut-Meikas**. Ovarian Follicle as the Environment of Oocyte Maturation: The Role of Granulosa Cells and Follicular Fluid at Pre-Ovulatory Development. 2014.
177. **Kristel Hälvin**. Determination of B-group Vitamins in Food Using an LC-MS Stable Isotope Dilution Assay. 2014.
178. **Mailis Päri**. Characterization of the Oligoadenylate Synthetase Subgroup from Phylum Porifera. 2014.
179. **Jekaterina Kazantseva**. Alternative Splicing of *TAF4*: A Dynamic Switch between Distinct Cell Functions. 2014.
180. **Jaanus Suurväli**. Regulator of G Protein Signalling 16 (RGS16): Functions in Immunity and Genomic Location in an Ancient MHC-Related Evolutionarily Conserved Synteny Group. 2014.
181. **Ene Viiard**. Diversity and Stability of Lactic Acid Bacteria During Rye Sourdough Propagation. 2014.
182. **Kristella Hansen**. Prostaglandin Synthesis in Marine Arthropods and Red Algae. 2014.
183. **Helike Lõhelaid**. Allene Oxide Synthase-lipoxygenase Pathway in Coral Stress Response. 2015.
184. **Normunds Stivrinš**. Postglacial Environmental Conditions, Vegetation Succession and Human Impact in Latvia. 2015.
185. **Mary-Liis Kütt**. Identification and Characterization of Bioactive Peptides with Antimicrobial and Immunoregulating Properties Derived from Bovine Colostrum and Milk. 2015.
186. **Kazbulat Šogenov**. Petrophysical Models of the CO_2 Plume at Prospective Storage Sites in the Baltic Basin. 2015.
187. **Taavi Raadik**. Application of Modulation Spectroscopy Methods in Photovoltaic Materials Research. 2015.
188. **Reio Põder**. Study of Oxygen Vacancy Dynamics in Sc-doped Ceria with NMR Techniques. 2015.
189. **Sven Siir**. Internal Geochemical Stratification of Bentonites (Altered Volcanic Ash Beds) and its Interpretation. 2015.
190. **Kaur Jaanson**. Novel Transgenic Models Based on Bacterial Artificial Chromosomes for Studying BDNF Gene Regulation. 2015.
191. **Niina Karro**. Analysis of ADP Compartmentation in Cardiomyocytes and Its Role in Protection Against Mitochondrial Permeability Transition Pore Opening. 2015.
192. **Piret Laht**. B-plexins Regulate the Maturation of Neurons Through Microtubule Dynamics. 2015.
193. **Sergei Žari**. Organocatalytic Asymmetric Addition to Unsaturated 1,4-Dicarbonyl Compounds. 2015.

194. **Natalja Buhhalko**. Processes Influencing the Spatio-temporal Dynamics of Nutrients and Phytoplankton in Summer in the Gulf of Finland, Baltic Sea. 2015.
195. **Natalia Maticiuc**. Mechanism of Changes in the Properties of Chemically Deposited CdS Thin Films Induced by Thermal Annealing. 2015.
196. **Mario Öeren**. Computational Study of Cyclohexylhemicucurbiturils. 2015.
197. **Mari Kalda**. Mechanoenergetics of a Single Cardiomyocyte. 2015.
198. **Ieva Grudzinska**. Diatom Stratigraphy and Relative Sea Level Changes of the Eastern Baltic Sea over the Holocene. 2015.
199. **Anna Kazantseva**. Alternative Splicing in Health and Disease. 2015.